

---

[All ETDs from UAB](#)

[UAB Theses & Dissertations](#)

---

2013

## An Examination of the Molecular Mechanism of E. coli ClpAP Catalyzed Polypeptide Translocation

Justin Mark Miller  
*University of Alabama at Birmingham*

Follow this and additional works at: <https://digitalcommons.library.uab.edu/etd-collection>

 Part of the [Arts and Humanities Commons](#)

---

### Recommended Citation

Miller, Justin Mark, "An Examination of the Molecular Mechanism of E. coli ClpAP Catalyzed Polypeptide Translocation" (2013). *All ETDs from UAB*. 2470.  
<https://digitalcommons.library.uab.edu/etd-collection/2470>

This content has been accepted for inclusion by an authorized administrator of the UAB Digital Commons, and is provided as a free open access item. All inquiries regarding this item or the UAB Digital Commons should be directed to the [UAB Libraries Office of Scholarly Communication](#).

An Examination of the Molecular Mechanism of  
*E. coli* ClpAP Catalyzed Polypeptide Translocation

by

Justin M. Miller

Aaron L. Lucius, CHAIR

David E. Graves

Kirill M. Popov

Christie G. Brouillette

Matthew B. Renfrow

A DISSERTATION

Submitted to the graduate faculty of The University of Alabama at Birmingham,  
in partial fulfillment of the requirements for the degree of  
Doctor of Philosophy

BIRMINGHAM, ALABAMA

2013

Copyright by  
Justin Mark Miller  
2013

An Examination of the Molecular Mechanism of  
*E. coli* ClpAP Catalyzed Polypeptide Translocation

Justin M. Miller

CHEMISTRY

ABSTRACT

ATP-dependent proteases catalyze the removal of both misfolded and properly folded proteins in cellular quality control pathways. ClpAP shares a structural homology with other ATP-dependent proteases where a hexameric ring of ClpA associates with one or both ends of the cylindrically-shaped protease ClpP, which contains serine protease active sites sequestered in its inner core. ClpA contains two nucleotide binding domains where ATP is bound and hydrolyzed, termed Domain 1 (D1) or 2 (D2). D1 has been shown to be primarily responsible for ClpA oligomerization, but both domains appear to support polypeptide translocation independently. We previously reported a molecular mechanism for ClpA catalyzed polypeptide translocation in the absence of ClpP, including estimates of the elementary rate constant, the overall translocation rate, and the kinetic step-size. We have applied here a single-turnover stopped-flow fluorescence method to examine polypeptide translocation catalyzed by ClpA in both the presence and absence of the proteolytic component ClpP. We propose models for ClpA and ClpAP catalyzed polypeptide translocation where D1 or D2 limits the rate of ClpA catalyzed polypeptide translocation when ClpP is either absent or present, respectively. In our models, the observed rate-limiting step occurs immediately after an ATP binding event in a cycle of translocation. For ClpA, this step repeats every  $\sim 14$  amino acids translocated with an observed rate constant of  $\sim 1.39 \text{ s}^{-1}$ , whereas for ClpAP this step repeats every  $\sim 2 - 5$  amino acids translocated with an observed rate constant of  $\sim 6.6 \text{ s}^{-1}$ . However, our model for

ClpAP catalyzed polypeptide translocation was based on data collected for conditions where a mixture of ClpAP complexes was favored. Thus, it was unclear whether ClpAP complexes with one or two associated ClpA hexamers translocate polypeptide with the same mechanisms. To address this, we report here an examination of the dependence of the mechanism for ClpAP catalyzed polypeptide translocation on the ClpAP species distribution. We conclude that ClpAP complexes with one or two ClpA hexamers associated translocate polypeptide with identical mechanisms. Therefore, our data are consistent with a model where the rate-limiting step for translocation is coupled to ATP hydrolysis at D2 for all ClpAP complexes.

**Keywords:** ATP Dependent Proteases; AAA+ Motor Proteins; pre-steady-state kinetics; protein unfoldases; steady-state kinetics

## DEDICATION

To my wife, Kayla. Without you, none of this would have been possible. Thank you for always being there to support me, both in good times and bad times. You pushed me to be productive when I lacked the desire to do so. You loved me when I was irritable. For all these reasons and more, I thank you for tagging along for the graduate school ride. I look forward to spending many more years together.

To our dog, Belle. Despite the jokes that we make, you will never be capable of reading this. However, I must extend thanks to you for your well-timed application of stress relief techniques. You have learned how to very efficiently extract a chuckle from me by dropping your bone on my head at the most inopportune times, pouncing on me for sole purpose of biting my nose, and through many other finely tuned stress relief methods.

## ACKNOWLEDGEMENTS

I would like to thank everybody that has helped me along the way over the years. The number of people included in this group are far too numerous to give individual thanks. Please know that I am eternally grateful to all of those that have contributed to my development, both personally and professionally throughout my undergraduate and graduate studies here at UAB. In particular, I would like to thank the past and present members of the Lucius lab for always pushing me to be better at what I do, including (in no particular order) Aaron Lucius, Keith Veronese, Ryan Stafford, Rajendar Burki, Tao Li, Jiabei Lin, Lolli Meeks, Hitesh Goel, Clarissa Weaver, Elizabeth Duran, Christina Bogan, Alfredo Jimenez, Nate Scull, and Zac Ingram. I would also like to thank all UAB department of chemistry staff, including Laura Knighten, Tammie Vines, Sharon Mahaffey, and Tanja Matthews. To my committee members, David Graves, Kirill Popov, Matthew Renfrow, Christie Brouillette, and Aaron Lucius, I thank you for your constructive criticism and support that you have offered from my first committee meeting to the last committee meeting. To the UAB department of chemistry faculty, I thank each and every one of you for helping me to grow in one way or another. I came to UAB as a freshman, and now, eight years later, I leave as a trained scientist. It is impossible to adequately thank all of you that contributed to my growth. However, I say thank you nonetheless.

I would also like to acknowledge my family and friends for all of their support along the way. Thanks to Gerri and Mark Miller, Marissa Miller, Tony and Angie

Retherford, Denise Retherford, Kyle Retherford, Trent and Ally Killian, Stephen and Jessica Bosley, Kirk and Morgan Ellison, Justin and Lisa Anne Surratt, and many others. None of this would have been possible without supportive friends and family. Thank you for tolerating my constant need to have a computer on somewhere nearby for data analysis purposes. Additionally, I would like to acknowledge the talented team of baristas located in the Mervyn H. Sterne library Starbucks conveniently located approximately 500 feet from my desk in the Lucius lab. They have insured that I have been consistently caffeinated for five years now.

Finally, to any future students that may be reading this, always remember that there is light at the end of the tunnel. You will be faced with challenges along the way, but remember that degrees are not earned overnight. You must take one step at a time in life and earning your Ph.D. is no different. Along the way, cultivate as many relationships as you can, learn as many techniques as you can, and do not neglect yourself in the process.

## TABLE OF CONTENTS

	Page
ABSTRACT.....	iii
DEDICATION.....	v
ACKNOWLEDGMENTS.....	vi
LIST OF TABLES.....	xi
LIST OF FIGURES.....	xii
LIST OF ABBREVIATIONS.....	xiv
 CHAPTER	
I. Introduction.....	1
The role of ATP-dependent proteases in disease.....	1
<i>Escherichia coli</i> ClpA.....	3
Observation of ClpA catalyzed polypeptide translocation.....	5
Dependence of the molecular mechanism of ClpA catalyzed polypeptide translocation on [ATP].....	6
ATP $\gamma$ S is required for the observation of translocation.....	8
Observation of polypeptide translocation by ClpAP involves multiple species....	10
2. Application of the Sequential n-Step Kinetic Mechanism to Polypeptide Translocases.....	12
Introduction.....	14
Single Turnover Fluorescence Stopped-Flow Method to Monitor Polypeptide Translocation.....	15
Substrate Design.....	17
Enzyme Trap.....	18
Application of the Sequential n-step Mechanism.....	20
Application of Scheme 1.....	21
Scheme 2: Biphasic Kinetics.....	24
Scheme 3: Finite Processivity.....	27
Determination of Kinetic Step-size.....	29
Application of Scheme 4.....	34

Determination of Translocation Directionality.....	36
Concluding Remarks.....	36
References.....	38
3. E. coli ClpA Catalyzed Polypeptide Translocation is Allosterically Controlled by the Protease ClpP.....	51
Introduction.....	53
Results.....	56
Application of a single-turnover method to examine polypeptide translocation by ClpAP.....	56
Analysis of the number of steps as a function of polypeptide substrate length.....	61
Dependence of translocation mechanism on [ATP].....	64
Discussion.....	66
Analysis of translocating species.....	68
Rate of ClpAP catalyzed polypeptide translocation.....	71
Interpretation of the kinetic step-size.....	72
A proposed molecular model for translocation.....	75
Materials and Methods.....	80
Materials.....	80
ClpP Purification.....	81
Methods.....	82
Analytical Ultracentrifugation.....	82
Sedimentation Velocity.....	82
Single-Turnover Stopped-Flow Fluorescence Experiments.....	83
NLLS Analysis.....	84
References.....	87
4. ATP $\gamma$ S Competes with ATP for Binding at Domain 1 but not Domain 2 during ClpA Catalyzed Polypeptide Translocation.....	104
Introduction.....	106
Results.....	109
Kinetics of ATP $\gamma$ S Hydrolysis Catalyzed by ClpA.....	109
Competition between ATP and ATP $\gamma$ S.....	111
Global NLLS analysis of translocation data.....	112
Impact of Parameter Correlation on the Determination of the Kinetic Parameters.....	114
ClpAP catalyzed polypeptide translocation.....	117
Discussion.....	120
Model for Polypeptide Translocation catalyzed by ClpA vs. ClpAP.....	121
Dependence of Correlation Coefficient on ATP $\gamma$ S.....	124
Type 1 AAA+ Molecular Chaperones.....	127
Materials and Methods.....	128
Materials.....	128
Methods.....	128
ATPase Activity Assay.....	128

Stopped-flow fluorescence assay .....	129
NLLS Analysis.....	130
References.....	134
5. <i>E.coli</i> ClpAP Complexes Share a Common Polypeptide Translocation Mechanism .....	148
Introduction.....	150
Results.....	155
Application of single-turnover stopped-flow fluorescence method.....	156
Apparent translocation rate depends on [ClpP <sub>14</sub> ] <sub>T</sub> .....	160
1:1 and 2:1 ClpAP complexes translocate polypeptide with similar rates.....	162
Dependence of kinetic parameters on molar ratio .....	167
Discussion.....	170
Polypeptide translocation catalyzed by 1:1 ClpAP versus 2:1 ClpAP ....	170
Binding of ClpA hexamers by ClpP tetradecamers .....	174
Proposed mechanism for ClpAP activation in the cytoplasm.....	176
Materials and Methods.....	178
Materials .....	178
Methods.....	178
NLLS Analysis.....	179
References.....	181
6. Summary .....	192
Conclusions.....	192
Directions.....	196
LIST OF REFERENCES FOR INTRODUCTION AND CONCLUSION .....	198
APPENDIX: Mathematical representation of [ATP]-dependent polypeptide translocation using the method of Laplace transforms.....	201

## LIST OF TABLES

<i>Tables</i>	<i>Page</i>
Application of the Sequential n-Step Kinetic Mechanism to Polypeptide Translocases	
1	Polypeptide Translocation Substrates .....50
E. coli ClpA Catalyzed Polypeptide Translocation is Allosterically Controlled by the Protease ClpP	
1	Polypeptide Translocation Substrates .....101
2	ClpAP Polypeptide Translocation NLLS Parameters as a Function of [ATP]....102
3	ClpAP Polypeptide Translocation Global NLLS Parameters as a Function of [ATP] .....103
ATP $\gamma$ S Competes with ATP for Binding at Domain 1 but not Domain 2 during ClpA Catalyzed Polypeptide Translocation	
1	Polypeptide Translocation Substrates .....145
2	ClpA Polypeptide Translocation NLLS Parameters as a Function of [ATP $\gamma$ S].....146
3	ClpAP Polypeptide Translocation NLLS Parameters as a Function of [ATP $\gamma$ S].....147
E.coli ClpAP Complexes Share a Common Polypeptide Translocation Mechanism	
1	Polypeptide Translocation Substrates .....190
2	ClpAP Polypeptide Translocation NLLS Parameters as a Function of [ClpP <sub>14</sub> ] <sub>T</sub> .....191

## LIST OF FIGURES

<i>Figures</i>		<i>Page</i>
Application of the Sequential n-Step Kinetic Mechanism to Polypeptide Translocases		
1	Schematic Representation of Single-Turnover Stopped-Flow Experiment.....	41
2	Schematic Representation of “Trap-Test” .....	42
3	Representative Time-Courses from Single-Turnover Stopped-Flow Fluorescence Experiment.....	43
4	Simulated Time-Courses from Scheme 1 .....	44
5	Simulated Time-Courses from Scheme 2 .....	45
6	Simulated Time-Courses from Scheme 3 .....	46
7	Fluorescence time-courses for ClpA catalyzed polypeptide translocation .....	47
8	Simulated Time-Courses from Scheme 4 .....	48
9	Schemes .....	49
E. coli ClpA Catalyzed Polypeptide Translocation is Allosterically Controlled by the Protease ClpP		
1	Schematic representation of single turnover stopped-flow translocation .....	92
2	Fluorescence time-courses for ClpAP catalyzed polypeptide translocation.....	93
3	Sedimentation coefficient distribution, $c(s)$ , dependence on ATP $\gamma$ S .....	94
4	The number of translocation steps depends on polypeptide length .....	95
5	Dependence of translocation parameters on [ATP] .....	96
6	Schematic representation of polypeptide translocation .....	97

7	Proposed model of polypeptide translocation.....	98
8	Scheme 1.....	99
9	Scheme 2.....	100

#### ATP $\gamma$ S Competes with ATP for Binding at Domain 1 but not Domain 2 during ClpA Catalyzed Polypeptide Translocation

1	Schematic representation of single turnover stopped-flow translocation .....	138
2	ClpA catalyzes ATP $\gamma$ S hydrolysis.....	139
3	Fluorescence time-courses for ClpA catalyzed polypeptide translocation.....	140
4	Molecular mechanism for ClpA catalyzed polypeptide translocation depends on [ATP $\gamma$ S] .....	141
5	Parameter correlation between the kinetic step-size and elementary rate constant depends on [ATP $\gamma$ S] for ClpA catalyzed polypeptide translocation in the absence of ClpP .....	142
6	Parameter correlation between the kinetic step-size and elementary rate constant depends on [ATP $\gamma$ S] for ClpA catalyzed polypeptide translocation in the presence of ClpP .....	143
7	Scheme 1: Sequential n-step model for polypeptide translocation.....	144

#### *E. coli* ClpAP Complexes Share a Common Polypeptide Translocation Mechanism

1	Schematic representation of the possible ClpAP oligomers .....	184
2	Schematic representation of single turnover stopped-flow translocation.....	185
3	Representative fluorescence time-courses for ClpAP catalyzed polypeptide translocation.....	186
4	The apparent overall rate of translocation $mk_{T,app}$ depends on [ClpP $_{14}$ ] <sub>T</sub> .....	187
5	Dependence of the apparent kinetic parameters on ClpAP species distribution.....	188
6	Sequential <i>n</i> -step model for polypeptide translocation .....	189

## LIST OF ABBREVIATIONS

ADP	Adenosine 5'-diphosphate
ATP	Adenosine 5'-triphosphate
ATP $\gamma$ S	Adenosine 5'-[gamma-thio]-triphosphate
AMP-PNP	Adenosine 5'-( $\beta,\gamma$ -imido)triphosphate
AMP-PCP	$\beta,\gamma$ -Methyleneadenosine 5'-triphosphate
ADP.BeF	Adenosine diphosphate beryllium fluoride
NLLS	nonlinear-least-squares
SSD	sum of squared residuals
EDTA	Ethylenediaminetetraacetic acid
FLU	Fluorescein 5-Maleimide dye
CY3	Cyanine 3 Maleimide dye
D1	Domain 1
D2	Domain 2

## Chapter One

### Introduction

#### *The role of ATP-dependent proteases in disease*

Many late-onset neurodegenerative disease states such as Alzheimer's disease, Parkinson's disease, and Huntington's disease are commonly caused by defects in protein folding and proteasomal degradation pathways.<sup>1</sup> Neurodegeneration can often be linked to mutations that render proteins to be more aggregate-prone than wild-type proteins.<sup>1</sup> For example, a major pathological hallmark of Alzheimer's disease is a result of mutations in amyloid precursor protein that lead to accumulation of amyloid plaques.<sup>2</sup> Similarly, point mutations in huntingtin protein that lengthen polyglutamine sequences correlate with increased propensity for aggregation and earlier onset of Huntington's disease.<sup>1</sup>

In healthy cells, energy-dependent protein degradation is required as a component of quality control pathways that help to avoid the toxic gains-of-function associated with protein aggregation. In eukaryotes, the major machine to have evolved for this purpose is the ATP-dependent 26S proteasome.<sup>3</sup> As such, the 26S proteasome is responsible for the removal of hundreds of regulatory proteins, which leads to an active role in a variety of cellular processes that include cell cycle control, stress responses, apoptosis, inflammation, signal transduction, protein quality control, and many others.<sup>4</sup> Defects in the proteasomal protein degradation pathway can lead to observations of protein

aggregation and toxic gains-of-function. Therefore, a thorough understanding of the mechanism of polypeptide substrate degradation will be required to devise treatments for the various forms of dementia.

The 26S proteasome represents the largest and most complex AAA+ protease (ATPases Associated with various cellular Activities).<sup>5</sup> While complete proteasomal assembly requires more than 30 different proteins, basic architectural features are found to be shared with ATP-dependent proteases in all organisms.<sup>3; 6; 7</sup> ATP-dependent proteases share a common architecture where a hexameric AAA+ ATPase can associate with one or both ends of a barrel-shaped peptidase that contains compartmentalized active sites in its interior.<sup>6; 8; 9</sup> In these systems, the AAA+ ATPase component is responsible for the recognition, unfolding, and translocation of specific protein substrates into the proteolytic core of the associated peptidase for degradation.

In *Escherichia coli*, there are five known ATP dependent proteases (Lon, ClpAP, ClpXP, HslUV, and the membrane-associated FtsH) that catalyze the removal of both misfolded and properly folded proteins in cellular protein quality control pathways.<sup>5; 8</sup> Lon and FtsH represent cases in which the ATPase and protease domains are contained within a single gene product. In contrast, ClpAP, ClpXP, and HslUV represent the canonical ATP-dependent proteases in which a AAA+ unfoldase associates with a compartmentalized protease. The scope of this work will be dedicated to the discussion of the canonical ATP dependent proteases. In particular, we will use ClpAP as a model system to understand how ATP dependent proteases like the 26S proteasome process their respective polypeptide substrates.

## *Escherichia coli ClpA*

AAA+ unfoldases couple the energy of ATP binding and hydrolysis to catalyze protein unfolding for a variety of purposes including protein degradation and remodeling. AAA+ proteins can be classified as belonging to either Class I or Class II.<sup>8:</sup>  
<sup>10</sup> Class I proteins contain two ATP binding and hydrolysis sites per monomer, while Class II proteins contain only one site per monomer. Class I enzymes include ClpA and ClpB, whereas Class II includes ClpX and HslU.

Despite the differences in number of ATPase sites, several AAA+ unfoldases are capable of unfolding the same polypeptide substrates, and even associating with the same protease in some cases. For example, ClpA and ClpX can both associate with ClpP to form the ATP dependent proteases ClpAP and ClpXP, respectively. However, it remains unclear as to why ClpA requires two ATP binding and hydrolysis sites per monomer, whereas ClpX only requires a single ATP binding and hydrolysis site per ClpX monomer.

The monomeric ClpA crystal structure demonstrates clearly that three domains are present in each ClpA monomer: an N-terminal domain, AAA+ Domain 1 (D1), and AAA+ Domain 2 (D2).<sup>11</sup> D1 and D2 each contain Walker A and Walker B motifs that form the ATP binding and hydrolysis sites. In both D1 and D2, a loop structure is formed between the Walker A and Walker B motif, which resides in the central channel of the ClpA hexamer. Hinnerwisch and coworkers showed through crosslinking studies that when ClpA was bound to an SsrA containing substrate in the presence of ATP $\gamma$ S, the D2 loop made contact with the SsrA sequence.<sup>12</sup> Although they did not observe crosslinking to the D1 loop, mutations in this loop eliminated translocation. Consequently, it was concluded that both the D1 and D2 loops are involved in polypeptide translocation.

In ClpA, the D2 loop contains a conserved aromatic-hydrophobic sequence, GYVG, which is present in nearly all AAA+ unfoldases.<sup>13</sup> Mutating the conserved tyrosine at residue 540 to either a cysteine or an alanine, i.e. Y540C or Y540A, decreases the rate of proteolysis observed when either mutant is incubated in the presence of ClpP and casein.<sup>14</sup> However, the same tyrosine mutations do not appear to dramatically alter the degradation rate of short peptides or observed ATPase rates.

To date, the best model for translocation is one where ClpA catalyzed translocation is driven by movement of the D1- and D2-loops that are coupled to the hydrolytic state of the bound nucleotide.<sup>15; 16</sup> The D2 loop has been observed to reside in a “down” position in the ADP-bound state from crystallographic studies,<sup>11</sup> whereas synchrotron protein footprinting experiments with ATP $\gamma$ S-bound ClpA suggest an alternate “up” position.<sup>15</sup> Furthermore, single-molecule methodology has been used to show that the ATP $\gamma$ S-bound pre-hydrolytic state of ClpA corresponds to a conformation with a higher affinity for polypeptide.<sup>14; 16</sup> That study also reported shorter dwell times for the ADP-bound post-hydrolytic state, corresponding to a less stable conformation with a lower affinity for polypeptide.

At thermodynamic equilibrium, ClpA resides in a mixture of monomers, dimers, and tetramers in the absence of nucleotide.<sup>17; 18</sup> Nucleoside triphosphate is required to assemble ClpA hexamers that are active in polypeptide binding, polypeptide translocation, and association with ClpP.<sup>19; 20; 21</sup> Maurizi and coworkers used ClpA mutants that were unable to bind ATP at either D1 or D2 to show that ATP binding at D1 was essential for assembly into hexameric rings and that D2 was responsible for the majority of the observed ATP hydrolysis.<sup>22</sup> However, more recent work has shown that

ClpA mutants deficient in ATPase activity at either D1 or D2 both support polypeptide translocation.<sup>23</sup> Therefore, both nucleotide binding sites are likely involved in polypeptide translocation.

As mentioned above, the canonical ATP-dependent protease is assembled through the association of a AAA+ unfoldase with a protease that contains active sites sequestered from surrounding solution. For ClpAP, ClpA hexamers that have been assembled in the presence of nucleoside triphosphate can associate with a single face of ClpP<sub>14</sub> to form a ClpAP complex with one hexamer per ClpP tetradecamer, 1:1 ClpAP. ClpA hexamers can also associate with both faces of ClpP<sub>14</sub> to form a ClpAP complex with two hexamers per ClpP tetradecamer, 2:1 ClpAP. In principle, the 2:1 ClpAP complex can bind one or two polypeptide substrates per active complex. Therefore, a dynamic equilibrium of free ClpA hexamers, 1:1 ClpAP, and 2:1 ClpAP complexes with either one or two polypeptides bound is possible.

#### *Observation of ClpA catalyzed polypeptide translocation*

Throughout the literature, ClpA catalyzed polypeptide translocation has been observed using steady-state degradation of model substrates such as green fluorescent protein<sup>24</sup> and casein<sup>14; 25</sup>, or via the observation of FRET upon substrate entry into ClpP.<sup>26; 27</sup> However, these strategies require ClpP to be present for observation of signal. Therefore, none of the reported experimental designs allow for the examination of ClpA catalyzed polypeptide translocation in the absence of ClpP. Thus, the question of whether or not ClpP exerts an allosteric effect on the mechanism of ClpA catalyzed polypeptide translocation cannot be addressed with existing methodologies.

To circumvent this problem, we developed a single turnover stopped-flow fluorescence method that allows us to examine ClpA catalyzed polypeptide translocation in the absence of the proteolytic component, ClpP.<sup>28</sup> Using this approach, we showed that ClpA, in the absence of ClpP, translocated polypeptide substrates with an overall rate of  $\sim 20 \text{ aa s}^{-1}$  and the repeating rate-limiting step repeats every  $\sim 14 \text{ aa}$ . The methodology of our single-turnover stopped-flow fluorescence assay is discussed in detail in Chapter 2 of this dissertation.

Our single-turnover translocation assay is discussed in detail in Chapter 2 of this dissertation. In this experimental design, preassembled ClpA that is prebound with polypeptide substrate is rapidly mixed in a stopped-flow fluorometer with ATP and protein trap to initiate translocation. Under these conditions, time courses only reflect the kinetics of translocation since we have removed the contributions of assembly kinetics and polypeptide binding kinetics. Therefore, the resulting kinetic time courses only reflect a single cycle of polypeptide translocation. The strength of this technique is that the kinetic time courses are sensitive to the molecular events in polypeptide translocation.

*Dependence of the molecular mechanism of ClpA catalyzed polypeptide translocation on [ATP]*

For a motor protein to translocate along a linear lattice, repeating cycles of certain events must occur. At a minimum, each cycle must include ATP binding, ATP hydrolysis,  $P_i$  release, potential conformational changes, etc. Therefore, each round of translocation requires that this cycle of events repeat multiple times until translocation is complete. Consequently, our single-turnover methodology is sensitive to the slowest repeating step in the cycle.

A common approach to the investigation of the mechanism of any translocase is to examine the dependence of the translocation mechanism on [ATP].<sup>28; 29</sup> The rationale for such an approach lies in the fact that each translocation step requires at least one cycle of ATP binding and hydrolysis, and this cycle must repeat multiple times in a single round of translocation. Therefore, if multiple kinetic steps are rate-limiting under conditions of saturating [ATP], where ATP binding is not rate-limiting, a reduction in [ATP] will potentially cause ATP binding to become rate-limiting and will lead to a change in the observed number of translocation steps. This is because a reduction in [ATP] will lead to the bimolecular ATP binding step becoming rate-limiting in translocation. An alternate outcome is that the ATP binding step is in rapid equilibrium with the step immediately following ATP binding. In this case, the step following ATP binding will become rate-limiting and the number of observed translocation steps remains unchanged. Thus, the dependence of the translocation parameters on [ATP] is often used to elucidate details of the translocation mechanism for a given enzyme.

In Chapter 3 of this dissertation, we report the results of an investigation of the dependence of the translocation mechanism for ClpA catalyzed polypeptide translocation on [ATP] in the presence of ClpP. This was performed in an effort to address the question of whether ClpP allosterically impacts the translocation mechanism of ClpA. We report that ClpA, in the presence of ClpP, translocates polypeptide substrate with an overall rate of  $\sim 36 \text{ aa s}^{-1}$ , contrary to our previous report of  $\sim 20 \text{ aa s}^{-1}$  in the absence of ClpP. We demonstrate that this is a result of both an increase in the elementary rate constant for translocation and a decrease in the frequency with which the observed rate-limiting step repeats. Furthermore, the dependence in translocation parameters on [ATP] leads to the

conclusion that the repeating rate-limiting step is a step that immediately follows ATP binding.

By coupling our observations presented in Chapter 3 with our previous observations of ClpA catalyzed polypeptide translocation in the absence of ClpP,<sup>28</sup> steady state ATP hydrolysis rates from Weber-Ban and coworkers,<sup>23</sup> and crosslinking experiments from Horwich and coworkers,<sup>12</sup> we proposed models for ClpA and ClpAP catalyzed polypeptide translocation. In these models, the rate-limiting step in translocation takes place at D1 when ClpP is absent, whereas the observed rate-limiting step occurs at D2 in the presence of ClpP.<sup>29</sup> We proposed that at D1 this step repeats every ~14 amino acids translocated with an observed rate constant of  $\sim 1.39 \text{ s}^{-1}$ , and at D2 this step repeats every ~2 – 5 amino acids translocated with an observed rate constant of  $\sim 6.6 \text{ s}^{-1}$ .<sup>16; 18</sup>

*ATP $\gamma$ S is required for the observation of translocation*

Our single-turnover methodology requires ClpA hexamers to be preassembled and prebound to polypeptide in the presence of a non- or slow-hydrolysable ATP analogue, and, in some cases, ClpP. This approach removes the contribution of assembly kinetics or polypeptide substrate binding kinetics from translocation time courses such that time courses are sensitive only to the kinetics of translocation. However, because a non- or slowly-hydrolysable ATP analogue is required for assembly of ClpA hexamers, there is the potential for competition between ATP and the ATP analogue.

To eliminate potential competition between ATP and the ATP-analogue, we have explored several pathways to assemble ClpA hexamers, prebind ClpA to polypeptide substrates, and initiate translocation. For example, we tried prebinding ClpA to

polypeptide in the presence of ATP and the absence of  $Mg^{+2}$  and initiating translocation by rapidly mixing with  $Mg^{+2}$ . However, translocation was not observed using this approach. We also investigated the effect of nucleotide analogue on translocation by assembling ClpA in the presence of ATP $\gamma$ S, AMP-PNP, AMP-PCP, ADP, and ADP.BeF.<sup>19</sup> There we showed that only AMP-PNP and ATP $\gamma$ S would assemble a prebound complex competent for polypeptide translocation. However, substantially higher concentrations of AMP-PNP compared to ATP $\gamma$ S are required, which was consistent with previous reports on assembling ClpA with AMP-PNP.<sup>20</sup> Consequently, ATP $\gamma$ S emerged as the most effective nucleotide analog for preassembling ClpA hexamers competent for ClpP association, polypeptide binding, and polypeptide translocation.

In Chapter 4, we report the results of an examination of the effect of [ATP $\gamma$ S] on ClpA catalyzed polypeptide translocation in both the presence and absence of ClpP. Using our single-turnover stopped-flow fluorescence method, we demonstrate that the rate of ClpA catalyzed translocation depends on [ATP $\gamma$ S] in the absence of ClpP, which is consistent with competition for binding between ATP and ATP $\gamma$ S. However, this dependence is not observed in the presence of ClpP. By incorporating these observations with our proposed models for ClpA and ClpAP catalyzed polypeptide translocation,<sup>29</sup> we propose in Chapter 4 that ATP $\gamma$ S competes for ATP binding at the D1 ATPase site, but not significantly at the D2 ATPase site. Because competition between ATP and ATP $\gamma$ S was observed in the absence of ClpP, but not in the presence, ATP $\gamma$ S must bind at D1 with a greater affinity than at D2. This conclusion is reasonable since D2 has been shown

to hydrolyze ATP more rapidly than D1, and this would only be possible if the two sites bound nucleotide with different affinities.

*Observation of polypeptide translocation by ClpAP involves multiple species*

In the absence of ClpP, the application of our single-turnover stopped-flow fluorescence method to observe ClpA catalyzed polypeptide translocation reports only on preassembled ClpA hexamers initially bound to polypeptide. In contrast, when the same experiments are performed in the presence of ClpP, up to four possible forms of ClpA and ClpAP may exist in solution, which include free ClpA hexamers, 1:1 ClpAP, and 2:1 ClpAP complexes with either one or two polypeptides bound. Because all four complexes are competent for polypeptide translocation, translocation time courses may contain contributions from multiple species. However, the contribution of each species to translocation time courses remains unclear.

Multiple models have been proposed to describe the translocation activities of 1:1 ClpAP and 2:1 ClpAP complexes. Using casein degradation as a signal, Maurizi and coworkers reported that the maximum proteolytic activity was observed when solution conditions favored the formation of 2:1 ClpAP complexes, and that the proteolytic activity was decreased only slightly when 1:1 ClpAP complexes were favored.<sup>25</sup> From this, it was concluded that the addition of a second ClpA hexamer to the ClpAP complex did not further activate ClpP for polypeptide degradation. In contrast, Weber-ban and coworkers used a stopped-flow FRET approach to observe polypeptide unfolding and translocation where a  $\lambda$ RSsrA construct was prepared that had been labeled with donor and acceptor fluorophores.<sup>30</sup> It was reported there that a 2:1 ClpAP complex with two

polypeptides bound could translocate polypeptide from both ends of ClpP<sub>14</sub> simultaneously and independently. Therefore, it was concluded that both ClpA hexamers present in a 2:1 ClpAP complex could simultaneously translocate polypeptide, and that the hexamers exerted no allosteric control of one another during translocation.

Because no general consensus exists with respect to the individual contributions of each ClpA hexamer to the observed translocation activity of ClpAP complexes, we asked the question; Do 1:1 and 2:1 ClpAP complexes share a common translocation mechanism or does each complex translocate polypeptide with a unique mechanism? While it is clear that the presence of ClpP impacts the ClpA catalyzed polypeptide translocation mechanism, it remains unclear as to whether ClpAP complexes with one versus two ClpA hexamers translocate polypeptide differently. To address this question, we applied our single-turnover stopped-flow fluorescence assay to examine how the translocation mechanism depends on the ClpAP species distribution. In Chapter 5, we demonstrate that the best model to describe translocation of a single polypeptide by 1:1 and 2:1 ClpAP complexes is one where both complexes utilize identical translocation mechanisms. Our data are consistent with a model where the addition of a second ClpA hexamer to ClpP does not upregulate ClpAP catalyzed polypeptide translocation. Therefore, we conclude that the allosteric impact of ClpP on the mechanism of ClpA catalyzed polypeptide translocation is the result of the association of a single ClpA hexamer with a ClpP tetradecamer, and that the addition of a second ClpA hexamer to a ClpAP complex does not further affect translocation catalyzed by ClpA.

Chapter Two

Application of the Sequential n-Step Kinetic Mechanism to Polypeptide Translocases

by

Aaron L. Lucius, Justin M. Miller, and Burki Rajendar

*Methods in Enzymology*

Copyright 2011

Used by permission

Format adapted for dissertation

## **Abstract**

Clp/Hsp100 proteins are essential motor proteins in protein quality control pathways in all organisms. Such enzymes couple the energy derived from ATP binding and hydrolysis to translocate and unfold polypeptide substrates. Often they perform this role in collaboration with proteases for protein removal or with other chaperones for protein disaggregation. Unlike other well characterized motor proteins, fundamental parameters such as the microscopic rate constants and overall rate of translocation, step-size (amino-acids translocated per step), processivity, and directionality are not available for many of these enzymes. We have recently developed a fluorescence stopped-flow method to elucidate these fundamental mechanistic details. In addition, we have developed a quantitative method to examine the single-turnover time courses that result from the rapid mixing experiments. With these two advances in hand, we have recently reported the first determination of the microscopic rate constants, overall rate of translocation, kinetic step-size, and processivity for the *E. coli* ClpA polypeptide translocase. Here, we report a description of both the fluorescence stopped-flow method to examine the mechanism of enzyme catalyzed polypeptide translocation and the mathematics required to quantitatively examine the resulting time-courses.

## Introduction

Motor proteins that translocate directionally on a linear lattice have been studied extensively. Such motor proteins couple the energy derived from NTP binding and hydrolysis to mechanical movement. Enzymes such as kinesin translocate directionally on microtubules.<sup>1; 2; 3</sup> Nucleic acid polymerases<sup>4</sup> and helicases<sup>5; 6; 7; 8</sup> translocate directionally on linear nucleic acid filaments. Clp/Hsp100 proteins translocate directionally on polypeptide chains while disrupting protein structure.<sup>9; 10; 11; 12</sup>

A complete characterization of the molecular mechanism of translocation on a linear lattice requires the determination of several fundamental physical parameters. These parameters include the microscopic rate-constants and overall rate of translocation, the distance traveled per translocation cycle (step-size), processivity, and the amount of NTP used per translocation step (coupling efficiency).

Elucidation of such parameters for nucleic acid motors like helicases and polymerases, and other enzymes like myosin and kinesin has long been an active area of research. As such, these fundamental kinetic parameters have been elucidated for many of these enzymes.<sup>13; 14; 15; 16</sup> In contrast, until recently, quantitative estimates of many of these fundamental physical parameters had not been reported for Clp/Hsp100 enzymes.<sup>10</sup> Here, we report a detailed description of both the fluorescence stopped-flow method to examine the mechanism of enzyme catalyzed polypeptide translocation and the mathematics required to quantitatively examine the resulting time-courses.

## **Single Turnover Fluorescence Stopped-Flow Method to Monitor Polypeptide Translocation**

A major difficulty in examining the mechanism of polypeptide translocation by Clp/Hsp100 enzymes like *E. coli* ClpA, ClpB, or ClpX is that the substrate enters and leaves the reaction without being covalently modified. ClpA, for example, binds a polypeptide substrate, directionally translocates the substrate and then releases the substrate with no covalent change in the substrate. If the polypeptide being translocated is a folded protein upon entering the reaction, then the only change in the substrate that is induced by the protein translocase is the disruption of protein structure. However, upon release, the protein substrate, most likely, promptly refolds making it difficult to monitor how the enzyme has transiently affected the protein secondary structure.

To overcome these difficulties we have developed a single-turnover fluorescence stopped-flow method to examine polypeptide translocation catalyzed by protein unfoldases that do not covalently modify the substrate they translocate. Although this has been developed and applied to *E. coli* ClpA catalyzed polypeptide translocation, in principle, this approach is applicable to a variety of molecular chaperones that directionally translocate on a linear lattice.

The strength of the single-turnover method is that it allows for the examination of the first turnover of translocation in the absence of any binding or rebinding of the enzyme. Therefore, single-turnover experiments are sensitive to the microscopic rate-constants that govern the reaction. This is in stark contrast to multiple-turnover or steady-state kinetic measurements, where multiple rounds of dissociation, binding, and catalysis occur. Such steady-state measurements are a reflection of the slowest step in the

repeating cycles of binding, catalysis, and dissociation. Often, the slowest step is binding or even macromolecular assembly. Thus, interpreting the steady-state kinetic parameters in terms of microscopic rate-constants is difficult. More importantly, elucidating parameters such as the kinetic step-size (average number of AA translocated per step) and processivity (the probability that the enzyme will translocate vs. dissociate) that are essential for our understanding of any motor protein is impossible.

Two strategies are employed to insure that the observed kinetic time courses are not sensitive to binding or re-binding of the enzyme. First, the enzyme and a fluorescently modified substrate are pre-mixed to allow for binding equilibrium to be achieved before the reaction is initiated with ATP. This insures that the acquired kinetic time course will not reflect any bimolecular steps and will only be sensitive to the events in the active site of the enzyme, thus simplifying the kinetic model. Second, after the enzyme and substrate have achieved binding equilibrium the translocation reaction is initiated by rapidly mixing with ATP and a large excess of enzyme trap, see Figure 1. This enzyme trap is anything that can serve to bind specifically to the enzyme in the substrate binding site that will inhibit rebinding of the fluorescently modified substrate, e.g. identical substrate without fluorescent modification. In summary, by pre-binding the enzyme to the substrate and including an enzyme trap, the observed signal is only a reflection of translocation catalyzed by enzyme that was bound to the substrate at time zero in the absence of binding or rebinding. Thus, any kinetic mechanism that will describe the time course that results upon rapid mixing with ATP will not contain any bimolecular steps thereby intensely simplifying the system of differential equations that describe the reaction (see Section 3).

Traditionally, single-turnover experiments are defined as maintaining the enzyme in large excess over the substrate. Although enzyme is often in large excess over the substrate in our experimental design, because a trap for free enzyme is included, no rebinding of the protein occurs (see Substrate Design). Thus, the single-turnover method presented here does not, necessarily, require the enzyme be in large excess over the substrate.

### *Substrate Design*

The first task at hand in the development of a single-turnover stopped-flow experiment to monitor translocation is the development of a suitable substrate. Some knowledge about where the enzyme binds and initiates translocation on the substrate is necessary, i.e. does the enzyme bind and initiate at a specific site or randomly along the entire substrate. The case of random binding has been described for single stranded DNA translocation catalyzed by the UvrD helicase and will not be discussed here.<sup>17; 18</sup> This is because, in the case of ClpA, the enzyme is known to bind specifically to the 11 amino acid (AA) SsrA sequence (AANDENYALAA) placed at the carboxy terminus of protein substrates. Thus, we synthesized a series of polypeptide substrates of various lengths each containing the SsrA sequence at the carboxy terminus, see Table 1. For the purposes of fluorescent modification we placed a single cysteine residue at the carboxy terminus. The single cysteine residue can then be fluorescently modified with the maleimide functional group that is commercially available on many fluorophores such as fluorescein-maleimide or Cy3-maleimide.

There are a plethora of fluorophores that the experimenter can choose from. Fluorescence is intensely sensitive to the environment. Thus, the predominant criterion in

selecting a fluorophore is finding one that is sensitive to the presence of the protein when bound to the substrate. We have investigated two different fluorophores that react in completely opposite ways. First, we have used Fluorescein-maleimide to fluorescently label our peptides. Polypeptide substrates that contain fluorescein exhibit a fluorescence quenching of the fluorescein when ClpA is bound to the polypeptide substrate. Thus, a distinct fluorescence enhancement is observed when pre-bound ClpA either dissociates from the substrate or translocates the substrate and subsequently dissociates. In contrast, the identical substrates labeled with Cy3-maleimide exhibit a fluorescence enhancement when ClpA is bound and a loss of signal upon ClpA dissociation.

The dependence of the observed kinetics on substrate length is essential for any experimental design that is aimed at determining the molecular mechanism for a translocating enzyme (see Section 3). With this in mind a series of substrates that ranged in length from the 11 AA SsrA sequence up to 50 AA were synthesized. As can be seen in Table I, the carboxy-terminus always contains the 11 AA SsrA binding sequence. From the SsrA sequence the substrate is extended at the amino-terminus. The rationale for this substrate design, for ClpA, is that we anticipate that it will translocate from the carboxy terminal binding site to the amino-terminus based on previous work performed with ClpAP.<sup>9</sup> However, we will discuss a method for examining directionality (See determination of directionality below).

#### *Enzyme Trap*

As discussed above and shown in Figure 1, a trap for free enzyme is included to maintain single turnover conditions. As mentioned, the trap serves to insure that rebinding of the enzyme to the fluorescently modified substrate cannot occur. The 11 AA

SsrA peptide is a logical choice for a trap for ClpA since the enzyme binds specifically to this substrate. However, in principle, any substrate that would efficiently compete for binding with the fluorescently modified substrates presented in Table 1 could serve as a trap. For example, one could always use a 100-fold excess of the sequence contained within the fluorescently modified substrate, but without the fluorophore. In this scenario, it could be assumed that, at most, only 1% rebinding could occur. In our case, the polypeptide substrates contain a cysteine that would be reactive and this would not be a practical choice. Moreover, synthetic polypeptide substrates become inordinately expensive as the length is increased. Thus, to use any polypeptide substrate above 20 amino acids as a trap would not be a practical choice.

Single turnover experiments performed to examine single stranded DNA translocation and double stranded DNA unwinding catalyzed by DNA helicases have employed heparin as a trap.<sup>17; 19</sup> Heparin is a long polyanion and is, therefore, a good mimic of single stranded DNA. Because ClpA binds to a heparin column during protein purification, we attempted to use heparin as a trap. However, at the highest concentrations achievable, heparin does not efficiently compete for ClpA binding.

The obligatory rapid-mixing kinetic experiment that is performed to test for adequate trapping is shown in Figure 2. The schematic representation shown in Figure 2 is essentially identical to the standard translocation experiment shown in Figure 1. In the standard translocation experiment shown in Figure 1, the enzyme at concentration 'x' is prebound to the substrate at concentration 'y'. This complex is rapidly mixed with ATP and trap. The question to be answered is; what concentration of trap is required to inhibit the 'x' concentration of enzyme from binding to the 'y' concentration of substrate when

the enzyme encounters the substrate in an excess concentration of enzyme trap? To answer this question one only need move the 'y' concentration of fluorescently modified substrate into Syringe 2, where ATP and 'z' concentration of trap is present. The two reactants in Figure 2 can then be rapidly mixed at various concentrations of trap until no signal change is observed. At the concentration of trap where no signal change is observed, there can be no rebinding of the substrate by the enzyme at these concentrations of trap, substrate, and enzyme. Once established the standard translocation experiment illustrated in Figure 1 can be performed at the determined concentration of trap. In our examination of ClpA we found that a final mixing concentration of 100  $\mu$ M SsrA substrate is sufficient for inhibiting 500 nM ClpA monomer from binding 50 nM fluorescently modified substrate.

### **Application of the Sequential *n*-step Mechanism**

The ClpA polypeptide translocase binds specifically to the carboxy terminus of the model substrates presented in Table 1. Since ClpA requires nucleoside triphosphate binding to assemble into a hexamer with polypeptide binding activity, ATP $\gamma$ S is included in Syringe 1 to preassemble and bind ClpA to the model substrate. The single-turnover polypeptide translocation experiment illustrated by Figure 1 is performed by preincubating ClpA with each of the model substrates in Table 1 and subsequently rapidly mixing with ATP and enzyme trap. When this experiment is done, a distinct lag in the fluorescence signal is observed.

The presence of the observed lag phase followed by a fluorescence increase indicates that the fluorescence remains constant upon rapid mixing with ATP and trap for

a period of time followed by enzyme dissociation, see Fig. 3. In order to observe a lag phase under single turnover conditions the enzyme must cycle through at least two steps with similar rate constants before dissociation. Although counter intuitive, a lag phase will not be observed due to a single slow step. Rather, a single slow step will be described by a single exponential function that intersects the origin.

### *Application of Scheme 1*

The simplest model that will give rise to a lag phase that incorporates the experimental design described above and illustrated in Fig. 1 is given by Scheme 1. In Scheme 1,  $E$  denotes the enzyme and  $P$  denotes the peptide substrate. Thus,  $(E \bullet P)_L$  denotes the prebound enzyme-peptide complex with substrate of length,  $L$ , that would be present in Syringe 1, see Figure 1. Upon rapid mixing with ATP, the enzyme will proceed through a translocation step with rate constant  $k_T$  to form the first intermediate,  $I_{(L-m)}$ , where  $L$  is the substrate length and  $m$  is the step-size (amino acids translocated per step). The enzyme will cycle through  $n$  steps with rate constant  $k_T$  until reaching the end and releasing the unchanged peptide substrate.

Many events must occur for every step that the enzyme translocates forward. At a minimum this would include ATP binding, hydrolysis, mechanical movement, various conformational changes and ADP + P<sub>i</sub> release. The mechanism presented in Scheme 1 assumes that a single step within each repeating cycle is rate-limiting. Thus, each step in Scheme 1 is considered to be the same. In the upcoming sections we will present a method for testing this assumption.

To either model experimental time courses or simulate the behavior of the various models, the first task is to determine an equation that describes the fraction of peptide released as a function of time,  $f_p(t)$ , defined by Eq. (1).

$$f_p(t) = \frac{P(t)}{(E \cdot P)_0} \quad (1)$$

Where  $(E \cdot P)_0$  is the concentration of enzyme peptide complex at  $t = 0$ , and  $P(t)$  is the concentration of peptide released as a function of time. The system of coupled differential equations that results from Scheme 1 is solved using the Laplace transform method as previously described.<sup>20</sup> The strength of using this method is that it reduces the system of coupled differential equations to a system of coupled algebraic equations that can be solved using matrix methods. Moreover, the resulting Laplace transform of  $f_p(t)$  is a continuous function of the number of steps,  $n$ , and is given by Eq. (2).

$$\mathcal{L}f_p(t) = F_p(s) \quad (2)$$

Where,  $\mathcal{L}$  is the Laplace transform operator, and  $F_p(s)$  is the Laplace transform of  $f_p(t)$ . For Scheme 1, the resulting Laplace transform of the fraction of peptide released as a function of time,  $f_p(t)$ , is given by Eq. (3).

$$F_p(s) = \frac{k_t^n}{s(k_t + s)^n} \quad (3)$$

where  $s$  is the Laplace variable. In order to analyze experimental time-courses one must determine  $f_p(t)$ , which is accomplished by finding the inverse Laplace transform of  $F_p(s)$  as described by Eq. (4).

$$\mathcal{L}^{-1}F_p(s) = f_p(t) \quad (4)$$

Where  $\mathcal{L}^{-1}$  is the inverse Laplace transform operator. Traditionally, the inverse Laplace transform can be found by consulting tables of Laplace transforms. However, these tables are also present in most modern symbolic mathematics software packages such as Mathematica, Maple, MathCad, etc.

Although for Scheme 1 a closed form expression of  $f_p(t)$  is easily found using Eqs. (3) and (4) and has been reported previously<sup>20</sup> a solution is not possible for most Schemes. Thus, for the analysis of experimental time courses or to simulate time-courses, we numerically solve Eq. (4). For example, experimental time-courses were simulated by combining Eqs. (3) and (4) for Scheme 1 with  $k_T = 1.67 \text{ s}^{-1}$  and  $n = 1 - 5$ , see Figure 4. As seen in Figure 4, for one step,  $n = 1$ , a time course that can be described by a single exponential function is observed. However, as the number of steps,  $n$ , increases the extent of the lag increases. Thus, Scheme 1 adequately describes a lag phase that increases with increasing numbers of steps.

Although Scheme 1 fulfills the requirement of describing an increasing lag phase with increasing numbers of steps, it does not adequately describe the shape of the curves that are experimentally observed. As seen in Figure 3 for ClpA catalyzed polypeptide translocation, the time courses clearly exhibit biphasic kinetics. That is to say, there is a

rapid phase that is complete in  $\sim 5$  s followed by a slow second phase that is complete in greater than 100 s. Since the signal is only sensitive to enzyme that was bound at time zero, the simplest explanation for biphasic kinetics is that there are two conformations of enzyme bound at time-zero. Scheme 2 describes a scenario where the enzyme peptide complex can exist in a non-productive conformation,  $(E \cdot P)_{NP}$ , that must proceed through a slow isomerization step with rate constant  $k_{NP}$  to form the productive complex,  $(E \cdot P)_L$ , that can immediately initiate translocation.

### *Scheme 2 Biphasic Kinetics*

Using the same Laplace transform approach described above, we derived an equation for  $F_p(s)$  for Scheme 2, Eq. (5).

$$F_p(s) = \frac{k_t^n (k_{NP} + sx)}{s(k_t + s)^n (k_{NP} + s)} \quad (5)$$

Where  $x$  is defined as the fraction of productively bound complexes, which is given by Eq. (6).

$$x = \frac{[(E \cdot P)_L]}{[(E \cdot P)_L] + [(E \cdot P)_{NP}]} \quad (6)$$

Fig. 5 a shows simulations using Scheme 2 (Eqs. (4) and (5)) with  $k_T = 1.67 \text{ s}^{-1}$ ,  $k_{NP} = 0.167 \text{ s}^{-1}$ ,  $x = 0.5$ , and  $n = 1 - 5$ . By comparing Fig. 4 to Fig 5 a it can be seen that the time courses simulated using Scheme 2 (Fig. 5 a) clearly exhibit biphasic kinetics in contrast to the time courses simulated from Scheme 1 (Fig. 4), which exhibit only a

single phase. Thus, Scheme 2 adequately describes the macroscopic features of the experimental time courses shown in Fig. 3, i.e. lag phase exhibiting biphasic kinetics.

Fig. 5 b is a series of simulations that were performed using Scheme 2 (Eqs. (4) and (5)) with  $k_T = 1.67 \text{ s}^{-1}$ ,  $k_{NP} = 0.167 \text{ s}^{-1}$ , and  $n = 5$ , with varying values of the fraction of productively bound complexes. The simulations show the effect that the various values of  $x$  have on the shape of the kinetic time courses. When the fraction of productively bound complexes,  $x$ , is equal to unity, the time course is identical to the time course in Fig. 4 for  $n = 5$ . This is the expected result since when  $x = 1$  all of the complexes initiate from the productively bound state and Scheme 2 collapses to Scheme 1. This can also be observed by recognizing that once  $x$  is set to 1 in Eq.(5), which is the Laplace transform of the time dependent equation describing peptide release for Scheme 2, Eq.(5) simplifies to Eq.(3), which is the Laplace transform of the time dependent equation describing peptide release for Scheme 1.

In contrast to Fig. 5 b, Fig. 5 c shows a series of simulations for peptide release from Scheme 2 (Eqs. (4) and (5)) with  $k_T = 1.67 \text{ s}^{-1}$ ,  $x = 0.5$ , and  $n = 5$ , with varying values of  $k_{NP}$ . What is observed is that when  $k_{NP}$  is faster than  $k_T$ , then the time course is identical to the time course simulated from the simplest model, Scheme 1, Fig. 4  $n = 5$ . This makes sense because the limit as  $k_{NP}$  goes to infinity of Eq. (5) is Eq. (3), which describes Scheme 1, see Eq. (7).

$$\lim_{k_{NP} \rightarrow \infty} \frac{k_t^n (k_{NP} + sx)}{s(k_t + s)^n (k_{NP} + s)} = \frac{k_t^n}{s(k_t + s)^n} \quad (7)$$

However, when  $k_{NP}$  is slower than  $k_T$  a second slower phase is clearly apparent. Finally, when  $k_{NP} = 0$ , the fraction of productively bound complexes becomes little more than an amplitude term. This can be seen mathematically by taking the limit of Eq. (5) as  $k_{NP}$  goes to zero.

$$\lim_{k_{NP} \rightarrow 0} \frac{k_t^n (k_{NP} + sx)}{s(k_t + s)^n (k_{NP} + s)} = \frac{k_t^n x}{s(k_t + s)^n} = x \frac{k_t^n}{s(k_t + s)^n} \quad (8)$$

Where  $x$  in Eq. (8) is a constant and thus is treated as a scalar multiplier of Eq. (3). That is to say, when the Inverse Laplace transform of the result in Eq (8) is determined the constant,  $x$ , is moved out in front of the operator as shown in Eq. (9).

$$\mathcal{L}^{-1} F_p(s) = \mathcal{L}^{-1} x \frac{k_t^n}{s(k_t + s)^n} = x \mathcal{L}^{-1} \frac{k_t^n}{s(k_t + s)^n} = x f_p(t) \quad (9)$$

This can be seen, graphically, in Fig. 5 c. In Fig. 5 c when  $x = 0.5$  and  $k_{NP} = 0$  the time course is scaled down from 1 to 0.5. Thus, at these limits, Scheme 2 describes a scenario where some fraction of enzyme binds but never initiates translocation when.

In summary, both Scheme 1 and Scheme 2 have been introduced and discussed previously.<sup>20</sup> In fact Scheme 2 has been used extensively to model helicases catalyzed DNA unwinding since biphasic kinetics, to our knowledge, have always been observed in single turnover DNA unwinding experiments.<sup>13; 14; 21</sup> Although the molecular explanation for why a second phase is observed in these experiments is not clear, it is interesting that polypeptide translocases and helicases both exhibit such kinetic behavior.

### Scheme 3 Finite Processivity

The fluorescence stopped-flow method that we have developed and applied to polypeptide translocases is sensitive to the dissociation of the motor from the linear lattice. For example, when ClpA is bound to the fluorescently modified peptide substrate containing fluorescein there is a fluorescence quenching. Upon rapidly mixing with ATP and enzyme trap an increase in fluorescence is observed upon dissociation. To describe this, we introduce Scheme 3 that includes a dissociation step with rate constant  $k_d$  at each intermediate. Because signal is observed at each intermediate dissociation step, the equation that describes product formation is substantially more complicated. That is to say, the equation,  $F_p(s)$ , for Scheme 3 has a contribution from dissociation at each step as well as dissociation from the end. The Laplace transform of  $f_p(t)$  for Scheme 3 is given by Eq. (10).

$$F_p(s) = \frac{\left( k_t^n (k_d + k_t)(k_d + s) + k_d (k_d + k_t + s)^n \left( k_t - \left( \frac{k_t}{k_d + k_t + s} \right)^n (k_d + k_t + s) \right) \right) (k_{np} + sx)}{sk_t (k_d + s)(k_{np} + s)(k_d + k_t + s)^n} \quad (10)$$

Equation (10) collapses to Eq.(5), which describes the Laplace transform of  $f_p(t)$  for Scheme 2, as the  $k_d$  approaches 0, see Eq. (11).

$$\lim_{k_d \rightarrow 0} \frac{\left( k_t^n (k_d + k_t)(k_d + s) + k_d (k_d + k_t + s)^n \left( k_t - \left( \frac{k_t}{k_d + k_t + s} \right)^n (k_d + k_t + s) \right) \right) (k_{np} + sx)}{sk_t (k_d + s)(k_{np} + s)(k_d + k_t + s)^n} = \frac{k_t^n (k_{NP} + sx)}{s(k_t + s)^n (k_{NP} + s)} \quad (11)$$

Thus, there is continuum of models from Scheme 3 to Scheme 1. That is to say, when  $k_d = 0$  in Eq. (10) (Scheme 3) collapses to Eq. (5) (Scheme 2). When  $x = 1$ , which says that

no enzyme binds in a nonproductive fashion, Eq. (5) (Scheme 2) collapses to Eq. (3) (Scheme 1).

By numerically solving  $F_p(s)$  for Scheme 3 (Eqs. (4) and (10)) we simulated a series of time courses with  $k_T = 1.67 \text{ s}^{-1}$ ,  $n = 5$ , and varying values of  $k_d$ . As can be seen in Fig. 6, since complete dissociation is being monitored all of the simulated time courses proceed to unity, i.e. eventually everything dissociates. As expected, when  $k_d = 0$  the time course is equivalent to the time course simulated from Scheme 1 with  $k_T = 1.67 \text{ s}^{-1}$  and  $n = 5$ , compare Fig. 1  $n = 5$  to Fig. 6  $k_d = 0$  and  $n = 5$ . Strikingly, when  $k_d = 0.08 \text{ s}^{-1}$  the lag no longer has zero slope as it does for  $k_d = 0$ , but has positive slope. Likewise, if  $k_d$  is increased to  $0.17 \text{ s}^{-1}$  then the slope in the lag region is further increased. Finally, if  $k_d$  is increased to  $0.25 \text{ s}^{-1}$  there is little ability to determine if there is any change in slope from the lag region to the rapid increase in signal. In fact, with the introduction of experimental error one would not be able to discern the presence or absence of a lag. It should be noted that the disappearance of the lag at  $k_d = 0.25 \text{ s}^{-1}$  is relative to  $k_T = 1.67 \text{ s}^{-1}$ , which likely suggests that a discernable lag can only be observed if  $k_d < \sim 0.15 k_T$ .

With a measurement of the dissociation rate constant,  $k_d$ , a measure of the processivity of the enzyme is possible. The processivity,  $P_r$ , is defined as the probability that the enzyme will either proceed through the next step or dissociate and is defined by Eq. (12).

$$P_r = \frac{k_T}{k_T + k_d} \quad (12)$$

It can be easily seen from Eq.(12) that when  $k_d = 0$  the processivity,  $P_r = 1$ , and this describes an infinitely processive enzyme, were every enzyme that binds fully translocates the substrate. In contrast, when  $k_d$  is finite  $P_r$  varies between 0 and 1 and describes finite processivity.

Interestingly, as stated above, in order to observe a lag phase for Scheme 3,  $k_d$  must be less than approximately  $0.15 k_T$ . By making this substitution into Eq. (12) a  $P_r = 0.87$  results. This shows that the simple observation of a lag phase in the kinetic time course qualitatively suggests a minimum processivity of  $\sim 0.87$ , although the processivity may be much higher.

#### *Determination of Kinetic Step-size*

The kinetic step-size is defined as the average number of amino acids translocated per rate-limiting step. It is important to note that others have defined the step-size as the number of ATP molecules hydrolyzed per catalytic cycle. However, we define the number of ATP molecules hydrolyzed per catalytic cycle as the coupling efficiency and, here, the step-size will always be referred to as the number of amino acids translocated per step. To determine the kinetic step-size,  $m$  (average number of amino acids translocated between two rate-limiting steps), the dependence of the observed number of steps,  $n$ , on substrate length is examined. This is accomplished by subjecting the time-courses to nonlinear-least-squares analysis using the models discussed.

Graphically, the information on the number of steps required to translocate a given substrate is contained within the extent of the lag. That is to say, as the enzyme proceeds through more steps a longer lag in the kinetic time course is expected. Single-

turnover polypeptide translocation experiments are performed on multiple substrates that differ in length to determine if the extent of the lag increases with increasing length of substrate. In the case of ClpA, a distinct increase in the extent of the lag with increasing substrate length is observed. To determine the kinetic step-size,  $m$ , the relationship between the number of steps to describe each time course,  $n$ , and substrate length,  $L$ , must be determined. To do this, one must always collect time courses for multiple substrates since the number of steps,  $n$ , and the translocation rate constant,  $k_T$ , are highly correlated. Thus it would be impossible to have confidence in values of  $k_T$  and  $n$  or  $m$  if determined from a single time course collected for a single substrate of a given length,  $L$ . Therefore, the best way to determine a unique value for both of these parameters is through global nonlinear least squares analysis of a series of time courses collected for different lengths of substrates.

Upon collecting a series of time courses for various substrate lengths the first diagnostic examination of the data is done by subjecting the data to NLLS analysis using Scheme 1 if no second phase is present or Scheme 2 if a second phase is present. The inherent assumption that is made in doing this is that the observed steps all have the same rate constant. This analysis is done by first assuming that  $k_T$  is the same for all lengths, but each length is described by a different number of steps,  $n$ , with rate constant  $k_T$ . That is to say,  $k_T$  is a global parameter and  $n$  is a local parameter.

Figure 7 shows a series of time courses collected for the 30, 40 and 50 amino acid substrates with Fluorescein attached to the carboxy terminus, shown in Table 1. The solid lines are the result of a global NLLS analysis using Scheme 2, where the rate constants  $k_T$  and  $k_{NP}$  are constrained to be the same for all lengths and  $n$  is a local parameter for each

length. Figure 7 d shows a plot of the number of steps to describe each time course vs. substrate length,  $L$ . If all of the observed rate limiting steps are the same then a plot of  $n$  vs.  $L$  should be linear with a zero intercept. That is to say, the observed number of steps should be related to substrate length by the equation  $n = L / m$ , where  $m$  is the kinetic step-size (average number of amino acids translocated between two rate-limiting steps). However, as can be seen in Figure 7 c, a positive y-intercept is observed. Thus, the simple linear equation,  $n = L / m$ , does not apply and a better description is  $n = L / m + b$ , where  $b$  describes an intercept term.

Qualitatively, the  $n$  vs.  $L$  plot shown in Fig. 7 c suggests that at a length of  $L = 0$  there are still some number of steps taken by the enzyme. As we have shown previously, the observation of a positive y-intercept in an  $n$  vs.  $L$  plot is a diagnostic observation indicating that there are additional steps not equal to  $k_T$ . To describe this, we introduce Scheme 4, which includes an additional step with rate constant  $k_C$ . The equation that describes the Laplace transform of product formation as a function of time,  $f_p(t)$ , is given by Eq. (13),

$$F_p(s) = \frac{\left( k_c^h k_i^n (k_d + k_i)(k_d + s) + k_d (k_d + k_i + s)^n (-k_i)(k_c + k_d + s)^h \left( \left( \frac{k_c}{k_c + k_d + s} \right)^h - 1 \right) + k_c^h \left( k_i - \left( \frac{k_i}{k_d + k_i + s} \right)^n (k_d + k_i + s) \right) \right) (k_{np} + sx)}{sk_i(k_d + s)(k_{np} + s)(k_c + k_d + s)^h (k_d + k_i + s)^n} \quad (13)$$

where  $h$  is the number of steps with rate constant  $k_C$ . Strictly speaking, the Laplace transform of the equation that describes product formation as a function of time for Scheme 4 would have  $h = 1$ . However, we have derived Eq.(13) such that it can accommodate  $h$  number of steps with rate constant  $k_C$ . Thus, Eq. (13) represents a

function that is continuous on both the number of steps with rate constant  $k_T$ ,  $n$ , and the number of steps with rate constant  $k_C$ ,  $h$ . Although Scheme 4 contains the step with rate constant  $k_C$  at the beginning of the reaction, because of the symmetry in Eq.(13), there is no information on whether the step is at the beginning, the end, or somewhere in the middle. To say it another way, if the step with rate constant  $k_C$  is placed at any position in the reaction scheme, given by Scheme 4, upon solving the system of couple differential equations the same solution given by Eq. (13) will result.

Conveniently, Eq. (13) exhibits the expected behavior at the extremes of the parameters. Namely, Eq. (13) collapses to Eq. (10), which describes Scheme 3, when  $k_C \gg k_T$ . Therefore, as discussed above, at the appropriate limits the Laplace transform of the equation that describes product formation for Scheme 3 can be used to describe Scheme 2 and subsequently Scheme 1. Thus, all four Schemes presented here can be modeled by one equation, Eq.(13), which, in its current form, describes Scheme 4.

We simulated and analyzed a series of mock time courses to determine if time courses simulated using Scheme 4, which contains a step with rate constant  $k_C$ , and examined them using Scheme 3, which assumes all steps are the same, would yield a positive y-intercept in an  $n$  vs.  $L$  plot, as observed experimentally (see Fig. 7 D). These time courses were simulated by numerically solving Eqs. (4) and (13) with  $n = 5$ ,  $k_T = 1.67 \text{ s}^{-1}$ ,  $k_d = 0$  and various values of  $k_C$ , see Fig. 8 A. In this simulation it was assumed that all bound enzyme started in the productive state by setting  $x = 1$ . Time courses were simulated and 1 % error was introduced. The time courses were then subjected to NLLS analysis using Eqs. (4) and (10), which is the Laplace transform of  $f_p(t)$  for Scheme 3. The global NLLS analysis was performed by constraining the rate constants to be the

same for all time courses, i.e. global parameters, and the number of steps to be different for each time course, i.e. local parameters.

Figure 8 B is a plot of the number of steps to describe each time course as a function of substrate length for various values of  $k_C$ . As expected, the number of steps increases linearly with increasing substrate length. Although the plot is linear it clearly exhibits a positive y intercept and therefore cannot be described by the relationship  $n = L / m$ . This result shows that when data comes from a model with an additional slow step, Scheme 4, upon analyzing this data with a simpler model, Scheme 3, the resulting  $n$  vs.  $L$  plot will exhibit a positive y-intercept indicating the presence of the slow step.

Interestingly, the  $n$  vs.  $L$  plots that were generated for different values of  $k_C$  all result in a y-intercept that is above one, but does not exceed two. Thus, the intercept represents a qualitative predictor of the number of  $k_C$  steps. As the value of the rate constant is increased the resulting  $n$  vs.  $L$  plot becomes steeper. Thus, one cannot simply fit the line to an equation such as  $n = L / m + b$  and determine the kinetic step size,  $m$  as this would result in an underestimate. Clearly, there is some dependence of the slope on the value of the rate constant  $k_C$ . Finally, once the value of  $k_C$  exceeds that of  $k_T$ , the  $n$  vs.  $L$  plot again intersects the origin. In summary, the  $n$  vs.  $L$  plot should be used as a diagnostic plot to determine what model may better describe the experimental data.

Simulations were performed to determine the dependence of the y-intercept in the  $n$  vs.  $L$  plot on the number of steps with rate constant  $k_C$ ,  $h$ . Time courses were simulated using Eqs. (4) and (13) by replacing  $n$  with  $L / m$ , and  $m = 10$  AA step<sup>-1</sup>,  $L = 30, 40$ , and  $50$  AA with  $k_T = 1.67$  s<sup>-1</sup>,  $k_d = 0$ ,  $k_C = 0.08$  s<sup>-1</sup>, and  $h$  equal to integer values between 0

and 4. Representative time courses with 1 % random error introduced are shown in Fig. 8 C. In this simulation, for simplicity, it was again assumed that all bound enzyme started in the productive state by setting  $x = 1$ . As expected, when  $h = 0$  the line describing the data points intersects the origin. In all other cases, with  $h > 0$ , the intercept always exhibits a value that exceeds the number of steps with rate constant  $k_C$ ,  $h$ . However, the intercept never exceeds the true value of  $h$  by a whole integer value, reiterating the conclusion that the intercept may serve as a qualitative estimate of the number of steps with rate constant  $k_C$ .

#### *Application of Scheme 4 to ClpA Catalyzed Polypeptide Translocation*

The time courses shown in Figure 7 were initially analyzed using Eq. (10) that describes the Laplace transform of  $f_p(t)$  for Scheme 3. All attempts to float the value of  $k_d$  resulted in  $k_d$  floating to an infinitely small number. Thus, we concluded that, on such short substrates, no appreciable dissociation was occurring until the enzyme full translocates the substrate. This conclusion is not only drawn from the NLLS analysis but also from simple inspection of the curves. If one compares the experimental time courses shown in Fig. 7 to the simulated time-courses shown in Fig. 6 that were generated from Eq. (10) that includes  $k_d$ , it is immediately obvious that the experimental time courses do not exhibit any measurable slope in the lag region.

The experimental time courses shown in Figure 7 were analyzed using Eq. (11) that describes the Laplace transform of  $f_p(t)$  for Scheme 4. Multiple observations led to applying Scheme 4 to the experimental time courses. First, we observe biphasic kinetics and thus we must incorporate  $k_{NP}$ . Second, the n vs. L plot generated from the analysis of

the experimental time courses exhibit a positive y-intercept slightly above one. This observation indicates that there is at least one additional step not involved in polypeptide translocation. Third, the data do not require a significant dissociation rate constant to be described adequately.

The first strategy in the analysis of the experimental time courses was to analyze the kinetic time courses using Scheme 4 but allowing the number steps,  $n$ , to float for each time course. Upon doing this, the  $n$  vs.  $L$  plot could again be constructed by removing the contribution from the additional step with rate constant  $k_C$ . Strikingly, the positive y-intercept vanishes and an x-intercept is observed. Empirically, we take the observation that the line intersects the x-axis to mean that some number of amino acids in the substrate are in contact with the enzyme and are not translocated. That is to say, the enzyme does not bind at the extreme end of the carboxy-terminus and translocate the full substrate. Rather, in the case of ClpA, it is in contact with the eleven amino acid SsrA sequence. Thus, the actual length of substrate being translocated is  $L - d$ , where  $d$  is the contact site size. Therefore, the number of steps,  $n$ , is replaced with  $n = (L - d) / m$ .

Upon incorporating the relationship of the number of steps to the substrate length, i.e.  $n = (L - d) / m$ , the data were globally analyzed using Scheme 4. The resultant parameters are  $k_T = (1.45 \pm 0.05) \text{ s}^{-1}$ ,  $k_C = (0.210 \pm 0.003) \text{ s}^{-1}$ ,  $k_{NP} = (0.0455 \pm 0.0005) \text{ s}^{-1}$ ,  $k_d = 0$ ,  $m = (12.6 \pm 0.5) \text{ AA step}^{-1}$ , and  $d = (11.7 \pm 0.4) \text{ AA}$ . The product of the kinetic step-size,  $m$ , and the translocation rate constant,  $k_T$ , yields the macroscopic rate of polypeptide translocation and from this analysis is  $mk_T = (18.2 \pm 1.3) \text{ AA s}^{-1}$  at saturating ATP concentrations and 25 °C.

### *Determination of Translocation Directionality*

To examine translocation directionality the dependence of the observed signal on the position of the fluorophore is tested. For ClpA catalyzed polypeptide translocation, we observed a distinct lag phase when the Fluorophore is placed at the amino-terminus and the SsrA binding sight is at the carboxy-terminus. However, when the fluorophore is placed at the carboxy-terminus, see C-Cys-30 and C-Cys-40 in Table I, no lag is observed. In fact, not only is a lag not observed, but the time courses are identical.<sup>10</sup> This indicates that all of the enzymes are translocating away from the fluorophore and thus an immediate change in the signal is observed with no lag time.

### **Concluding Remarks**

We have developed a novel method to examine the molecular mechanism of polypeptide translocation catalyzed by polypeptide translocases. Two major advances are summarized here and reported previously.<sup>10</sup> First, we have developed an experimental strategy to perform fluorescence stopped flow experiments to examine a single turnover of polypeptide translocation catalyzed by ClpA. Second, we describe a method to quantitatively analyzing the experimental data by applying sequential  $n$ -step kinetic models.

Polypeptide translocases or protein unfoldases, such as ClpA, are often associated with a proteolytic component, like ClpP. For example, the 26 S proteasome is composed of a motor component termed the 19 S cap and a proteolytic component termed the 20 S core.<sup>22; 23</sup> These motor proteins, like ClpA, likely employ a similar mechanism to translocate a ubiquitinilated protein into the proteolytic cavity for degradation. Because

these motor components are often associated with a protease the observation of proteolytic fragments has often been used to infer information on the activities of the motor component. With the development of the method presented here, we are able to acquire information on the translocation of a polypeptide substrate without the need for covalent modification of the substrate. This will allow us to answer a variety of fundamental questions regarding the molecular mechanism. For example, does the proteolytic component exert allosteric control over the motor component? That is to say, is the mechanism employed by the motor alone the same as the mechanism employed when associated with the protease. Preliminary observations have suggested that the rate for ClpA alone is different than that of ClpAP.

Equally important, ClpB is a protein unfoldase with high homology to ClpA. However, ClpB does not associate with any known protease. In contrast to ClpA, ClpB disaggregates protein aggregates *in vivo* and, in collaboration with DnaK, resolubilizes protein aggregates.<sup>24; 25</sup> However, because the enzyme does not covalently modify the substrate it translocates, little detail on the molecular mechanism of polypeptide translocation catalyzed by ClpB is available. This is underscored in a recent report where multiple mutations were made in ClpB to force it to interact with the protease ClpP so that proteolytic degradation could be used to monitor the activities of ClpB.<sup>26</sup> However, with the approach presented here, we may be able to shine new light on the mechanism of ClpB catalyzed polypeptide translocation.

**Acknowledgements** This work was supported by NSF grant MCB-0843746 to ALL.

## References

1. Vale, R. D. & Fletterick, R. J. (1997). The design plan of kinesin motors. *Annu Rev Cell Dev Biol* **13**, 745-77.
2. Howard, J., Hudspeth, A. J. & Vale, R. D. (1989). Movement of microtubules by single kinesin molecules. *Nature* **342**, 154-8.
3. Block, S. M., Goldstein, L. S. & Schnapp, B. J. (1990). Bead movement by single kinesin molecules studied with optical tweezers. *Nature* **348**, 348-52.
4. Kornberg, A. & Baker, T. A. (1992). *DNA replication*. 2nd edit, W.H. Freeman, New York.
5. Lohman, T. M. & Bjornson, K. P. (1996). Mechanisms of helicase-catalyzed DNA unwinding. *Annu Rev Biochem* **65**, 169-214.
6. Matson, S. W. & Kaiser-Rogers, K. A. (1990). DNA helicases. *Annu Rev Biochem* **59**, 289-329.
7. Pyle, A. M. (2008). Translocation and unwinding mechanisms of RNA and DNA helicases. *Annu Rev Biophys* **37**, 317-36.
8. Lohman, T. M., Tomko, E. J. & Wu, C. G. (2008). Non-hexameric DNA helicases and translocases: mechanisms and regulation. *Nat Rev Mol Cell Biol* **9**, 391-401.
9. Reid, B. G., Fenton, W. A., Horwich, A. L. & Weber-Ban, E. U. (2001). ClpA mediates directional translocation of substrate proteins into the ClpP protease. *Proc Natl Acad Sci U S A* **98**, 3768-72.
10. Rajendar, B. & Lucius, A. L. (2010). Molecular mechanism of polypeptide translocation catalyzed by the Escherichia coli ClpA protein translocase. *J Mol Biol* **399**, 665-79.
11. Hoskins, J. R., Singh, S. K., Maurizi, M. R. & Wickner, S. (2000). Protein binding and unfolding by the chaperone ClpA and degradation by the protease ClpAP. *Proc Natl Acad Sci U S A* **97**, 8892-7.

12. Kim, Y. I., Burton, R. E., Burton, B. M., Sauer, R. T. & Baker, T. A. (2000). Dynamics of substrate denaturation and translocation by the ClpXP degradation machine. *Mol Cell* **5**, 639-48.
13. Ali, J. A. & Lohman, T. M. (1997). Kinetic measurement of the step size of DNA unwinding by Escherichia coli UvrD helicase. *Science* **275**, 377-80.
14. Jankowsky, E., Gross, C. H., Shuman, S. & Pyle, A. M. (2000). The DExH protein NPH-II is a processive and directional motor for unwinding RNA. *Nature* **403**, 447-51.
15. Svoboda, K., Schmidt, C. F., Schnapp, B. J. & Block, S. M. (1993). Direct observation of kinesin stepping by optical trapping interferometry. *Nature* **365**, 721-7.
16. Uyeda, T. Q., Kron, S. J. & Spudich, J. A. (1990). Myosin step size. Estimation from slow sliding movement of actin over low densities of heavy meromyosin. *J Mol Biol* **214**, 699-710.
17. Fischer, C. J. & Lohman, T. M. (2004). ATP-dependent translocation of proteins along single-stranded DNA: models and methods of analysis of pre-steady state kinetics. *J Mol Biol* **344**, 1265-86.
18. Fischer, C. J., Maluf, N. K. & Lohman, T. M. (2004). Mechanism of ATP-dependent translocation of E.coli UvrD monomers along single-stranded DNA. *J Mol Biol* **344**, 1287-309.
19. Lucius, A. L., Jason Wong, C. & Lohman, T. M. (2004). Fluorescence stopped-flow studies of single turnover kinetics of E.coli RecBCD helicase-catalyzed DNA unwinding. *J Mol Biol* **339**, 731-50.
20. Lucius, A. L., Maluf, N. K., Fischer, C. J. & Lohman, T. M. (2003). General methods for analysis of sequential "n-step" kinetic mechanisms: application to single turnover kinetics of helicase-catalyzed DNA unwinding. *Biophys J* **85**, 2224-39.
21. Lucius, A. L., Vindigni, A., Gregorian, R., Ali, J. A., Taylor, A. F., Smith, G. R. & Lohman, T. M. (2002). DNA unwinding step-size of E. coli RecBCD helicase determined from single turnover chemical quenched-flow kinetic studies. *J Mol Biol* **324**, 409-28.
22. Eytan, E., Ganoth, D., Armon, T. & Hershko, A. (1989). ATP-dependent incorporation of 20S protease into the 26S complex that degrades proteins conjugated to ubiquitin. *Proc Natl Acad Sci U S A* **86**, 7751-5.

23. Hough, R., Pratt, G. & Rechsteiner, M. (1987). Purification of two high molecular weight proteases from rabbit reticulocyte lysate. *J Biol Chem* **262**, 8303-13.
24. Glover, J. R. & Lindquist, S. (1998). Hsp104, Hsp70, and Hsp40: a novel chaperone system that rescues previously aggregated proteins. *Cell* **94**, 73-82.
25. Goloubinoff, P., Mogk, A., Zvi, A. P., Tomoyasu, T. & Bukau, B. (1999). Sequential mechanism of solubilization and refolding of stable protein aggregates by a bichaperone network. *Proc Natl Acad Sci U S A* **96**, 13732-7.
26. Weibezahn, J., Tessarz, P., Schlieker, C., Zahn, R., Maglica, Z., Lee, S., Zentgraf, H., Weber-Ban, E. U., Dougan, D. A., Tsai, F. T., Mogk, A. & Bukau, B. (2004). Thermotolerance requires refolding of aggregated proteins by substrate translocation through the central pore of ClpB. *Cell* **119**, 653-65.
27. Rapoport, T. A. (2007). Protein translocation across the eukaryotic endoplasmic reticulum and bacterial plasma membranes. *Nature* **450**, 663-9.

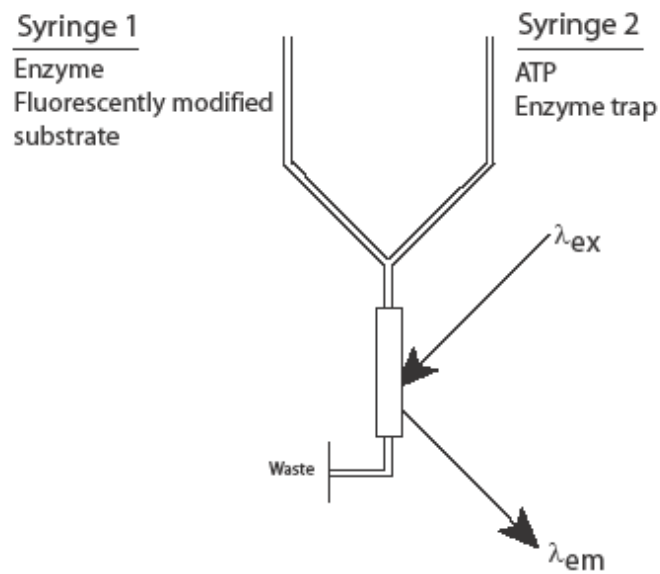


**Figure 1. Schematic Representation of Single-Turnover Stopped-Flow Experiment.** In Syringe 1 the enzyme and fluorescently modified substrate are pre-incubated. Syringe 2 contains ATP and a trap for free enzyme. The two are rapidly mixed together in the chamber, where the reactants are irradiated by light at a wavelength,  $\lambda_{ex}$  and emission is observed by a photomultiplier tube at  $\lambda_{em}$ .

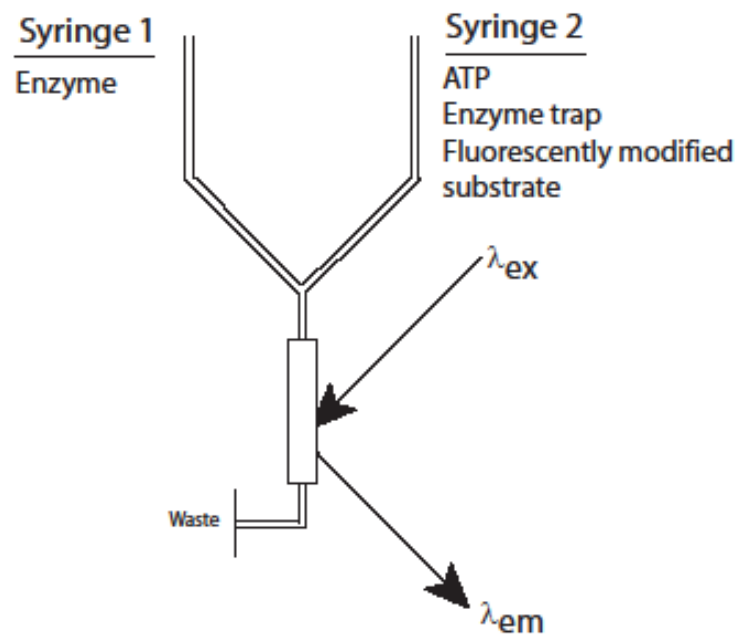


**Figure 2. Schematic Representation of “Trap-Test”.** Schematic shows the standard method for determining if the enzyme trap is effective at inhibiting binding to the substrate. The experimental design is the same as Fig. 1, with the exception that the Fluorescently modified substrate has been moved to Syringe 2. The two reactants are rapidly mixed together at increasing concentrations of enzyme trap until no signal is observed.

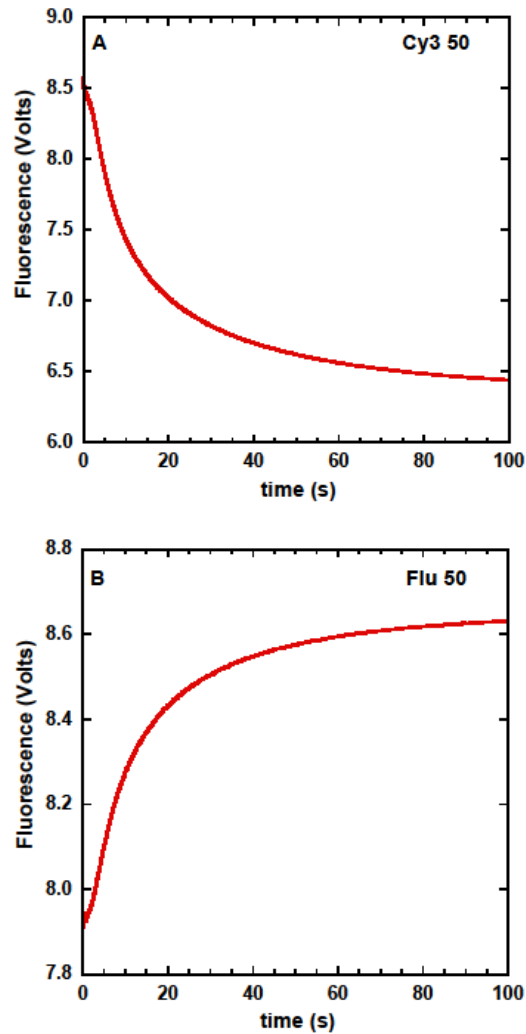


**Figure 3. Representative Time-Courses from Single-Turnover Stopped-Flow Fluorescence Experiment.** Shows a representative time course for an stopped-flow fluorescence experiment performed as shown schematically in Fig. 1 with 1  $\mu$ M ClpA, 100 nM A) Cy3-50 or B) Fluorescein-50 in Syringe 1 and rapidly mixing with 10 mM ATP and 300  $\mu$ M SsrA peptide. All concentrations are syringe concentrations and the final mixing concentration is two-fold lower.

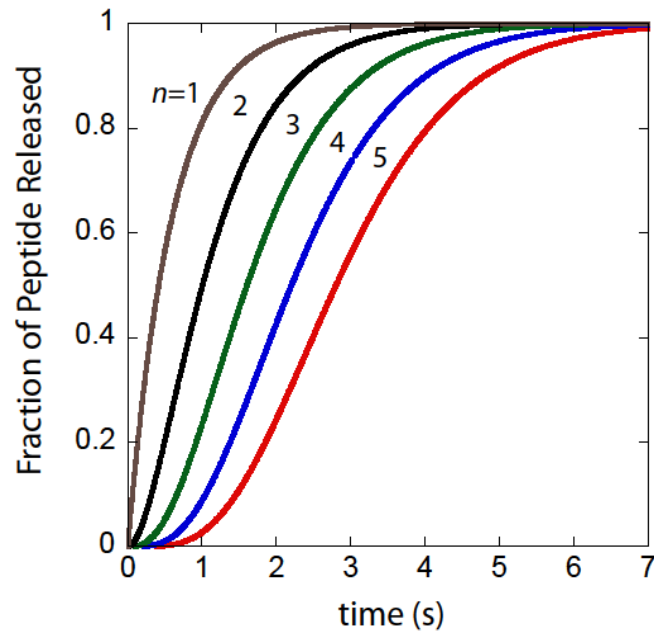


**Figure 4. Simulated Time-Courses from Scheme 1.** Simulated time courses were generated by numerically solving the inverse Laplace transform for fraction of peptide released as a function of time,  $f_p(t)$ , for Scheme 1. This was accomplished using Eqs. (4) and (3) with  $k_T = 1.67 \text{ s}^{-1}$  and  $n = 1 - 5$ . Plot illustrates an increase in the extent of the lag with increasing numbers of steps,  $n$ .

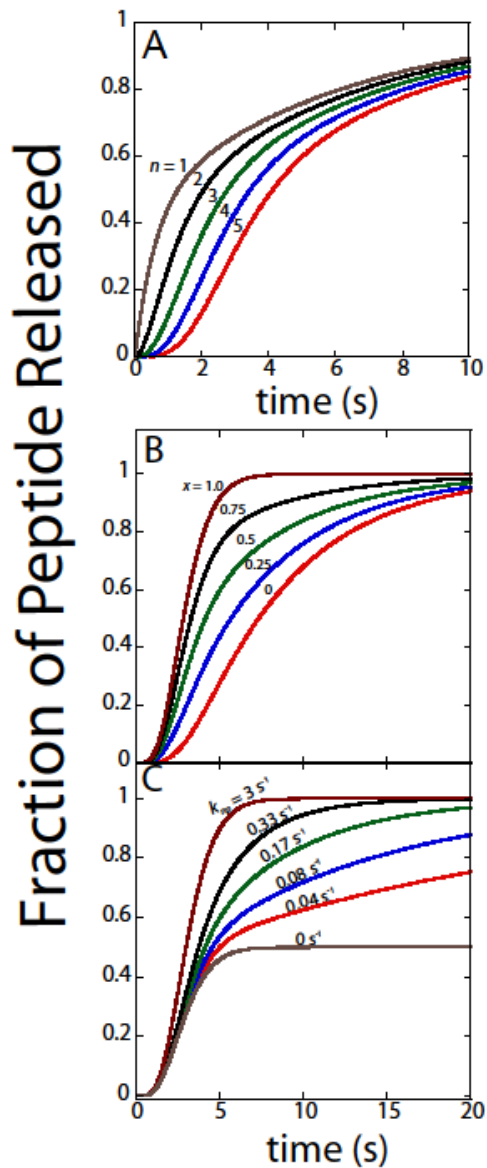


**Figure 5. Simulated Time-Courses from Scheme 2.** Simulated time courses were generated by numerically solving the inverse Laplace transform for fraction of peptide released as a function of time,  $f_p(t)$ , for Scheme 2 using Eqs. (4) and (5). A)  $k_T = 1.67 \text{ s}^{-1}$ ,  $k_{NP} = 0.167 \text{ s}^{-1}$ ,  $x = 0.5$ , and  $n = 1 - 5$ . B)  $k_T = 1.67 \text{ s}^{-1}$ ,  $k_{NP} = 0.167 \text{ s}^{-1}$ ,  $n = 5$ , and  $x = 0 - 1$ . C)  $k_T = 1.67 \text{ s}^{-1}$ ,  $x = 0.5$ ,  $n = 5$ , and  $k_{NP} = 0 - 3 \text{ s}^{-1}$ .

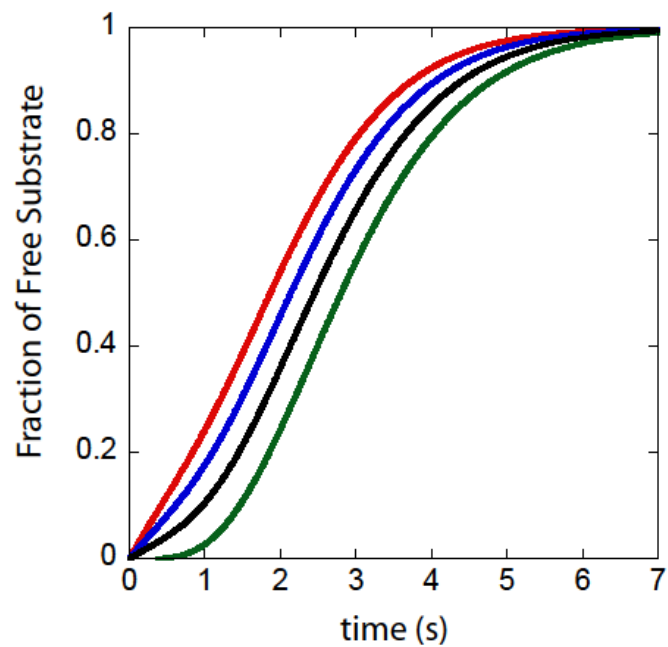


**Figure 6. Simulated Time-Courses from Scheme 3.** Simulated time courses were generated by numerically solving the inverse Laplace transform for fraction of peptide released as a function of time,  $f_p(t)$ , for Scheme 3 using Eqs. (4) and (10). Time courses were simulated with  $k_T = 1.67 \text{ s}^{-1}$ ,  $n = 5$ , and  $k_d = 0 - 0.25 \text{ s}^{-1}$ .

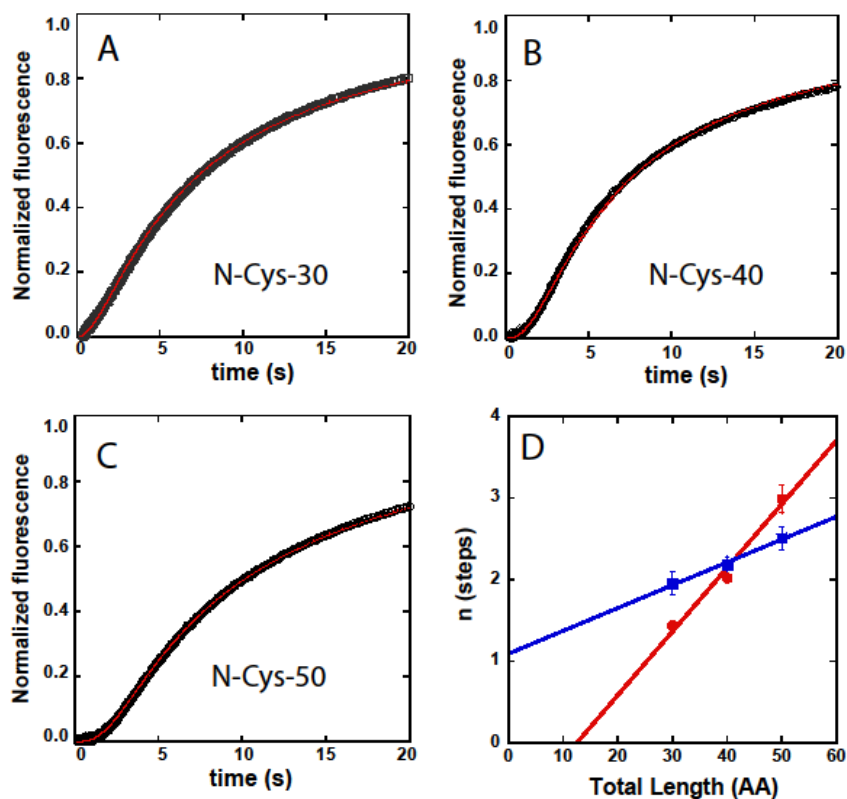


**Figure 7. Fluorescence time-courses for ClpA catalyzed polypeptide translocation.** Time-courses were collected as described in Fig. 1. A) N-Cys-30, B) N-Cys-40, C) N-Cys-50. The solid lines in panel A – C represent a global NLLS fit using Scheme 4 (Eqs. (4) and (11)) for time-courses collected with substrates I – III in Table I. The resultant parameters are  $k_T = (1.45 \pm 0.05) \text{ s}^{-1}$ ,  $k_C = (0.210 \pm 0.003) \text{ s}^{-1}$ ,  $k_{NP} = (0.0455 \pm 0.0005) \text{ s}^{-1}$ ,  $k_d = 0$ ,  $m = (12.6 \pm 0.5) \text{ AA step}^{-1}$ ,  $d = (11.7 \pm 0.4) \text{ AA}$ . D) Dependence on polypeptide length of the numbers of steps,  $n$ , determined from analysis of time-courses presented in panel b – d. Each time-course was analyzed by constraining the parameters  $k_T$ ,  $k_C$ ,  $k_{NP}$ , and  $h$  to be global parameters, while  $A_t$ ,  $x$ , and  $n$  were allowed to float for each time-course. The solid squares represent a determination of the number of steps,  $n$ , required to describe each time-course in panel A – C using Scheme 4 (Eqs. (4) and (11) with  $h = 0$ ), i.e. no slow step with rate constant,  $k_C$ . The solid line through the solid squares represents a linear least squares fit with a slope = 0.028 and intercept = 1.09. The solid circles represent the analysis using Scheme 4 (Eqs. (4) and (11) with  $h = 1$ ), i.e. one slow step with rate constant,  $k_C$ . The solid line through the solid circles represents a linear least squares fit with a slope = 0.078 and intercept = -0.973.

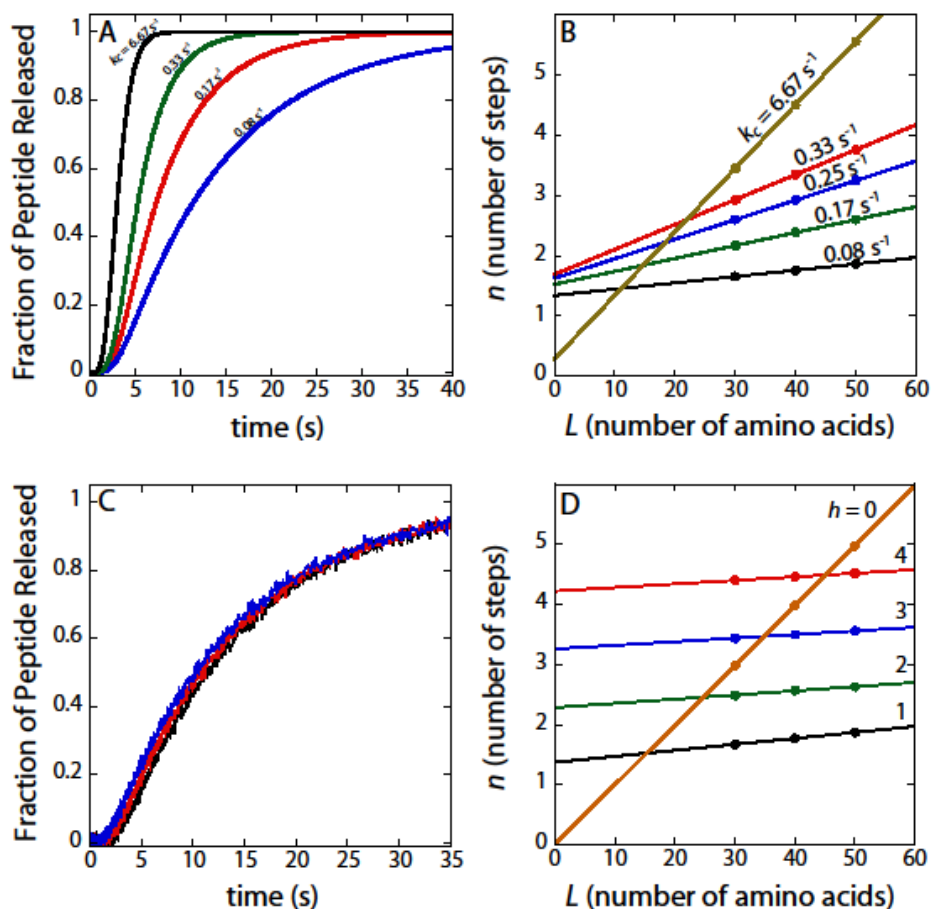
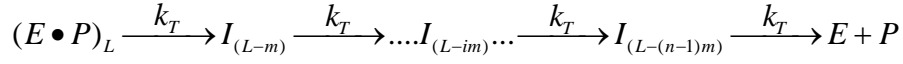


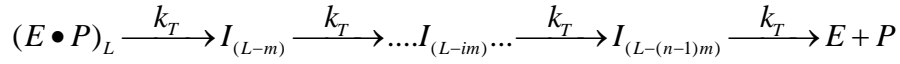
**Figure 8. Simulated Time-Courses from Scheme 4.** Simulated time courses were generated by numerically solving the inverse Laplace transform for fraction of peptide released as a function of time,  $f_p(t)$ , for Scheme 4 using Eqs. (4) and (10). Time courses in panel A were simulated with  $n = 5$ ,  $k_T = 1.67 \text{ s}^{-1}$ ,  $k_d = 0$  and various values of  $k_C$ . Simulations were performed for Scheme 4 using Eqs. (4) and (10) by replacing  $n$  with  $L/m$ , and  $m = 10 \text{ AA step}^{-1}$ ,  $L = 30, 40, \text{ and } 50 \text{ AA}$ ,  $k_T = 1.67 \text{ s}^{-1}$ ,  $k_d = 0$  and various values of  $k_C$ . Time courses were subjected to global NLLS analysis using Scheme 3 and the number of steps,  $n$ , to describe each time course was determined. B) is a plot of the dependence of  $n$  on substrate length,  $L$ . C) representative set of time courses for varying values of  $k_C = 0.08 \text{ s}^{-1}$ . D) dependence of the number of steps to describe each time course on substrate length,  $L$ , for various values of  $h$ . In all cases, the y-intercept approximates the number of steps with rate constant  $k_C$ .

## Schemes

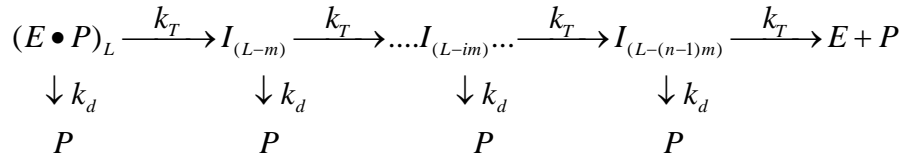
### Scheme 1



### Scheme 2



### Scheme 3



### Scheme 4

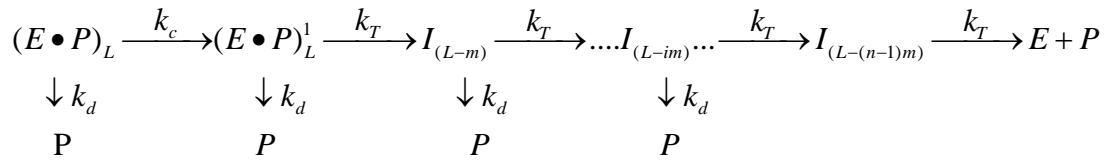


**Table 1.** Polypeptide Translocation Substrates

Substrate	Name	Length (AA)	Sequence
I	N-Cys-30	30	<b>CTKSAANLKVKELRSKKKLAA NDENYALAA</b>
II	N-Cys-40	40	<b>CTGEVSFQAANTKSAANLKVK ELRSKKKLAANDENYALAA</b>
III	N-Cys-50	50	<b>CLILHNKQLGMTGEVSFQAAN TKSAANLKVKELRSKKKLAA NDENYALAA</b>
IV	C-Cys-30	30	<b>TKSAANLKVKELRSKKKLAA NDENYALAAC</b>
V	C-Cys-40	40	<b>TGEVSFQAANTKSAANLKVKE LRSKKKLAANDENYALAAC</b>

Chapter Three

*E. coli* ClpA Catalyzed Polypeptide Translocation is Allosterically Controlled by the  
Protease ClpP

by

Justin M. Miller, Jiabei Lin, Tao Li, and Aaron L. Lucius

*Journal of Molecular Biology*

Copyright 2013

Used by permission

Format adapted for dissertation

## Abstract

There are five known ATP-dependent proteases in *Escherichia coli*, Lon, ClpAP, ClpXP, HslUV, and the membrane-associated FtsH, that catalyze the removal of both misfolded and properly folded proteins in cellular protein quality control pathways. Hexameric ClpA rings associate with one or both faces of the cylindrically-shaped tetradecameric ClpP protease. ClpA catalyzes unfolding and translocation of polypeptide substrates into the proteolytic core of ClpP for degradation through repeated cycles of ATP binding and hydrolysis at two nucleotide binding domains on each ClpA monomer. We previously reported a molecular mechanism for ClpA catalyzed polypeptide translocation in the absence of ClpP, including elementary rate constants, overall rate, and the kinetic step-size. However, the potential allosteric effect of ClpP on the mechanism of ClpA catalyzed translocation remains unclear. Using single-turnover fluorescence stopped flow methods, here we report that ClpA, when associated with ClpP, translocates polypeptide with an overall rate of ~35 amino acids per second and, on average, traverses ~5 amino acids between two rate limiting steps with reduced cooperativity between ATP binding sites in the hexameric ring. This is in direct contrast to our previously reported observation that, in the absence of ClpP, ClpA translocates polypeptide substrates with a maximum translocation rate of ~20 amino acids per second with cooperativity between ATPase sites. Our results demonstrate that ClpP allosterically impacts the polypeptide translocation activity of ClpA by reducing the cooperativity between ATP binding sites.

## Introduction

Virtually every major event in the cell is catalyzed by macromolecular machines.<sup>1; 2</sup> ~~Error! Bookmark not defined.~~ One example are the ATP dependent proteases, which are ATP-driven enzymes required in all organisms for the removal of both misfolded and properly folded proteins in cell cycle regulation.<sup>3; 4</sup> The ATP-dependent proteases share a common architecture where a hexameric AAA+ ATPase can associate with one or both ends of a barrel-shaped peptidase that contains active sites in its interior sequestered from bulk solvent.<sup>5; 6; 7</sup> In these systems, the AAA+ ATPase component is responsible for the recognition, unfolding, and subsequent translocation of specific protein substrates into the proteolytic core of the associated peptidase.

Clp/Hsp100 proteins can be classified as either Class I or Class II.<sup>2; 8</sup> Class I proteins contain two ATP binding and hydrolysis sites per monomer, while Class II proteins contain only one site per monomer. Class I enzymes include ClpA and ClpB, whereas Class II includes ClpX and HslU. Despite the differences in number of ATPase sites, both ClpA and ClpX can associate with ClpP to form the ATP dependent protease ClpAP or ClpXP, respectively. In both cases, the motor component, ClpA or ClpX, binds to protein displaying a degradation tag, and through repeating cycles of ATP binding and hydrolysis, translocates the protein substrate through the central channel of the motor component into the proteolytic core of ClpP.<sup>4; 9; 10; 11</sup>

Despite the similar functions of ClpA and ClpX, it is unclear as to why ClpA requires two ATP binding sites. The monomeric structure of ClpA shows that ClpA is composed of three domains: an N-domain, AAA+ Domain 1 (D1), and AAA+ Domain 2 (D2).<sup>12</sup> Both D1 and D2 contain Walker A and Walker B motifs, which form the ATP

binding and hydrolysis sites. In both AAA cassettes, the Walker A and Walker B motifs are separated by a loop that resides in the central channel of the hexameric ring. In the D2 domain of ClpA, this corresponds to a conserved aromatic-hydrophobic sequence, GYVG, which is present in nearly all AAA+ unfoldases.<sup>13</sup> Hinnerwisch et al showed through crosslinking studies that when ClpA was bound to an SsrA containing substrate in the presence of ATP $\gamma$ S, the D2 loop made contact with the SsrA sequence.<sup>14</sup> Although they did not observe crosslinking to the D1 loop, mutations in this loop eliminated translocation. From this, it was concluded that both the D1 and D2 loops are involved in polypeptide translocation.

In the absence of nucleotide, ClpA resides in a mixture of monomers, dimers, and tetramers at thermodynamic equilibrium.<sup>15; 16</sup> To form hexameric rings active in polypeptide binding and association with ClpP, ClpA requires nucleoside triphosphate binding. Maurizi and coworkers showed that ATP binding at D1 was essential for assembly into hexameric rings whereas D2 is responsible for the majority of the observed ATP hydrolysis.<sup>17</sup>

ClpAP catalyzed polypeptide translocation and degradation has been examined by either monitoring the steady state degradation of model substrates, often green fluorescent protein<sup>18</sup> or the appearance of FRET upon substrate entry into ClpP.<sup>19; 20</sup> Both strategies have the absolute requirement that ClpP is present. Thus, the question of whether or not ClpP exerts an allosteric effect on the mechanism of ClpA catalyzed polypeptide translocation cannot be addressed with either of these strategies. To overcome this limitation, we developed a single turnover fluorescence stopped-flow method that allows us to examine ClpA catalyzed polypeptide translocation in the

absence of the proteolytic component, ClpP.<sup>21</sup> Using this approach, we showed that ClpA, in the absence of ClpP, translocated polypeptide substrates with an overall rate of  $\sim 20 \text{ aa s}^{-1}$  and a kinetic step-size of  $\sim 14 \text{ aa step}^{-1}$ .

The kinetic step-size represents the average number of amino-acids translocated between two rate limiting steps and does not necessarily reflect mechanical movement.<sup>22; 23; 24; 25; 26; 27; 28; 29; 30</sup> We have previously reported that the observed kinetic step-size for ClpA translocation is independent of ATP concentration and that the observed rate-limiting step is kinetically coupled to repeating cycles of ATP binding and hydrolysis.<sup>21</sup> From this observation, it can be concluded that a single step is being monitored in each repeating cycle of polypeptide translocation. Thus, the observed step immediately follows ATP binding.<sup>25; 26</sup> Therefore, the observed step could be mechanical movement, ATP hydrolysis, or a slow conformational change, i.e. D1 or D2 loop movement.

In the case of ClpA, the interpretation of the kinetic step-size is further muddled by the fact that the enzyme contains two ATP binding and hydrolysis sites per monomer and both sites are hydrolyzing ATP at different rates.<sup>31</sup> Therefore, it is unclear if the step that limits the observation of translocation and repeats every  $\sim 14$  amino acids translocated is occurring at D1 or D2. Despite these limitations on the interpretation of the kinetic step-size, quantitative information on the elementary steps in polypeptide translocation can be obtained using such single-turnover kinetic approaches.

Here we report the results from applying our single-turnover fluorescence stopped flow technique to examine ClpA catalyzed polypeptide translocation in the presence of ClpP. This was done to address the question: does ClpP allosterically impact the ClpA

catalyzed polypeptide translocation mechanism? Here we report that ClpA, in the presence of ClpP, translocates polypeptide substrate with an overall rate of  $\sim 36$  aa  $s^{-1}$  in contrast to our previous report of  $\sim 20$  aa  $s^{-1}$  in the absence of ClpP, both at saturating [ATP]. We show that this is the consequence of both an increase in the elementary rate constant and an increase in the frequency with which the observed rate-limiting step repeats, i.e. a decrease in the kinetic step-size. Most strikingly, the dependence of the kinetic parameters on ATP concentration suggests that the cooperativity between ATP binding and hydrolysis sites is reduced during polypeptide translocation in the presence of ClpP. This is in stark contrast to what was observed for ClpA in the absence of ClpP, where the dependence of the kinetic parameters on ATP suggests cooperativity between ATP binding and hydrolysis sites.

## Results

### *Application of a single-turnover method to examine polypeptide translocation by ClpAP*

To examine ClpAP catalyzed polypeptide translocation, single-turnover translocation experiments were performed in Buffer H (see Materials and Methods) as previously described for ClpA.<sup>21</sup> Fig. 1 illustrates the experimental design. In syringe 1 of the stopped-flow apparatus is a solution containing 1  $\mu$ M ClpA monomer, 1.2  $\mu$ M ClpP monomer, 150  $\mu$ M ATP $\gamma$ S, and 20 nM fluorescein labeled polypeptide substrate (see Table 1 for sequences). Each polypeptide substrate contains the SsrA sequence, AANDENYALAA (shown in bold in Table 1), at the carboxy terminus and a single cysteine residue at the amino terminus that has been labeled with fluorescein-5-maleimide. ClpA binds the SsrA sequence at the carboxy terminus of the substrate and

translocates toward the amino terminus.<sup>19; 21</sup> Inclusion of ATP $\gamma$ S is required for assembly of hexameric ClpA that is active in both polypeptide binding and ClpP association.<sup>6; 21; 32</sup> The structure shown in Fig. 1 is a schematic representation of the contents of syringe 1 from a model of the ClpA hexamer<sup>12</sup> and the crystal structure of the ClpP tetradecamer, since there is not an available crystal structure of hexameric ClpA bound to tetradecameric ClpP.<sup>33</sup>

Syringe 2 contains a solution of ATP and 300  $\mu$ M SsrA polypeptide. The inclusion of a non-fluorescently modified SsrA polypeptide in syringe 2 serves as a protein trap that insures single-turnover conditions. Upon mixing the contents of the two syringes, free ClpAP or any ClpAP that dissociates will rapidly bind the non-fluorescently modified SsrA trap, thus insuring that the observed signal is only sensitive to ClpAP that was bound at time zero.

Reaction progress is monitored by exciting fluorescein at 494 nm and observing the emissions at 515 nm and above using a 515 nm long pass filter. Upon binding to the polypeptide substrate in the presence of ATP $\gamma$ S, ClpAP quenches the fluorescence, identical to what was observed and reported for ClpA.<sup>21</sup> Thus, the reactant in syringe 1 represents a pre-bound complex with quenched fluorescence and will exhibit a fluorescence increase when ClpAP dissociates.

Fig. 2 shows the fluorescence time courses collected from rapidly mixing the contents of syringe 1 and 2, as illustrated in Fig. 1, at a final ATP concentration of 300  $\mu$ M after mixing. The representative time courses are from three experiments performed with polypeptide substrate lengths of 30, 40, and 50 amino acids (see Table 1). Similar to

what was observed for ClpA in the absence of ClpP, the three fluorescence time courses exhibit a lag followed by a fluorescence enhancement.<sup>21</sup> Consistently, the extent of the lag increases with increasing substrate length. Under single-turnover conditions, a lag phase in the kinetic time course is observed if two or more rate-limiting steps occur with similar rate constants.<sup>22; 26; 29</sup> Likewise, ClpAP is proceeding through more rate limiting steps with each increase in substrate length since the extent of the lag is increasing with increasing substrate length.

The time courses shown in Fig. 2 are only sensitive to the enzyme that was bound at time zero. In our previous examination of ClpA catalyzed polypeptide translocation, the only active form of the enzyme would be hexameric ClpA.<sup>21</sup> However, in the experiments shown here, signal will come from hexameric ClpA or hexameric ClpA associated with ClpP. Moreover, ClpP can be associated with either one or two hexamers of ClpA, i.e. a 1:1 or 2:1 complex, respectively. In the experimental design, shown in Fig. 1, the monomeric ClpA concentration is 1  $\mu$ M and the concentration of ClpP tetradecamers is 86 nM. If it is assumed that all of the ClpA monomers are in the hexameric state, then the concentration of hexamers would be 166.7 nM, i.e. 1  $\mu$ M ClpA monomer divided by 6 monomers per hexamer. Thus, the hexameric concentration of ClpA would be in two fold excess over the concentration of ClpP, a condition that has been used in many studies.<sup>5; 7; 19; 20; 34</sup> However, we previously reported that 18  $\mu$ M ClpA monomer in the presence of 1 mM ATP $\gamma$ S did not sediment as a single ideal species in sedimentation velocity experiments.<sup>32</sup> Rather, there were a distribution of oligomers where the hexameric state exhibited a sedimentation coefficient of  $\sim$ 15.5 S.<sup>32</sup>

The single turnover experiments schematized in Fig. 1 are performed with 1  $\mu\text{M}$  ClpA monomer and 150  $\mu\text{M}$  ATP $\gamma$ S in the pre-incubation syringe. Under these conditions, the ClpA concentration is 18-fold lower and the ATP $\gamma$ S concentration is nearly 7-fold lower than in our previous report on the assembly state of ClpA.<sup>32</sup> Since the free monomer concentration and the free nucleotide concentration are the thermodynamic driving forces for hexamer formation, one would predict that the hexameric state would be even less populated under these lower concentration conditions than in our previous study. To address this, we performed sedimentation velocity experiments to determine the concentration of hexamers in the preincubation syringe illustrated in Fig. 1. with 1  $\mu\text{M}$  ClpA and three different concentrations of ATP $\gamma$ S between 50 and 150  $\mu\text{M}$  ATP $\gamma$ S.

Fig. 3a shows the  $c(s)$  distributions from the analysis of sedimentation velocity experiments performed with 1  $\mu\text{M}$  ClpA monomer and 50, 100, and 150  $\mu\text{M}$  ATP $\gamma$ S. We have previously published sedimentation coefficients for monomer and hexamer to be 4.5 S and 15.5 S, respectively.<sup>16; 32</sup> Consistently, the  $c(s)$  distribution shows a clear reaction boundary at  $\sim 4.5$  S and  $\sim 15.5$  S. Moreover, as the nucleotide concentration is increased, the reaction boundary for the monomer decreases and the hexamer increases (see Fig. 3a). The  $c(s)$  distribution clearly indicates that not all of the ClpA resides in the hexameric state and that ClpA resides in a dynamic equilibrium of hexamers, monomers, and potentially smaller oligomers.

The sedimentation boundaries were subjected to analysis using the non-interacting discrete species model to determine the number of oligomers present and the fraction of each component (see Materials and Methods). Knowledge of the total loading

concentration of ClpA and the fraction of this concentration in the hexameric state yields the concentration of hexamers present. Fig. 3b shows the concentration of hexamers at the three different concentrations of ATP $\gamma$ S. The determined concentration of hexamers in our pre-incubation conditions (1  $\mu$ M ClpA and 150  $\mu$ M ATP $\gamma$ S) is (130  $\pm$  11) nM, which is ~22 % lower than the 167 nM hexamers predicted if one assumes all of the ClpA is in the hexameric state.

ClpP can bind one or two hexamers to form a 1:1 or 2:1 complex, respectively. A mixture of 1:1 and 2:1 complexes will be present since the ClpP concentration is 86 nM and the ClpA hexamer concentration is ~130 nM under these conditions. However, there should not be a significant concentration of free hexamers based on an affinity constant of ~4 nM for ClpA hexamer binding to ClpP.<sup>6</sup> Therefore, the observed signal shown in Fig. 2 should only reflect ClpAP bound to polypeptide substrate. The signal will represent the translocation activity of a mixture of 1:1 and 2:1 complexes. On the other hand, since the polypeptide substrate concentration in these experiments is 20 nM and the enzyme concentration is in large excess, on average, only one polypeptide should be bound per complex whether 2:1 or 1:1. It has been previously concluded that only one polypeptide can bind to one hexamer.<sup>35</sup> Moreover, only one hexamer can bind to these short polypeptide substrates and ClpA binds to the SsrA sequence ~6-fold tighter than to a random unstructured sequence (T. Li and A. L. Lucius, manuscript submitted). Thus, the time courses only reflect translocation catalyzed by ClpA at one side of the ClpAP complex, whether it is a 2:1 or a 1:1 ClpA to ClpP complex.

### *Analysis of the number of steps as a function of polypeptide substrate length*

The kinetic mechanism that we previously reported for ClpA in the absence of ClpP exhibited a slow step with rate constant  $k_C$  that was not involved in polypeptide translocation.<sup>21</sup> To diagnose whether this step is present for ClpA when ClpP is present, i.e. ClpAP, the dependence of the number of observed translocation steps,  $n$ , on the total length of polypeptide,  $L$ , was investigated. To accomplish this, the time courses shown in Fig. 2 were subjected to NLLS analysis using the simplified  $n$ -step sequential model shown as Scheme 1. In Scheme 1, ClpAP begins pre-bound to polypeptide substrate,  $S$ , in both a productive and nonproductive form,  $(E\bullet S)_L$  and  $(E\bullet S)_{NP}$ , respectively, which accounts for the observed slow second phase. Upon mixing with ATP,  $(E\bullet S)_{NP}$  can isomerize with rate constant  $k_{NP}$  into the productive form,  $(E\bullet S)_L$ , which can either dissociate from the polypeptide substrate with rate constant  $k_d$  or translocate polypeptide substrate in discrete steps, with rate constant  $k_T$ . Once the enzyme has taken a single translocation step, the first intermediate,  $I_{(L-m)}$ , of length  $L-m$  is formed, where  $L$  is the length of the polypeptide and  $m$  is the kinetic step-size. The kinetic step-size is defined here as the average number of amino acids translocated between two rate-limiting steps. ClpAP can then continue to translocate polypeptide through  $n$  translocation steps until reaching the end and dissociating to form free enzyme and free polypeptide substrate,  $S$ .

In this analysis the time courses collected for each length of fluorescein-labeled polypeptide were subjected to NLLS analysis using Scheme 1 by constraining  $k_T$  and  $k_{NP}$  to be the same for each substrate length, and thus global parameters. In contrast, the amplitudes,  $A_x$ , the fraction of productively bound complexes,  $x_x$ , and the observed

number of translocation steps,  $n_x$ , are treated as local parameters and are different for each polypeptide length, where the subscript 'x' represents the substrate length.

From the NLLS analysis, we determined the total number of steps,  $n$ , required to describe each time course and plotted  $n$  as a function of total polypeptide length. Fig. 4 shows that when Scheme 1 is used for analysis, the number of steps required to describe each time course increases linearly with polypeptide length (red solid circles in Fig. 4). This indicates that ClpAP must proceed through additional steps for each increase in substrate length, consistent with translocation initiating at the carboxy-terminal binding site and proceeding to the amino-terminal fluorophore. A linear least-squares analysis of these data results in the observation of a positive y-intercept of approximately 1.3 (red line in Fig. 4). We have previously shown that the observation of a positive y-intercept in a plot of the number of steps,  $n$ , versus total polypeptide substrate length,  $L$ , can serve as a diagnostic for the presence of additional steps in the molecular mechanism that are not involved in translocation.<sup>21; 25; 26; 29</sup>

To test the possibility that the observation of a positive n-intercept in the  $n$  vs.  $L$  plot is the consequence of additional kinetic steps in the molecular mechanism for polypeptide translocation, the time courses shown in Fig. 2 for each length of fluorescein-labeled substrate were subjected to NLLS analysis using Scheme 2. Scheme 2 is identical to Scheme 1 with the exception of the inclusion of a step with rate constant  $k_C$ . From this analysis, the number of steps required to describe each time course was determined and plotted as a function of substrate length (solid blue circles in Fig. 4). Similar to the analysis using Scheme 1, the analysis using Scheme 2 also exhibited a linear increase in the number of steps,  $n$ , with increasing substrate length,  $L$ . When the number of steps,  $n$ ,

vs. substrate length,  $L$ , is fit with a linear equation, a negative y-intercept is observed (blue line in Fig.4). Moreover, the line intersects the x-axis at  $\sim 11$  amino acids. Thus, Scheme 2 accounts for the observation of a rate limiting step that is not part of repeating cycles of polypeptide translocation. The observation of an x-intercept at  $\sim 11$  amino acids is consistent with a contact site size of  $\sim 11$  amino acids, which is the same length as the SsrA binding sequence.

We take the observation of a positive x-intercept to mean that some number of amino acids contained in the polypeptide substrate are in contact with the enzyme, but should not be considered as part of the total length of the substrate.<sup>21; 23; 29</sup> To account for this observation in our analysis, we have removed the contribution of the SsrA binding sequence to the translocation time courses by subtracting eleven from the total length of each polypeptide sequence shown in Table 1. This is illustrated in more detail in Fig. 4 (green line), by showing that when the number of observed translocation steps resulting from NLLS analysis using Scheme 2 is plotted as a function of the corrected polypeptide substrate length, the fit line extrapolates to the origin.

Scheme 2 describes all of the macroscopic observations of the three time courses shown in Fig. 2. Thus, the time courses in Fig. 2 were subjected to global NLLS analysis using Scheme 2 by relating the number of observed steps,  $n$ , to the substrate length,  $L$ , using a global kinetic step-size,  $m$ , where  $n = L / m$ . In this analysis,  $k_T$ ,  $k_C$ ,  $k_{NP}$ , and  $m$  were all constrained to be global parameters. The solid red line in Fig. 2 represents the results of the global NLLS analysis. The resultant parameters are  $k_T = (4.69 \pm 0.09) \text{ s}^{-1}$ ,  $k_C = (0.12 \pm 0.01) \text{ s}^{-1}$ ,  $k_{NP} = (0.02 \pm 0.002) \text{ s}^{-1}$ ,  $m = (4.6 \pm 0.3) \text{ aa step}^{-1}$ , and  $mk_T = (21.5 \pm 1.1) \text{ aa s}^{-1}$ . Strikingly, at similar ATP concentrations, ClpA, in the absence of ClpP,

exhibited an observed translocation rate of  $\sim 0.2 \text{ s}^{-1}$  compared to  $\sim 4.7 \text{ s}^{-1}$  observed here in the presence of ClpP. Likewise, the overall rate of translocation when ClpP is present is  $\sim 22 \text{ aa s}^{-1}$  compared to  $\sim 3 \text{ aa s}^{-1}$  when ClpP is absent.<sup>21</sup> Equally, the kinetic step-size is reduced  $\sim 3$ -fold from  $\sim 14 \text{ aa step}^{-1}$  in the absence of ClpP compared to  $\sim 4.6 \text{ aa step}^{-1}$  when ClpP is present.

We propose three potential explanations for the observation that the rate constant and kinetic step-size are different in the presence and absence of ClpP. First, the observed rate limiting step could be the same step as observed in the absence of ClpP, but it has been accelerated in the presence of ClpP and the frequency with which it repeats has been increased, i.e. increased number of steps,  $n$ , to fully translocate the substrate and thus a reduced kinetic step-size,  $m$ . Second, the kinetic time courses could be sensitive to a different step that repeats with greater frequency. Third, if the kinetic step-size truly represents mechanical movement, then the distance traveled between two rate limiting steps could be different for ClpAP than for ClpA.

#### *Dependence of translocation mechanism on [ATP]*

To begin to distinguish between the three possibilities, we examined the ATP concentration dependence of the kinetic parameters. Single-turnover fluorescence stopped-flow experiments were performed as schematized in Fig. 1 by varying the [ATP] in syringe 2. Time courses were collected using substrates I-III (see Table 1) at a final mixing concentration of ATP equal to 125, 200, 300, 500, 750  $\mu\text{M}$ , and 1, 3, 5, 7, and 9 mM. Each data set was subjected to NLLS analysis to determine the parameters  $k_T$ ,  $m$ ,  $mk_T$ ,  $k_C$ , and  $k_{NP}$  at each [ATP] (see Table 2).

The kinetic step-size and the translocation rate constant exhibit a high degree of negative parameter correlation. As such, the associated uncertainties on these parameters are large (see Table 2). However, the translocation rate constant clearly exhibits an ATP concentration dependence, while the kinetic step-size appears to be constant with an average value of  $(4 \pm 1)$  aa step<sup>-1</sup>.

In an attempt to determine the kinetic parameters with higher precision, all of the time courses collected at different ATP concentrations were combined and subjected to global NLLS analysis. The kinetic step-size was constrained to be a global parameter for all thirty time courses since the kinetic step-size appears to be independent of ATP concentration. In contrast,  $k_T$ ,  $k_C$ , and  $k_{NP}$  were local parameters to each ATP concentration. As seen in Table 3, the certainty on the kinetic parameters is substantially improved (compare values in Table 2 to Table 3). Similarly, the global kinetic step-size was determined to be  $(4.6 \pm 0.3)$  aa step<sup>-1</sup>.

The microscopic translocation rate constant,  $k_T$ , and the macroscopic rate,  $mk_T$ , are plotted as functions of [ATP] in Figs. 5a and 5b, respectively. This global fitting strategy produced results similar to the fitting strategy discussed above in which all data were fit individually. A plot of either the macroscopic rate or microscopic rate constant of translocation exhibits a hyperbolic dependence on [ATP], rather than the sigmoidal dependence upon [ATP] that is observed for ClpA in the absence of ClpP.<sup>21</sup> Despite this, both curves were initially subjected to NLLS analysis using an infinitely cooperative binding model given by Eq. (4) as was done for ClpA in the absence of ClpP.<sup>21</sup> For the analysis of  $k_T$  and  $mk_T$ , the Hill coefficient,  $t$ , is  $1.2 \pm 0.2$  and  $1.1 \pm 0.1$ , and the equilibrium constant,  $K_a$ , is  $(4.8 \pm 1.1) \times 10^3 \text{ M}^{-1}$  and  $(4.8 \pm 1.1) \times 10^3 \text{ M}^{-1}$ , respectively.

Since the Hill coefficient is within error of one, the parameter was constrained to one, i.e. a 1:1 binding isotherm, and the data were subjected to NLLS analysis. The results of this analysis are shown as solid lines in Figs. 5a and 5b. The resultant parameter  $K_a$  for  $mk_T$  and  $k_T$  is  $(4.8 \pm 0.5) \times 10^3 \text{ M}^{-1}$  and  $(4.8 \pm 0.5) \times 10^3 \text{ M}^{-1}$ , respectively. The analysis of  $k_T$  and  $mk_T$  also yielded estimates of the maximum translocation rate constant and maximum macroscopic rate of translocation as  $(7.9 \pm 0.2) \text{ s}^{-1}$  and  $(36.1 \pm 0.7) \text{ aa s}^{-1}$ , respectively, at saturating ATP concentrations.

Scheme 2 includes both a kinetic step,  $k_C$ , that is slow relative to translocation and a pre-translocation equilibrium that proceeds from a non-productive state to a productive state with rate constant,  $k_{NP}$ . As shown in Fig. 5c,  $k_C$  and  $k_{NP}$  both show a dependence on [ATP]. Similar to  $mk_T$  and  $k_T$ ,  $k_C$  and  $k_{NP}$  exhibit rectangular hyperbolic character when plotted on a linear [ATP] scale. When  $k_C$  and  $k_{NP}$  were subjected to NLLS analysis using Eq. (4) with the Hill coefficient constrained to equal one, the equilibrium constant,  $K_a$ , was  $(2.8 \pm 0.2) \times 10^3 \text{ M}^{-1}$  and  $(2.5 \pm 0.1) \times 10^3 \text{ M}^{-1}$ , respectively. The analysis of  $k_C$  and  $k_{NP}$  also yielded estimates of the maximum value at saturating [ATP] as  $(0.26 \pm 0.003) \text{ s}^{-1}$  and  $(0.045 \pm 0.001) \text{ s}^{-1}$ , respectively.

## Discussion

We recently developed and reported a single-turnover fluorescence stopped flow method that is sensitive to polypeptide translocation catalyzed by ClpA in the absence of ClpP.<sup>21; 36</sup> Equally important, we developed methods to analyze the kinetic time courses and yield quantitative estimates of a number of parameters describing the elementary steps in the mechanism of ClpA catalyzed polypeptide translocation.<sup>29</sup> These parameters

include the kinetic step-size, the elementary rate constants, the overall rate of translocation, and the processivity. With these methods in hand, we reported a minimal kinetic mechanism to describe a single round of polypeptide translocation catalyzed by ClpA in the absence of ClpP.

That work represented a significant advance because much of our knowledge regarding ClpA catalyzed polypeptide translocation had been elucidated by examining the steady-state proteolysis catalyzed by ClpAP with the assumption that ClpA catalyzes polypeptide translocation employing the same molecular mechanism whether bound to ClpP or not.<sup>6; 18</sup> Reid et al reported the development of a FRET based stopped-flow method, where a donor fluorophore is in the central cavity of ClpP and an acceptor fluorophore is on a substrate protein being translocated into the central cavity. Thus, upon arrival of the substrate into the cavity, a FRET signal change is observed. Because this approach also requires the presence of ClpP, one could not address the question of whether or not ClpP exerts allosteric control over the mechanism of ClpA catalyzed polypeptide translocation. An alternative FRET experiment was performed by Weber-Ban and coworkers, where a donor-acceptor pair was placed far away from each other in the primary structure of a substrate protein, but close in proximity in the folded protein.<sup>20</sup> Upon translocation catalyzed by ClpA in the absence of ClpP, a FRET change was observed. However, none of the time courses acquired using either of these FRET methods were subjected to quantitative analysis that would lead to a determination of the elementary rate constants in the reaction cycle.

### *Analysis of translocating species*

In the work reported here, we set out to determine the effect of ClpP on the kinetic mechanism of polypeptide translocation catalyzed by ClpA. However, one immediate question arises in the experimental design schematized in Fig. 1: what form of ClpAP is catalyzing translocation? This question arises because ClpAP can exist as a complex consisting of either one ClpA hexamer associated with one ClpP tetradecamer (1:1 complex) or 2 hexamers associated with one ClpP tetradecamer (2:1 complex).

To predict the concentrations of 1:1 ClpAP, 2:1 ClpAP, and free ClpA hexamers, one needs the interaction constant for ClpA hexamer binding to ClpP tetradecamers, the ClpP tetradecamer concentration, and the ClpA hexamer concentration. The dissociation equilibrium constant for ClpA hexamers associating with ClpP tetradecamers has been reported to be in the range of 4 – 25 nM from activity assays.<sup>6; 37</sup> However, to determine the concentration of hexameric ClpA and tetradecameric ClpP, knowledge of the assembly state is required. In analytical ultracentrifugation experiments, ClpP sediments as a single ideal species with a molecular weight consistent with a tetradecameric species.<sup>6</sup> Thus, it is sufficient to determine the total monomer concentration and divide by fourteen to yield the ClpP tetradecamer concentration. In the case of ClpA, we recently reported results from sedimentation velocity experiments showing that ClpA did not sediment as a single ideal species in the presence of saturating concentrations of nucleoside triphosphate.<sup>32</sup> Thus, determining the concentration of ClpA hexamers under a given set of conditions is a more complex task than simply determining the total monomer concentration and dividing by six.

Those previous sedimentation velocity experiments showing that ClpA resides in a mixture of oligomers was carried out at 18  $\mu\text{M}$  ClpA monomer and 1 mM ATP $\gamma$ S.<sup>32</sup> In contrast, the stopped-flow experiments reported here were performed with a pre-mixing concentration of 1  $\mu\text{M}$  ClpA monomer and 150  $\mu\text{M}$  ATP $\gamma$ S (Fig. 1, Syringe 1). Thus, the population of hexamers in the stopped-flow pre-incubation syringe (Fig. 1, Syringe 1) is predicted to be even lower than in our previously reported sedimentation velocity experiments. This prediction is made simply based on mass action. Consequently, the population of ClpA hexamers must depend on both the free ClpA monomer concentration and the free ATP $\gamma$ S concentration.

The sedimentation velocity experiments reported here show that ~78 % of ClpA monomers reside in the hexameric state at 1  $\mu\text{M}$  ClpA monomer and 150  $\mu\text{M}$  ATP $\gamma$ S. Hence, the concentration of hexamers in the preincubation syringe would be ~130 nM. However, this assumes that neither ClpP binding nor polypeptide binding induces hexamer formation, which is an assumption we are currently investigating. Since the ClpP tetradecamer concentration is 86 nM, the hexamer concentration is in a 1.5-fold excess over the ClpP tetradecamer concentration. Thus, the kinetic time courses reported here likely reflect translocation catalyzed by a mixture of 1:1 and 2:1 complexes. Although this fact complicates our interpretation of the kinetic data, the results are comparable to a variety of published studies performed with similar ClpA and ClpP concentrations where it is assumed that ClpA resides only in the hexameric state and thus only the 2:1 complex is catalyzing the reaction.<sup>5; 18; 31</sup>

One natural question is; why not simply increase the ATP $\gamma$ S concentration in syringe 1 to shift the equilibrium to hexamers? The answer is that we want to minimize the impact of competition in binding between hydrolysable ATP and ATP $\gamma$ S upon mixing. We have found through sedimentation velocity experiments that the population of hexamers does not change significantly between 100  $\mu$ M and 1 mM ATP $\gamma$ S (Lin et al, manuscript in preparation). Consistently, Fig 3b suggests that the dependence of the concentration of hexameric ClpA on [ATP $\gamma$ S] is beginning to saturate at 150  $\mu$ M ATP $\gamma$ S. In the experiments reported here, the concentration of ATP $\gamma$ S is 75  $\mu$ M after mixing with 5 mM hydrolysable ATP. Thus, the competition between ATP and ATP $\gamma$ S binding should be minimized, while maintaining [ATP $\gamma$ S] sufficiently high to saturate ClpA hexamerization.

The interpretation of the kinetic time courses is complicated by the fact that there is a mixture of species present in solution. Nevertheless, we have reduced the complexity by maintaining enzyme concentration in excess of polypeptide substrate concentration. Under these conditions, binding of a single polypeptide to one hexamer in the 2:1 complex is favored. As such, our interpretation of the data assumes that a ClpA hexamer in a 2:1 complex translocates polypeptide with the same mechanism as a hexamer in a 1:1 complex. However, this assumption is currently being tested by determining the molecular mechanism of polypeptide translocation under a variety of ClpA to ClpP mixing ratios (J. Miller, manuscript in preparation).

### *Rate of ClpAP catalyzed polypeptide translocation*

Semi-quantitative approaches have previously been used to propose that ClpAP translocates polypeptide with an overall rate of 50 amino acids per second.<sup>20</sup> In the same study, it was concluded from qualitative inspection of kinetic time courses resulting from ClpA translocating a polypeptide labeled with a FRET pair that ClpA, in the absence of ClpP, translocated polypeptide more slowly than ClpAP. We previously reported that ClpA, in the absence of ClpP, translocates at a rate of  $(19 \pm 1)$  aa s<sup>-1</sup> at saturating ATP concentrations.<sup>21</sup> Here we show that ClpAP translocates with a rate of  $(36.1 \pm 0.7)$  aa s<sup>-1</sup> at saturating ATP concentrations. Consistent with previous reports, ClpAP does translocate polypeptide with a faster rate than ClpA.

The overall rate of translocation is the product of the average distance translocated between two rate limiting steps and the rate constant for the step. Thus, the difference in the overall rate of polypeptide translocation by ClpA vs. ClpAP can be interpreted in terms of the effects on these two parameters. We previously reported that the translocation rate constant and kinetic step-size for ClpA in the absence of ClpP is  $k_T = (1.39 \pm 0.06)$  s<sup>-1</sup> and  $m = (14 \pm 1)$  aa step<sup>-1</sup> in the presence of 5 mM ATP.<sup>21</sup> In contrast, we report here that the translocation rate constant and kinetic step-size for ClpA in the presence of ClpP is  $k_T = (7.9 \pm 0.2)$  s<sup>-1</sup> and  $m = (4.6 \pm 0.3)$  aa step<sup>-1</sup> at 5 mM ATP. The observed increase in overall rate for ClpAP is due to an increase in the rate constant by ~6-fold. However, the overall rate constant is only increased by ~1.5-fold, which is a consequence of the ~3-fold reduction in the kinetic step-size.

### *Interpretation of the kinetic step-size*

Polypeptide translocation must occur through repeating cycles of ATP binding, hydrolysis, mechanical movement, various conformational changes, and ADP and  $P_i$  release, among other potentially significant kinetic steps as shown in Fig. 6b. This listing of potential kinetically significant steps is not intended to imply an order because the order of these events for ClpA and ClpAP is unknown. Fig. 6b illustrates the cycle where enzyme,  $E$ , begins prebound to polypeptide substrate,  $S$ , which is represented as  $ES$ . The  $ES$  complex binds ATP with rate constant  $k_1$  to form the  $E.S.ATP$  ternary complex, followed by ATP hydrolysis and simultaneous translocation to form the first intermediate bound to enzyme,  $E.I_1$ , and ATP hydrolysis products. Upon ADP and  $P_i$  release,  $E.I_1$  can bind additional molecules of ATP to repeat the cycle. The observed rate constant ( $k_{obs}$  in Fig. 6a) in the single-turnover experiments presented here represents the slowest step within the repeating cycle illustrated by Fig. 6b.

An initial examination of translocation is typically performed with saturating ATP concentrations, so that repeating cycles of ATP binding are not rate limiting.<sup>21; 25</sup> Under such conditions, the step being observed in each cycle would occur with rate constant  $k_2$  or  $k_3$  (see supplemental), where the rate constants are defined in Fig. 6b. If either step with rate constant  $k_2$  or  $k_3$  is rate limiting, then  $k_{obs} = k_2$  or  $k_3$  (see Supplemental Eqs. (S.6), (S.7), and (S.8) in Appendix 1). Because each step repeats once per cycle, the number of times this step repeats is equal to the number of times the cycle repeats. Consequently, if the mechanical step occurs only once per cycle, the kinetic step-size would equal the mechanical step-size. Conversely, if  $k_2 = k_3$ , the observed number of translocation steps would be two-fold larger than the actual number of steps required to

physically translocate the substrate because one would observe two steps for every repetition of the cycle (see supplemental Eq. (S.9) in Appendix 1). For example, if ClpA translocates a 50 amino acid substrate with a mechanical step-size of 5 aa step<sup>-1</sup> and ATP is saturating such that ATP binding is not rate limiting, the number of steps required to fully translocate the substrate would be  $n = 10$  steps. If only a single step in the repeating cycle is rate limiting, i.e. either  $k_2$  or  $k_3$  is rate limiting, the cycle would be observed to repeat 10 times (see supplemental Eqs. (S.8) and (S.9) in Appendix 1). Hence, the kinetic step-size would be determined to be 5 aa step<sup>-1</sup>, which would be equal to the mechanical step-size, because the number of steps,  $n$ , is equal to the substrate length,  $L$ , divided by the kinetic step-size,  $m$ , ( $n = L/m$ ). Alternatively, if  $k_2$  and  $k_3$  are equal and rate limiting, the observed rate constant would be  $k_{obs} = k_2 = k_3$ , and two steps would be observed for every repetition of the cycle. The observed number of steps would increase to  $n = 20$  instead of 10 (see supplemental Eq. (S.9) in Appendix 1). Using the equation  $n = L/m$  would result in a kinetic step-size of 2.5, which is two-fold smaller than the mechanical step-size. With these examples in mind, we conclude that it is imperative to determine the number of steps being observed per repeating cycle.

To test for these possibilities, the ATP concentration dependence of the kinetic parameters is often examined.<sup>25</sup> If multiple steps per cycle are rate limiting under conditions where ATP binding is not rate limiting, i.e. high [ATP], then a reduction in ATP concentration will lead to a corresponding change in the observed number of translocation steps and therefore a change in the observed kinetic step-size. This is because as the ATP concentration is reduced, the bimolecular ATP binding step must become rate limiting. Alternatively, if the ATP binding step is in rapid equilibrium ( $k_{-1}$

>>  $k_2$  in Fig. 6b) with the step immediately following ATP binding, then the step immediately following ATP binding will become rate limiting because it is kinetically coupled to ATP binding.<sup>25</sup> In either case, a transition from observing multiple steps per cycle to observing only a single step per cycle will occur. Accordingly, a change in the observed number of steps to fully translocate a substrate will occur and therefore a change in the kinetic step-size will be observed as the ATP concentration is reduced. This is a consequence of the ATP binding step or a step coupled to ATP binding becoming rate-limiting.<sup>21; 25</sup>

The kinetic step-size will not exhibit an ATP concentration dependence if the ATP binding step is in rapid equilibrium relative to the next step and if the step immediately following ATP binding is rate limiting at saturating concentrations of ATP.<sup>25</sup> Under these conditions, the step that immediately follows ATP binding is kinetically coupled to the ATP binding step. That is to say,  $k_{obs}$  will exhibit an ATP concentration dependence given by  $k_{obs} = k_2(K_1[ATP]/(1 + K_1[ATP]))$ , where  $K_1 = k_1/k_{-1}$ . Moreover, the same step is being observed at all concentrations of ATP and it only occurs one time per cycle of translocation.

The fact that the kinetic step-sizes for both ClpA and ClpAP are observed to be independent of ATP concentration shows that only one step per repeating cycle of polypeptide translocation is being observed at all ATP concentrations. Equally important, we can conclude that the observed step is not ATP binding because  $k_T$  does not exhibit a linear dependence. Rather, the observed rate constant exhibits a hyperbolic dependence. The hyperbolic dependence indicates that the step must be kinetically coupled to ATP binding and must be the step that immediately follows ATP binding. In order for this step

to be kinetically coupled to ATP binding it must immediately follow the ATP binding step and no other step can come between ATP binding and the step we are observing.<sup>25</sup> Accordingly, the number of possibilities for what is being observed in our experiments is significantly reduced. The step being observed is either ATP hydrolysis, a conformational change, or mechanical movement. However, it cannot be product release since product release must come after hydrolysis.

#### *A proposed molecular model for translocation*

Hinnerwisch and coworkers showed through crosslinking studies that polypeptide substrate crosslinked with the D2 loop in the central channel of ClpA.<sup>14</sup> The D2 loop in the primary structure resides between the Walker A and Walker B motifs, which form the ATP binding pocket.<sup>12</sup> From these observations, Hinnerwisch and coworkers proposed that the D2 loop was responsible for mechanical pulling on the substrate polypeptide being translocated. They proposed a cycle of translocation to consist of ATP binding at D2 with the D2 loop in the up conformation, followed by ATP hydrolysis that drives movement of the D2 loop to the down conformation and concurrent movement of the polypeptide substrate that is bound to the D2 loop. More recently, synchrotron footprinting data revealed that the D2 loop proceeds through a nucleotide-dependent conformational change, consistent with a prehydrolytic up conformation.<sup>38</sup>

From the single turnover experiments reported here, we show that the step we observe in each repeating cycle of translocation is the step that immediately follows ATP binding. Combining our observations with the Hinnerwisch model, the step is either ATP hydrolysis or movement of the D2 loop. In either case, since we are observing a single

step in each cycle, loop movement in ClpAP may represent movement by  $\sim 4.6$  amino acids.

The suggestion that the D2 loop is responsible for movement of the distance of the kinetic step-size  $m$  of  $\sim 4.6$  amino acids assumes that there is not a significant concentration of free ClpA hexamers simultaneously catalyzing polypeptide translocation. This is because ClpA hexamers exhibit a kinetic step-size of  $\sim 14$  aa  $\text{step}^{-1}$ . Similarly, the interpretation assumes that 1:1 and 2:1 ClpAP translocate with the same mechanism. This is important to note because we have observed from simulations that if multiple species are translocating with different overall translocation rates and/or different step-sizes, the observed kinetic step-size will be overestimated (simulations not shown). From single molecule measurements, this is the same as what has been described as heterogeneity or static disorder.<sup>39</sup> At the single-molecule level, heterogeneity in the rate constant has been shown to give rise to overestimates of the kinetic step-size determined in bulk experiments.<sup>40</sup> Similarly, if there is a significant population of ClpA hexamers translocating in addition to ClpAP, then the kinetic step-size will also be overestimated. As a result, we conclude that the kinetic step-size of  $\sim 4.6$  aa  $\text{step}^{-1}$  represents an upper limit since it could represent an overestimate as a consequence of both static disorder and structural heterogeneity, i.e. hexameric ClpA, 1:1 ClpA:ClpP, and 2:1 ClpA:ClpP. Similarly, the kinetic step-size for ClpA, in the absence of ClpP, of  $\sim 14$  aa  $\text{step}^{-1}$  also may represent an upper limit since it could be overestimated if there are differences in the rate constant and/or step-size from molecule to molecule. However, in the case of ClpA in the absence of ClpP there is less structural heterogeneity since only hexameric ClpA catalyzes translocation.

If heterogeneity in the rate results in overestimation of the kinetic step-size for both ClpA and ClpAP, then the heterogeneity is predicted to be independent of [ATP]. That is to say, the width of the distribution of rate constants that would be observed from single molecule experiments would have to be the same at all ATP concentrations. If not, the kinetic step-size that we observe in these bulk measurements would exhibit a change in kinetic step-size as a consequence of changes in the heterogeneity in the rate as a function of [ATP]. Since both ClpAP and ClpA in the absence of ClpP exhibit a kinetic step-size that is independent of [ATP] this predicts that the heterogeneity is independent of [ATP].

If the kinetic step-size of less than 4.6 aa  $\text{step}^{-1}$  for ClpAP truly represents mechanical movement by less than 4.6 amino acids, then why does ClpA exhibit a different kinetic step-size of  $\sim 14$  aa  $\text{step}^{-1}$ ? The answer to this question appears to lie in the dependence of the overall translocation rate on [ATP]. We previously reported that  $k_T$  for ClpA in the absence of ClpP exhibited a sigmoidal dependence on ATP concentration, which is consistent with cooperativity between ATP binding sites.<sup>21</sup> The isotherm was not well described by a single site isotherm and therefore was analyzed with the Hill model, which assumes infinite cooperativity. This analysis resulted in a Hill coefficient of  $\sim 2.5$ . Since ClpA contains two ATP binding sites per monomer, the observation of a sigmoidal dependence of the rate of translocation on [ATP] suggests that there is cooperativity between multiple ATP binding sites that are involved in polypeptide translocation. In stark contrast, the ATP concentration dependence of  $k_T$  for ClpAP can be described by a simple 1:1 binding model. This suggests that when ClpA is associated

with ClpP, the cooperativity is reduced between ATP binding sites that are involved in translocation compared to ClpA alone.

With these observations in mind we propose a working model for ClpA and ClpAP catalyzed polypeptide translocation that leads to a number of testable hypotheses that will require further investigation. Fig. 7 illustrates our working model for both ClpA and ClpAP that incorporates known structural information, results from various biochemical/biophysical studies, and the work reported here. Fig. 7a illustrates ClpA, in the absence of ClpP, with the D1 and D2 loops both in the up conformation and ATP bound to both domains. The polypeptide substrate is shown in black and is making contact with both the D1 and D2 loops. Crosslinking studies have shown that contacts between polypeptide substrate and ClpA were only observed with the D2 loop, but mutations in the D1 loop abolished translocation activity.<sup>14</sup> Moreover, our work indicates that both ATPase sites are involved in translocation for ClpA in the absence of ClpP.<sup>21</sup> These two observations implicate the D1 loop in translocation. The next step would be for D1 to hydrolyze ATP and cause the D1 loop to move down and translocate the substrate by up to 14 amino acids creating a loop inside of ClpA. The loop in the substrate can be accommodated in ClpA since it has been shown that ClpA forms a cavity between the D1 and D2 loops.<sup>41; 42</sup> D1 would contain ADP and P<sub>i</sub> in the ATP binding site and therefore the D1 loop would have a reduced affinity for the polypeptide, which would allow for rebinding at another D1 loop loaded with ATP in a neighboring subunit in the hexamer.<sup>32; 43</sup> The D2 loop would cycle through multiple rounds of ATP hydrolysis coupled to translocation of the substrate by 2 – 5 amino acids per cycle with a rate constant of  $\sim 4 \text{ s}^{-1}$ . This will occur several times thereby shortening the loop inside the

cavity of ClpA before D1 translocates another ~14 amino acids into the cavity with a rate constant of  $1.4 \text{ s}^{-1}$ .

Fig. 7b illustrates our working model for how ClpA translocates when associated with ClpP. Since the ATP concentration dependence of the rate of ClpAP catalyzed polypeptide translocation suggests reduced cooperativity between ATP binding sites we hypothesize that D2 drives translocation. Repeating cycles of ATP binding and hydrolysis could occur at D1, but they do not limit the observation of translocation. Therefore, this model predicts repeating cycles of ATP binding and hydrolysis at D2 would lead to translocation of the substrate by distances of  $2 - 5 \text{ aa step}^{-1}$ . The conclusion that D2 alone is responsible for translocation in ClpAP is based on the observation that the substrate makes contacts with the D2 loop from crosslinking studies. However, the crosslinking studies were not carried out in the presence of ClpP. Given the differences we observe between the mechanisms for ClpA vs. ClpAP, revisiting the crosslinking studies in the presence of ClpP is warranted.

Our working model predicts that in the absence of ClpP, D1 should hydrolyze ATP with a rate constant of  $(1.39 \pm 0.06) \text{ s}^{-1}$  and D2 should hydrolyze ATP with a rate constant of one-half of  $(7.9 \pm 0.2) \text{ s}^{-1}$  in the presence of polypeptide substrate. Kress et al examined the steady state rate of ATP hydrolysis catalyzed by ClpA both in the presence and absence of ClpP.<sup>31</sup> Further, they made two variants of ClpA that are deficient in ATP hydrolysis at either D1 or D2, which allow for the examination of ATP hydrolysis at each domain in the absence of hydrolysis at the other domain, and in the presence or absence of ClpP and SsrA substrate. Interestingly, in the absence of ClpP and the presence of GFP-SsrA, D1 hydrolyzes ATP with a rate constant of  $(0.8 \pm 0.2) \text{ s}^{-1}$ , which is

comparable to the rate constant we determined for translocation of  $(1.39 \pm 0.06) \text{ s}^{-1}$ . Similarly, in the presence of ClpP and GFP-SsrA, D2 hydrolyzes ATP with a rate constant of  $(6.3 \pm 0.5) \text{ s}^{-1}$ , which is similar to our estimate of  $(7.9 \pm 0.2) \text{ s}^{-1}$ .

In 2010, we reported the first estimate of a step-size (aa  $\text{step}^{-1}$ ) for any AAA+ polypeptide translocase.<sup>21; 36</sup> In 2011, single-molecule experiments on ClpXP were reported by both Sauer, Baker and coworkers and Bustamante and coworkers.<sup>44; 45</sup> Both groups showed that ClpX translocated with a step-size of  $\sim 5 - 8$  amino acids per step. Unlike ClpA, ClpX contains only one nucleotide binding and hydrolysis site per monomer. However, the D2 ATPase site in ClpA is structurally related to the single site in ClpX. Thus, it is striking that the step-size we observe to occur coupled to ATP hydrolysis at D2 is closer to that observed with ClpX.

## **Materials and Methods**

### *Materials*

All solutions were prepared in double-distilled water produced from a Purelab Ultra Genetic system (Siemens Water Technology) and using reagent grade chemicals purchased commercially. All peptide substrates were synthesized by CPC Scientific (Sunnyvale, CA). All peptides were  $>90\%$  pure as judged by HPLC and mass spectral analysis. Fluorescein was covalently attached to the free cysteine residue at the amino terminus of the polypeptide as previously described. *E. coli* ClpA was purified as described.<sup>16</sup>

### *ClpP Purification*

*E. coli* ClpP was purified with several modifications according to the method previously reported by Maurizi and coworkers.<sup>46</sup> All purification steps were performed at 4 °C. *E. coli* ClpP was overexpressed from the pET30a vector in BL21(DE3). From the harvested cell paste, a 250 mg/mL solution was made in cell lysis solution containing 2 mM 2-mercaptoethanol, 10 mM EDTA acid, 40 mM Tris (pH 8.0 at 4°C), 200 mM NaCl, and 10% (w/v) sucrose. The resuspended cells were passed through a chilled French pressure cell multiple times at 20,000 psi to ensure optimal cell lysis. Nucleic acid was then precipitated through the addition of PEI to the cell extract such that the final concentration was 0.1% (v/v) PEI. The supernatant was precipitated using 35% saturation ammonium sulfate. The resulting supernatant was dialyzed overnight against buffer B (2 mM EDTA, 50 mM Tris, 2 mM 2-mercaptoethanol, and 10% (v/v) glycerol) supplemented with 50 mM NaCl. The sample was loaded on to a Q-Sepharose 6 FF column (GE Healthcare) that had previously been equilibrated with buffer B supplemented with 50 mM NaCl. The sample was eluted with a linear gradient from 50 mM NaCl to 400 mM NaCl. All ClpP containing fractions were then pooled and loaded on to a Hiprep 26/60 Sephacryl S-300 HR column (GE Healthcare) that had previously been equilibrated with buffer B supplemented with 200 mM NaCl. Previously constructed standard curves allow for the prediction of the elution volumes of all oligomeric species of ClpP. To ensure that active ClpP was being collected, only fractions corresponding to elution volumes of ClpP heptamers were pooled for further purification. Pooled fractions were then dialyzed overnight against buffer B (2 mM EDTA, 50 mM Tris, 2 mM 2-mercaptoethanol, and 10% (v/v) glycerol) supplemented

with 50 mM NaCl. As a final purification step, the dialyzed sample was loaded on to a Blue Sepharose FF column (GE Healthcare) that had previously been equilibrated in buffer B supplemented with 50 mM NaCl. The sample was eluted with a linear gradient from 50 mM NaCl to 2 M NaCl and the ClpP containing peak stored in the resulting elution conditions (Buffer B with additional 1 M NaCl) at -80°C. Prior to storage, purity was judged to be >95% by Coomassie staining. ClpP concentration was determined spectrophotometrically in buffer H using an extinction coefficient of  $\epsilon_{280} = 9.1 \times 10^3 \text{ M}^{-1} \text{ cm}^{-1}$ .

## *Methods*

### *Analytical Ultracentrifugation*

Sedimentation velocity experiments were performed using a Beckman Optima XL-I analytical ultracentrifuge. Protein samples (380  $\mu\text{L}$ ) were loaded into a double sector Epon charcoal-filled centerpiece and subjected to an angular velocity of 40,000 rpm. Absorbance scans as a function of radial position were collected by scanning the sample cells at a wavelength of 230 nm at intervals of 0.003 cm. Scans were collected every minute. For all analytical ultracentrifugation experiments, an identical concentration of nucleotide was included in both the sample and reference sector. All experiments were prepared in buffer H (25 mM HEPES, pH 7.5 at 25 °C, 10 mM  $\text{MgCl}_2$ , 2 mM 2-mercaptoethanol, 300 mM NaCl, and 10% v/v glycerol).

### *Sedimentation Velocity*

Sedimentation velocity experiments were performed with 1  $\mu\text{M}$  ClpA and various concentrations of  $\text{ATP}\gamma\text{S}$ . The apparent peak positions are independent of  $[\text{ATP}\gamma\text{S}]$

indicating slow dissociation on the time scale of the sedimentation velocity experiments.<sup>47</sup> As expected for a nucleotide linked hexamerization reaction, the area under the apparent peak at ~4.5 S decreases and the area under the apparent peak at ~ 15.5 S increases with increasing [ATP $\gamma$ S].

The size and relative population of each species can be approximated using a non-interacting discrete species model using Sedfit (Peter Schuck, NIH), since the oligomers are in slow exchange and are well resolved.<sup>48</sup> The variance of the fit at the 68% confidence level was determined using the F-statistics in SedFit.<sup>49</sup>

#### *Single-Turnover Stopped-Flow Fluorescence Experiments*

Fluorescence stopped-flow experiments were performed as previously described and shown in Fig. 1.<sup>21</sup> All reactions were prepared in buffer H (25 mM HEPES, pH 7.5 at 25 °C, 10 mM MgCl<sub>2</sub>, 2 mM 2-mercaptoethanol, 300 mM NaCl, and 10% v/v glycerol). All experiments were performed in an SX.20 stopped-flow fluorometer, Applied Photophysics (Letherhead, UK). Prior to each reaction, 1  $\mu$ M ClpA was preincubated with 150  $\mu$ M ATP $\gamma$ S for 25 minutes. ClpP was then added such that the final concentration was 1.2  $\mu$ M and incubated for another 25 minutes to allow for assembly of ClpAP complexes competent for polypeptide translocation. Fluorescently modified polypeptide substrate was then added such that the final concentration was 20 nM, and the mixture was loaded into syringe 1 of the stopped-flow fluorometer. Syringe 2 contained a solution of ATP and 300  $\mu$ M SsrA peptide prepared in buffer H. The concentration of ATP in syringe 2 was varied from 250  $\mu$ M to 18 mM. Prior to mixing, both solutions were incubated for an additional 10 minutes at 25°C in the stopped-flow

instrument. Increasing the incubation time of either solution in the stopped-flow instrument had no effect on the observed fluorescence time courses. Upon mixing, the final concentrations were 0.5  $\mu\text{M}$  ClpA monomer, 0.6  $\mu\text{M}$  ClpP monomer, 10 nM peptide substrate, 150  $\mu\text{M}$  SsrA peptide, 75  $\mu\text{M}$  ATP $\gamma\text{S}$ , and the final concentration of ATP is indicated in the text. The fluorescein dye was excited at  $\lambda_{\text{ex}} = 494$  nm and fluorescence emission was observed above 515 nm with a 515 nm long pass filter. All kinetic traces shown represent the average of at least 8 individual determinations. The sequence of the polypeptide substrates shown in Table 1 are based on the sequence of the Titin I 27 domain and have been used previously in the study of both ClpXP and ClpA in the absence of ClpP.<sup>21; 50</sup>

#### *NLLS Analysis*

The system of coupled differential equations that result from Scheme 2 was solved using the method of Laplace transforms to obtain an expression for product formation as a function of the Laplace variable,  $S(s)$ , given by Eq. (1),

$$S(s) = \frac{1}{s} \left( \sum_{j=1}^h \frac{k_d k_C^{j-1} (k_{NP} + sx)}{(k_C + k_d + s)^j (k_{NP} + s)} + \sum_{i=1}^{n-1} \frac{k_d k_T^i k_T^{i-1} (k_{NP} + sx)}{(k_C + k_d + s)^h (k_{NP} + s) (k_d + k_T + s)^i} + \frac{(k_T + k_d) k_C^h k_T^{n-1} (k_{NP} + sx)}{(k_C + k_d + s)^h (k_{NP} + s) (k_d + k_T + s)^n} \right) \quad 1$$

where capital  $S$  represents the substrate and lower case  $s$  is the Laplace variable,  $h$  is the number of steps with rate constant  $k_C$ ,  $n$  is the number of steps with rate constant  $k_T$ ,  $k_{NP}$  is the rate of transition from a nonproductive complex to the productive complex, and  $x$  is the fraction of ClpA bound in the productive form given by Eq. (2).

$$x = \frac{[ClpAP \cdot S]_L}{[ClpAP \cdot S]_L + [ClpAP \cdot S]_{NP}} \quad 2$$

Eq. (1) was then numerically solved using Eq. (3) to describe product formation as a function of time,  $S(t)$ ,

$$S(t) = A_T \mathcal{L}^{-1} S(s) \quad 3$$

where  $A_T$  is the total amplitude of the time-course, and  $\mathcal{L}^{-1}$  is the inverse Laplace transform operator. This was accomplished using the NLLS fitting routine, Conlin, and the inverse Laplace transform function using the IMSL C Numerical libraries from Visual Numerics (Houston, TX), as previously described.<sup>26; 29</sup>

The ATP concentration dependence of the rate and rate constant displayed in Figs. 5 a – c was subjected to NLLS analysis using the infinitely cooperative model or the Hill model given by Eq. (4),

$$k_{x,apparent} = \frac{k_{x,max} (K_a [ATP])^t}{1 + (K_a [ATP])^t} \quad 4$$

where  $k_{x,apparent}$  is either the apparent translocation rate constant,  $k_T$ , or the apparent translocation rate,  $mk_T$ ;  $k_{x,max}$  is the maximum microscopic or macroscopic translocation rate constant;  $K_a$  is the association equilibrium constant;  $t$  is the Hill coefficient.

## **Acknowledgements**

We would like to thank Karl Maluf and Clarissa Weaver for critical discussions of this manuscript. We thank Peter Prevelige and the Department of Microbiology for use of the Beckman XL-A analytical ultracentrifuge. We thank Walter Stafford and the Boston Biomedical Research Institute (BBRI) for gifting of a Beckman XL-I analytical ultracentrifuge. This work was supported by NSF grant MCB-0843746 to ALL, National Institute of Biomedical Imaging and Bioengineering (NIBIB) grant number T32EB004312 to JMM, and the University of Alabama at Birmingham Department of Chemistry. The content discussed here is solely the responsibility of the authors and does not necessarily represent the official views of the National Institute of Biomedical Imaging and Bioengineering or the National Institutes of Health.

## References

1. Alberts, B. (1998). The cell as a collection of protein machines: preparing the next generation of molecular biologists. *Cell* **92**, 291-4.
2. Neuwald, A. F., Aravind, L., Spouge, J. L. & Koonin, E. V. (1999). AAA+: A class of chaperone-like ATPases associated with the assembly, operation, and disassembly of protein complexes. *Genome Res* **9**, 27-43.
3. Gottesman, S. (1996). Proteases and their targets in Escherichia coli. *Annu Rev Genet* **30**, 465-506.
4. Sauer, R. T. & Baker, T. A. (2011). AAA+ Proteases: ATP-Fueled Machines of Protein Destruction. *Annual review of biochemistry* **80**, 587-612.
5. Maglica, Z., Kolygo, K. & Weber-Ban, E. (2009). Optimal efficiency of ClpAP and ClpXP chaperone-proteases is achieved by architectural symmetry. *Structure* **17**, 508-16.
6. Maurizi, M. R., Singh, S. K., Thompson, M. W., Kessel, M. & Ginsburg, A. (1998). Molecular properties of ClpAP protease of Escherichia coli: ATP-dependent association of ClpA and clpP. *Biochemistry* **37**, 7778-86.
7. Ishikawa, T., Beuron, F., Kessel, M., Wickner, S., Maurizi, M. R. & Steven, A. C. (2001). Translocation pathway of protein substrates in ClpAP protease. *Proc Natl Acad Sci U S A* **98**, 4328-33.
8. Kress, W., Maglica, Z. & Weber-Ban, E. (2009). Clp chaperone-proteases: structure and function. *Research in microbiology* **160**, 618-28.
9. Hoskins, J. R., Pak, M., Maurizi, M. R. & Wickner, S. (1998). The role of the ClpA chaperone in proteolysis by ClpAP. *Proc Natl Acad Sci U S A* **95**, 12135-40.
10. Licht, S. & Lee, I. (2008). Resolving individual steps in the operation of ATP-dependent proteolytic molecular machines: from conformational changes to substrate translocation and processivity. *Biochemistry* **47**, 3595-605.
11. Thompson, M. W., Singh, S. K. & Maurizi, M. R. (1994). Processive degradation of proteins by the ATP-dependent Clp protease from Escherichia coli. Requirement for the multiple array of active sites in ClpP but not ATP hydrolysis. *J Biol Chem* **269**, 18209-15.

12. Guo, F., Maurizi, M. R., Esser, L. & Xia, D. (2002). Crystal structure of ClpA, an Hsp100 chaperone and regulator of ClpAP protease. *J Biol Chem* **277**, 46743-52.
13. Martin, A., Baker, T. A. & Sauer, R. T. (2008). Pore loops of the AAA+ ClpX machine grip substrates to drive translocation and unfolding. *Nat Struct Mol Biol* **15**, 1147-51.
14. Hinnerwisch, J., Fenton, W. A., Furtak, K. J., Farr, G. W. & Horwich, A. L. (2005). Loops in the central channel of ClpA chaperone mediate protein binding, unfolding, and translocation. *Cell* **121**, 1029-41.
15. Veronese, P. K. & Lucius, A. L. (2010). Effect of Temperature on the Self-Assembly of the Escherichia coli ClpA Molecular Chaperone. *Biochemistry* **49**, 9820-9.
16. Veronese, P. K., Stafford, R. P. & Lucius, A. L. (2009). The Escherichia coli ClpA Molecular Chaperone Self-Assembles into Tetramers. *Biochemistry* **48**, 9221-9233.
17. Singh, S. K. & Maurizi, M. R. (1994). Mutational analysis demonstrates different functional roles for the two ATP-binding sites in ClpAP protease from Escherichia coli. *J Biol Chem* **269**, 29537-45.
18. Weber-Ban, E. U., Reid, B. G., Miranker, A. D. & Horwich, A. L. (1999). Global unfolding of a substrate protein by the Hsp100 chaperone ClpA. *Nature* **401**, 90-3.
19. Reid, B. G., Fenton, W. A., Horwich, A. L. & Weber-Ban, E. U. (2001). ClpA mediates directional translocation of substrate proteins into the ClpP protease. *Proc Natl Acad Sci U S A* **98**, 3768-72.
20. Kolygo, K., Ranjan, N., Kress, W., Striebel, F., Hollenstein, K., Neelsen, K., Steiner, M., Summer, H. & Weber-Ban, E. (2009). Studying chaperone-proteases using a real-time approach based on FRET. *J Struct Biol* **168**, 267-77.
21. Rajendar, B. & Lucius, A. L. (2010). Molecular mechanism of polypeptide translocation catalyzed by the Escherichia coli ClpA protein translocase. *J Mol Biol* **399**, 665-79.
22. Ali, J. A. & Lohman, T. M. (1997). Kinetic measurement of the step size of DNA unwinding by Escherichia coli UvrD helicase. *Science* **275**, 377-80.
23. Fischer, C. J. & Lohman, T. M. (2004). ATP-dependent translocation of proteins along single-stranded DNA: models and methods of analysis of pre-steady state kinetics. *J Mol Biol* **344**, 1265-86.
24. Fischer, C. J., Maluf, N. K. & Lohman, T. M. (2004). Mechanism of ATP-dependent translocation of E.coli UvrD monomers along single-stranded DNA. *J Mol Biol* **344**, 1287-309.

25. Lucius, A. L. & Lohman, T. M. (2004). Effects of temperature and ATP on the kinetic mechanism and kinetic step-size for E.coli RecBCD helicase-catalyzed DNA unwinding. *J Mol Biol* **339**, 751-71.
26. Lucius, A. L., Maluf, N. K., Fischer, C. J. & Lohman, T. M. (2003). General methods for analysis of sequential "n-step" kinetic mechanisms: application to single turnover kinetics of helicase-catalyzed DNA unwinding. *Biophys J* **85**, 2224-39.
27. Lucius, A. L., Vindigni, A., Gregorian, R., Ali, J. A., Taylor, A. F., Smith, G. R. & Lohman, T. M. (2002). DNA unwinding step-size of E. coli RecBCD helicase determined from single turnover chemical quenched-flow kinetic studies. *J Mol Biol* **324**, 409-28.
28. Galletto, R., Jezewska, M. J. & Bujalowski, W. (2004). Unzipping mechanism of the double-stranded DNA unwinding by a hexameric helicase: quantitative analysis of the rate of the dsDNA unwinding, processivity and kinetic step-size of the Escherichia coli DnaB helicase using rapid quench-flow method. *J Mol Biol* **343**, 83-99.
29. Lucius, A. L., Miller, J. M. & Rajendar, B. (2011). Application of the Sequential n-Step Kinetic Mechanism to Polypeptide Translocases. *Methods Enzymol* **488**, 239-64.
30. Jankowsky, E., Gross, C. H., Shuman, S. & Pyle, A. M. (2000). The DExH protein NPH-II is a processive and directional motor for unwinding RNA. *Nature* **403**, 447-51.
31. Kress, W., Mutschler, H. & Weber-Ban, E. (2009). Both ATPase domains of ClpA are critical for processing of stable protein structures. *J Biol Chem* **284**, 31441-52.
32. Veronese, P. K., Rajendar, B. & Lucius, A. L. (2011). Activity of Escherichia coli ClpA Bound by Nucleoside Di- and Triphosphates. *Journal of molecular biology* **409**, 333-47.
33. Wang, J., Hartling, J. A. & Flanagan, J. M. (1997). The structure of ClpP at 2.3 Å resolution suggests a model for ATP-dependent proteolysis. *Cell* **91**, 447-56.
34. Choi, K. H. & Licht, S. (2005). Control of peptide product sizes by the energy-dependent protease ClpAP. *Biochemistry* **44**, 13921-31.
35. Piszczek, G., Rozycki, J., Singh, S. K., Ginsburg, A. & Maurizi, M. R. (2005). The molecular chaperone, ClpA, has a single high affinity peptide binding site per hexamer. *J Biol Chem* **280**, 12221-30.
36. Lohman, T. M. (2010). Clipping along. *J Mol Biol* **399**, 663-4.

37. Hinnerwisch, J., Reid, B. G., Fenton, W. A. & Horwich, A. L. (2005). Roles of the N-domains of the ClpA unfoldase in binding substrate proteins and in stable complex formation with the ClpP protease. *J Biol Chem* **280**, 40838-44.
38. Bohon, J., Jennings, L. D., Phillips, C. M., Licht, S. & Chance, M. R. (2008). Synchrotron protein footprinting supports substrate translocation by ClpA via ATP-induced movements of the D2 loop. *Structure* **16**, 1157-65.
39. Xie, X. S. & Lu, H. P. (1999). Single-molecule enzymology. *J Biol Chem* **274**, 15967-70.
40. Park, J., Myong, S., Niedziela-Majka, A., Lee, K. S., Yu, J., Lohman, T. M. & Ha, T. (2010). PcrA helicase dismantles RecA filaments by reeling in DNA in uniform steps. *Cell* **142**, 544-55.
41. Beuron, F., Maurizi, M. R., Belnap, D. M., Kocsis, E., Booy, F. P., Kessel, M. & Steven, A. C. (1998). At sixes and sevens: characterization of the symmetry mismatch of the ClpAP chaperone-assisted protease. *Journal of structural biology* **123**, 248-59.
42. Guo, F., Esser, L., Singh, S. K., Maurizi, M. R. & Xia, D. (2002). Crystal structure of the heterodimeric complex of the adaptor, ClpS, with the N-domain of the AAA+ chaperone, ClpA. *J Biol Chem* **277**, 46753-62.
43. Farbman, M. E., Gershenson, A. & Licht, S. (2007). Single-Molecule Analysis of Nucleotide-Dependent Substrate Binding by the Protein Unfoldase ClpA. *J Am Chem Soc.*
44. Aubin-Tam, M. E., Olivares, A. O., Sauer, R. T., Baker, T. A. & Lang, M. J. (2011). Single-molecule protein unfolding and translocation by an ATP-fueled proteolytic machine. *Cell* **145**, 257-67.
45. Maillard, R. A., Chistol, G., Sen, M., Righini, M., Tan, J., Kaiser, C. M., Hodges, C., Martin, A. & Bustamante, C. (2011). ClpX(P) generates mechanical force to unfold and translocate its protein substrates. *Cell* **145**, 459-69.
46. Maurizi, M. R., Thompson, M. W., Singh, S. K. & Kim, S. H. (1994). Endopeptidase Clp: ATP-dependent Clp protease from Escherichia coli. *Methods Enzymol* **244**, 314-31.
47. Dam, J., Velikovskiy, C. A., Mariuzza, R. A., Urbanke, C. & Schuck, P. (2005). Sedimentation velocity analysis of heterogeneous protein-protein interactions: Lamm equation modeling and sedimentation coefficient distributions  $c(s)$ . *Biophys J* **89**, 619-34.

48. Schuck, P. (2000). Size-distribution analysis of macromolecules by sedimentation velocity ultracentrifugation and Lamm equation modeling. *Biophysical Journal* **78**, 1606-1619.
49. Straume, M. & Johnson, M. L. (1994). Comments on the analysis of sedimentation equilibrium experiments. In *Modern Analytical Ultracentrifugation* (Schuster TM and Laue TM, e., ed.), pp. p.37-65. Birkhauser, Boston.
50. Kenniston, J. A., Baker, T. A., Fernandez, J. M. & Sauer, R. T. (2003). Linkage between ATP consumption and mechanical unfolding during the protein processing reactions of an AAA+ degradation machine. *Cell* **114**, 511-20.

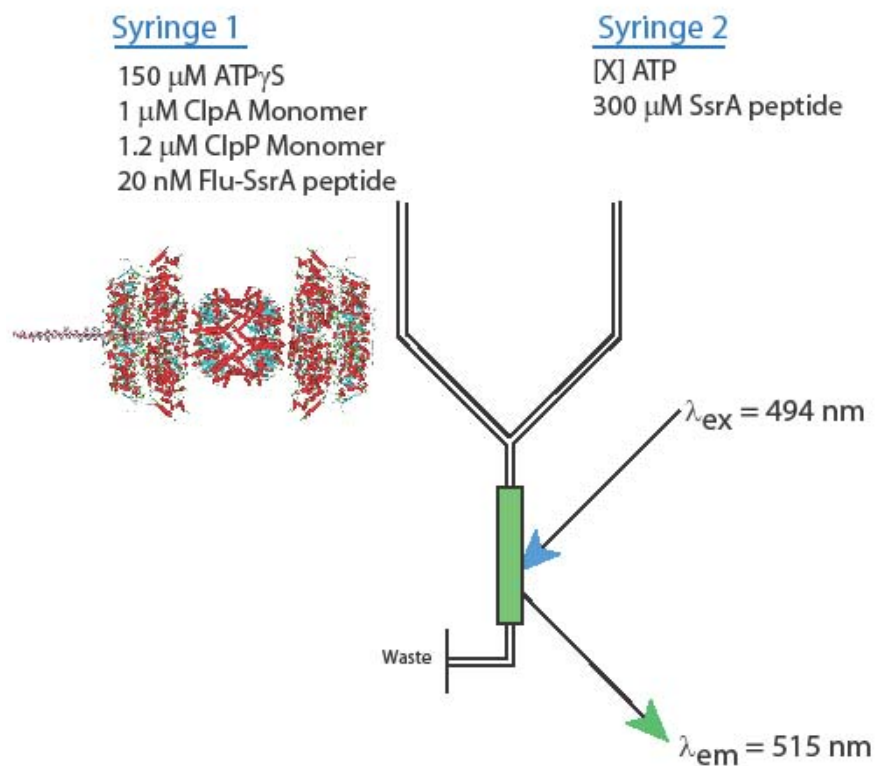


**Figure 1. Schematic representation of single turnover stopped-flow translocation experiments.** Syringe 1 contains the indicated reagents, ClpA, ClpP,  $\text{ATP}\gamma\text{S}$ , and fluorescein-labeled polypeptide. The structure shown illustrates the contents of syringe 1 with the formation of the ClpAP complex with a single polypeptide bound (illustration is a schematic created by superimposing model structures for ClpA, ClpP, and model polypeptide substrate). Syringe 2 contains ATP to fuel polypeptide translocation and 300  $\mu\text{M}$  SsrA peptide to serve as a trap for unbound ClpAP or any ClpAP that dissociates from polypeptide during the course of the reaction. The two reactants are rapidly mixed in the green colored chamber and fluorescein is excited at  $\lambda_{\text{ex}} = 494 \text{ nm}$ . Fluorescein emissions are observed above 515 nm with a 515 nm long pass filter. Upon mixing, the concentrations are two-fold lower than in the preincubation syringe.

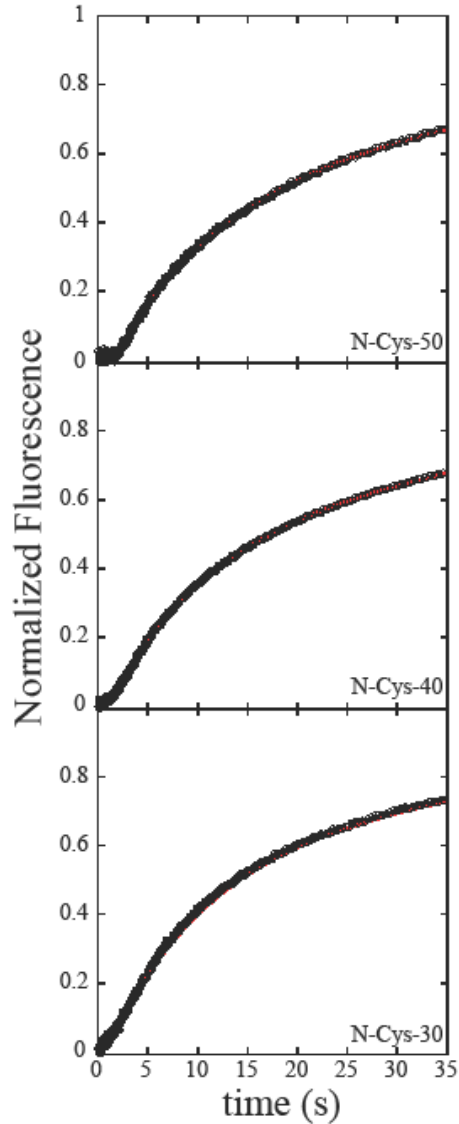


**Figure 2. Fluorescence time-courses for ClpAP catalyzed polypeptide translocation.**

As shown, 1  $\mu\text{M}$  ClpA, 1.2  $\mu\text{M}$  ClpP, 150  $\mu\text{M}$  ATP $\gamma\text{S}$ , and 20 nM fluorescein-labeled polypeptide substrate were pre-assembled prior to rapid mixing with 600  $\mu\text{M}$  ATP and 300  $\mu\text{M}$  SsrA. Shown are time courses for ClpAP catalyzed translocation of N-Cys-50, N-Cys-40, and N-Cys-30 polypeptide substrates. The solid red lines represent a global NLLS fit using Scheme 2 for time-courses collected with substrates I – III in Table 1. The resultant parameters are  $k_T = (4.69 \pm 0.09) \text{ s}^{-1}$ ,  $k_C = (0.12 \pm 0.01) \text{ s}^{-1}$ ,  $k_{NP} = (0.02 \pm 0.002) \text{ s}^{-1}$ ,  $m = (4.6 \pm 0.3) \text{ aa step}^{-1}$ , and  $mk_T = (21.5 \pm 1.1) \text{ aa s}^{-1}$ . Each time-course was analyzed under a given set of conditions by constraining the parameters  $k_T$ ,  $k_C$ ,  $k_{NP}$ , and  $h$  to be global parameters, while  $A_x$ ,  $x_x$ , and  $n_x$  were allowed to float for each polypeptide length, where the subscript ‘x’ represents the polypeptide substrate length.

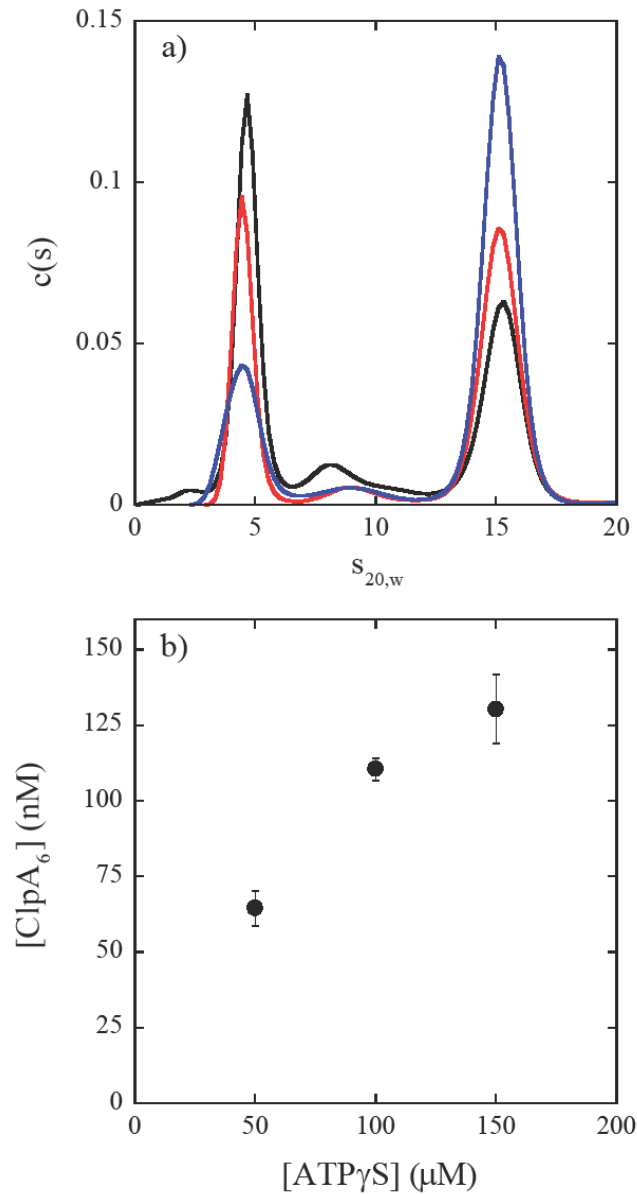


**Figure 3. Sedimentation coefficient distribution,  $c(s)$ , dependence on ATP $\gamma$ S concentration.** a)  $c(s)$  distributions for 1  $\mu\text{M}$  ClpA in the presence of 50 (black), 100 (red), and 150  $\mu\text{M}$  ATP $\gamma$ S from the analysis of sedimentation velocity experiments performed as described in the materials and methods section in Buffer H. b) The concentration of ClpA hexamers was determined from analysis of the  $c(s)$  distributions collected at the three [ATP $\gamma$ S] using a non-interacting discrete species model. For 1  $\mu\text{M}$  ClpA and 150  $\mu\text{M}$  ATP $\gamma$ S, the concentration of ClpA hexamers was determined to be  $[\text{ClpA}_6] = (130 \pm 11)$  nM, which represents the average and standard deviation of eight replicates.

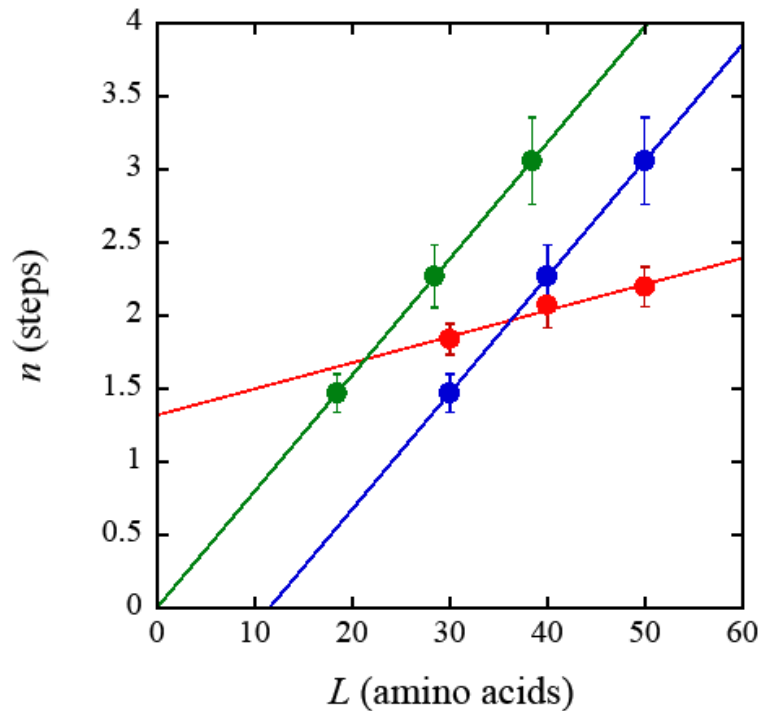


**Figure 4.** The dependence on polypeptide substrate length of the observed number of steps,  $n$ , determined from the analysis of ClpAP polypeptide translocation time-courses shown in Fig. 2. Each time course was analyzed by constraining the parameters  $k_T$ ,  $k_C$ ,  $k_{NP}$ , and  $h$  to be global parameters, while  $A_x$ ,  $x_x$ , and  $n_x$  were allowed to float for each time course. The solid red circles represent the determination of the number of steps,  $n$ , required to describe each time-course in Fig. 2 using Scheme 1 (Eqs. (1) and (3) with  $h=0$ ). The solid red line represents a linear least squares fit with a slope = 0.018 and y-intercept = 1.32. The solid blue circles represent the analysis of each time-course in Fig. 2 using Scheme 2 (Eqs. (1) and (3) with  $h=1$ ). The solid blue line represents a linear least squares fit with a slope = 0.08 and y-intercept = -0.92. The solid green circles represent the analysis of each time-course in Fig. 2 using Scheme 2, but with each polypeptide length lacking the eleven amino acid SsrA sequence in analysis. The solid green line represents a linear least squares fit with a slope = 0.08 and y-intercept =  $1.2 \times 10^{-6}$ .

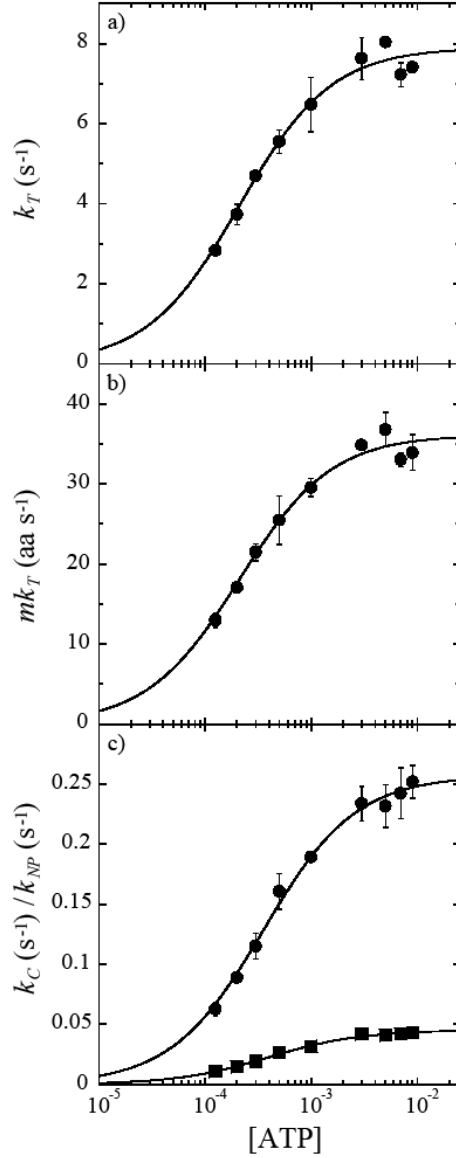


**Figure 5.** a) Dependence of  $k_T$  on [ATP], where the solid line is the result of a NLLS fit to Eq. (4) with the Hill coefficient constrained to equal one for  $k_{T,max} = (7.9 \pm 0.2 s^{-1}) s^{-1}$  and  $K_a = (4.8 \pm 0.5) \times 10^3 M^{-1}$ . b) Dependence of  $mk_T$  on [ATP], where the solid line is the result of a NLLS fit to Eq. (6) with the Hill coefficient constrained to equal one for  $mk_{T,max} = 36.1 \pm 0.7 aa s^{-1}$  and  $K_a = (4.8 \pm 0.5) \times 10^3 M^{-1}$ . c) Dependence of  $k_C$  (solid circles) and  $k_{NP}$  (solid squares) on [ATP], where the solid line is the result of a NLLS fit to Eq. (4) with the Hill coefficient constrained to equal one. For  $k_C$  and  $k_{NP}$ , the equilibrium constant,  $K_a$ , is  $(2.8 \pm 0.1) \times 10^3 M^{-1}$  and  $(2.5 \pm 0.1) \times 10^3 M^{-1}$ , respectively. The analysis of  $k_C$  and  $k_{NP}$  also yielded estimates of the maximum microscopic and macroscopic rates of translocation as  $0.26 \pm 0.003 s^{-1}$  and  $0.045 \pm 0.001 s^{-1}$ , respectively.

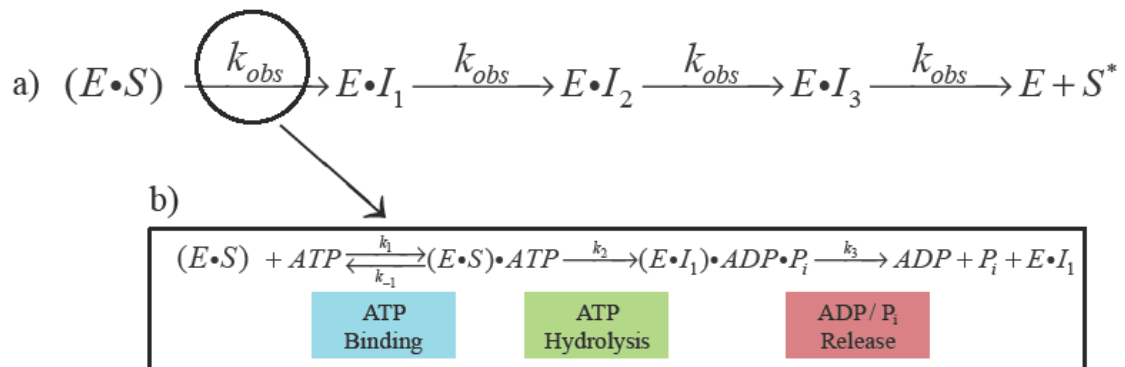


**Figure 6. Schematic representation of polypeptide translocation.** In the n-step sequential model of polypeptide translocation, enzyme that is prebound to polypeptide substrate translocates polypeptide in discrete steps until reaching the end of the substrate and dissociating (a). Polypeptide translocation must occur through repeating cycles of ATP binding, hydrolysis, mechanical movement, various conformational changes, and ADP and Pi release, among other potentially significant kinetic steps (b). The observed rate constant,  $k_{obs}$ , in the single-turnover experiments presented here represents the slowest step within this repeating cycle.

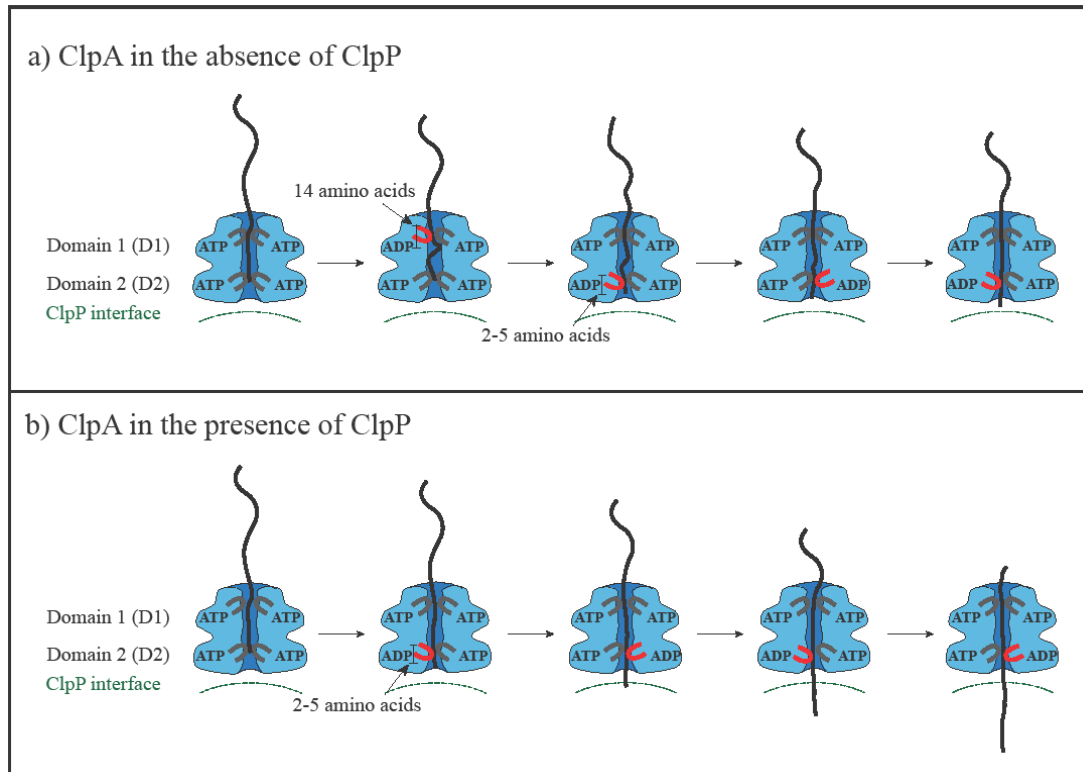
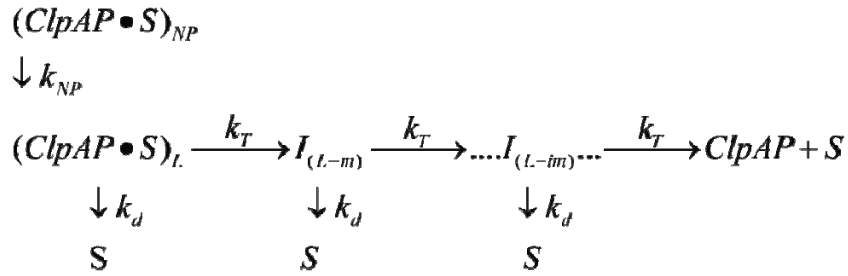
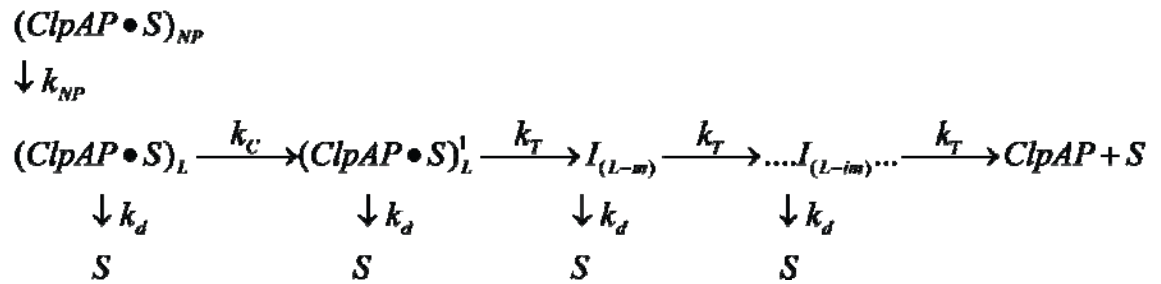


**Figure 7. Proposed model of polypeptide translocation.** In the absence of ClpP, ClpA translocates polypeptide with a mechanism that includes contributions from both ATP binding domains on each ClpA monomer. The D1 domain translocates polypeptide into the central cavity of ClpA by ~14 amino acids. In the time before D1 takes another translocation step, D2 must take three translocation steps of ~5 amino acids per step. Upon association of ClpP, the D1 domain of ClpA undergoes a conformational change such that repeated cycles of ATP binding and hydrolysis no longer take place and the rate of polypeptide translocation is limited by ATP hydrolysis and/or conformational changes taking place at D2 with each translocation step.



**Scheme 1. Simplest sequential n-step model.**  $(ClpAP \bullet S)_L$  and  $(ClpAP \bullet S)_{NP}$  represent ClpAP bound to polypeptide substrate in the productive and nonproductive forms, respectively, and  $S$  is the unbound polypeptide substrate.  $k_T$  is the translocation rate constant,  $k_d$  is the dissociation rate constant,  $L$  is the polypeptide length,  $m$  is the average distance translocated between two steps with rate constant  $k_T$ , and ‘ $i$ ’ in  $I_{(L-im)}$  represents  $i$  number of translocation steps.



**Scheme 2. Sequential  $n$ -step model with slow step relative to  $k_T$ .** All parameters are the same as in Scheme 1, with the exception of  $k_c$ , which represents a step slower than translocation

**Table 1.** Polypeptide translocation Substrates

Substrate	Name	Length (aa)	Sequence
I	N-Cys-50	50	CLILHNKQLGMTGEVSFQAA NTKSAANLKVKELRSKKKLA <b>ANDENYALAA</b>
II	N-Cys40	40	CTGEVSFQAANTKSAANLKV KELRSKKKLA <b>ANDENYALAA</b>
III	N-Cys40	30	CTKSAANLKVKELRSKKKLA <b>ANDENYALAA</b>

\* Fluorescein dye covalently attached to N-terminal cysteine residue

**Table 2.** ClpAP Polypeptide Translocation NLLS Parameters as a Function of [ATP]

[ATP] ( $\mu\text{M}$ )	$k_T$ ( $\text{s}^{-1}$ )	$mk_T$ ( $\text{aa s}^{-1}$ )	$k_C$ ( $\text{s}^{-1}$ )	$k_{NP}$ ( $\text{s}^{-1}$ )	$m$ ( $\text{aa step}^{-1}$ )
125	$1.93 \pm 7.04$	$12.8 \pm 0.9$	$0.06 \pm 0.01$	$0.011 \pm 0.001$	$6.8 \pm 1.9$
200	$4.7 \pm 1.1$	$17.0 \pm 0.1$	$0.09 \pm 0.01$	$0.015 \pm 0.0002$	$3.7 \pm 0.8$
300	$4.9 \pm 3.3$	$20.2 \pm 0.4$	$0.11 \pm 0.02$	$0.019 \pm 0.002$	$5.3 \pm 3.7$
500	$12 \pm 9$	$25.6 \pm 2.9$	$0.152 \pm 0.002$	$0.026 \pm 0.001$	$2.9 \pm 2.4$
750	$9.8 \pm 4.7$	$27.7 \pm 2.1$	$0.17 \pm 0.01$	$0.029 \pm 0.0004$	$3.2 \pm 1.3$
[ATP] (mM)					
1	$9.9 \pm 5.6$	$28.2 \pm 0.7$	$0.18 \pm 0.01$	$0.032 \pm 0.002$	$3 \pm 2$
3	$13.6 \pm 0.02$	$33.4 \pm 2.5$	$0.23 \pm 0.02$	$0.042 \pm 0.003$	$2.5 \pm 0.2$
5	$6.6 \pm 0.9$	$34.9 \pm 1.9$	$0.23 \pm 0.01$	$0.042 \pm 0.002$	$5.3 \pm 1.1$
7	$8.9 \pm 1.9$	$32.8 \pm 0.7$	$0.24 \pm 0.02$	$0.042 \pm 0.003$	$3.7 \pm 0.8$
9	$9.4 \pm 2.8$	$32.8 \pm 1.4$	$0.24 \pm 0.02$	$0.043 \pm 0.001$	$3.7 \pm 1.2$

$k_T$  is the translocation rate constant,  $k_d$  is the dissociation rate constant,  $k_C$  is a slow conformational change defined by Scheme 2,  $m$  is the kinetic step size, and  $mk_T$  is the macroscopic rate of translocation.

**Table 3.** ClpAP Polypeptide Translocation Global NLLS Parameters as a Function of [ATP]

[ATP] ( $\mu\text{M}$ )	$k_T$ ( $\text{s}^{-1}$ )	$mk_T$ ( $\text{aa s}^{-1}$ )	$k_C$ ( $\text{s}^{-1}$ )	$k_{NP}$ ( $\text{s}^{-1}$ )	
125	2.83±0.01	12.96±0.90	0.063±0.006	0.011±0.001	$m$ (AA step <sup>-1</sup> ) 4.58±0.31
200	3.73±0.26	17.04±0.03	0.089±0.004	0.015±0.0002	
300	4.69±0.09	21.47±1.06	0.115±0.011	0.019±0.002	
500	5.55±0.29	25.47±3.06	0.161±0.015	0.026±0.001	
750	6.43±1.39	29.21±4.37	0.174±0.007	0.029±0.001	
[ATP] (mM)					
1	6.48±0.68	29.55±1.11	0.189±0.002	0.032±0.002	$k_d$ ( $\text{s}^{-1}$ )
3	7.63±0.53	34.86±0.07	0.234±0.014	0.042±0.004	ND
5	8.04±0.09	36.80±2.10	0.232±0.018	0.041±0.002	
7	7.23±0.30	33.04±0.88	0.242±0.021	0.042±0.003	
9	7.41±0.02	33.93±2.22	0.252±0.014	0.043±0.0004	

$k_T$  is the translocation rate constant,  $k_d$  is the dissociation rate constant,  $k_C$  is a slow conformational change defined by Scheme 2,  $m$  is the kinetic step size, and  $mk_T$  is the macroscopic rate of translocation.

Chapter Four

ATP $\gamma$ S Competes with ATP for Binding at Domain 1 but not Domain 2 during ClpA  
Catalyzed Polypeptide Translocation

By

Justin M. Miller and Aaron L. Lucius

Submitted to *Journal of Biophysical Chemistry*

Format adapted for dissertation

## Abstract

ATP-dependent proteases catalyze the removal of both misfolded and properly folded proteins in cellular quality control pathways. ClpAP shares structural homology with other ATP-dependent proteases where a hexameric ring of ClpA associates with one or both ends of the cylindrically-shaped protease ClpP, which contains serine protease active sites sequestered in its inner core. ClpA contains two nucleotide binding domains where ATP is bound and hydrolyzed, termed Domain 1 (D1) or 2 (D2). D1 has been shown to be primarily responsible for ClpA oligomerization, while both domains appear to support polypeptide translocation independently. We have previously proposed that D1 or D2 limit the rate of ClpA catalyzed polypeptide translocation when ClpP is either absent or present, respectively. ATP $\gamma$ S is often used to preassemble ClpA hexamers before mixing with ATP to initiate polypeptide translocation. However, the observed reaction is occurring under conditions where ATP and ATP $\gamma$ S may compete for binding to ClpA. Here we show that the rate of ClpA catalyzed polypeptide translocation strongly depends on [ATP $\gamma$ S] in the absence of ClpP, but exhibits no such dependence in the presence of ClpP. We observe that ATP $\gamma$ S non-cooperatively binds to ClpA during polypeptide translocation with an affinity of  $\sim 6 \mu\text{M}$ , but that introduction of ClpP shifts this affinity such that translocation is no longer effected. Interpreting these data in light of our recently proposed model for translocation catalyzed by ClpA vs. ClpAP suggests that ATP $\gamma$ S competes for binding at D1 but not at D2.

## Introduction

AAA+ proteases are a ubiquitous class of ATP-driven enzymes that are required in all organisms for the removal of both misfolded and properly folded proteins as a means of cell cycle regulation.<sup>1; 2</sup> One example is the *E. coli* ATP-dependent protease ClpAP, which targets SsrA-polypeptides that have been tagged via the SsrA-SmpB system for degradation.<sup>3; 4; 5</sup> ClpAP shares structural homology with other ATP-dependent proteases where a hexameric ring of ClpA, a AAA+ protein (ATPases associated with various cellular activities), associates with one or both ends of the cylindrically-shaped protease ClpP, where ClpP contains serine protease active sites sequestered in its inner core away from bulk solvent.<sup>5; 6; 7; 8; 9; 10; 11</sup> Once associated with ClpP, ClpA is responsible for enzyme catalyzed protein unfolding and polypeptide translocation through repeated cycles of ATP binding and hydrolysis.

ClpA is a Class I AAA+ protein unfoldase, which indicates that each monomer contains two nucleotide binding domains. In addition to other conserved domains, each nucleotide binding domain contains the canonical Walker A and Walker B motifs.<sup>2</sup> The two nucleotide binding domains are labeled as Domain 1 or 2, D1 or D2, respectively, and are each thought to serve a particular function. D1 is hypothesized to be primarily responsible for ClpA oligomerization, while D2 is thought to play a larger role in polypeptide translocation.<sup>12; 13</sup> However, variants of ClpA that are deficient in ATP hydrolysis at either D1 or D2 both support polypeptide translocation, which likely indicates that both ATP hydrolysis sites are involved in translocation of polypeptide substrate. One model for polypeptide translocation proposes that loops formed between each Walker A and Walker B motif protrude into the axial channel of hexameric ClpA

and make contact with polypeptide substrates. ATP hydrolysis then modulates up and down movement of the loops thereby translocating the polypeptide chain through the axial channel.<sup>14; 15; 16</sup>

It has been well established that ClpA requires nucleotide binding to assemble into hexameric rings competent for association with ClpP.<sup>6; 17</sup> As a consequence, 1 – 2 mM ATP $\gamma$ S is often used in experiments where there is a need to preassemble ClpA into hexameric rings.<sup>6; 13; 18; 19; 20; 21; 22</sup> In some cases, this preassembled complex is then mixed with hydrolysable ATP and it is assumed that the ATP will exchange with ATP $\gamma$ S, which is likely a good assumption. However, since the experiment is being carried out in the presence of both ATP and ATP $\gamma$ S, the observed reaction is occurring under conditions where ATP and ATP $\gamma$ S may compete for binding to ClpA. For example, in our previous examination of ClpA catalyzed polypeptide translocation, we prebound ClpA to a polypeptide substrate in the presence of 150  $\mu$ M ATP $\gamma$ S.<sup>23</sup> The sample was then rapidly mixed with 10 mM ATP and protein trap, resulting in a final concentration of 75  $\mu$ M ATP $\gamma$ S and 5 mM ATP (see Figure 1 for schematic). In that study, even though the competition between ATP and ATP $\gamma$ S was not well understood, we chose to preincubate ClpA with an initial [ATP $\gamma$ S] of 150  $\mu$ M to minimize the effect of competition between ATP $\gamma$ S and hydrolysable ATP upon rapid mixing of the two reactants, if present. Despite the large excess of ATP over ATP $\gamma$ S, competition between the two nucleotides for binding to ClpA may still occur.

With the objective of eliminating the competing nucleotide, we have also explored a number of other strategies to assemble ClpA to hexamers, prebind ClpA to polypeptide, and initiate polypeptide translocation. For example, we prebound ClpA to

polypeptide in the presence of ATP and absence of  $Mg^{2+}$  and attempted to initiate translocation by rapidly mixing with  $Mg^{2+}$ . However, no translocation was observed (unpublished result). Further, we explored the possibility of assembling ClpA using a number of other nucleotides and nucleotide analogs. These included AMP-PNP, AMP-PCP, ADP, and ADP.BeF. In that study, we showed that only AMP-PNP would assemble a prebound complex that would initiate translocation.<sup>22</sup> However, substantially higher concentrations of AMP-PNP compared to ATP $\gamma$ S are required, which was consistent with previous reports on assembling ClpA with AMP-PNP.<sup>17</sup> Consequently, ATP $\gamma$ S has emerged as the most effective nucleotide analog for preassembling ClpA.

Despite ATP $\gamma$ S being the most effective nucleotide analog to assemble and prebind the complex, several concerns remain. First, ATP $\gamma$ S is slowly hydrolyzed by ClpA. This leads to the question; how fast is ATP $\gamma$ S hydrolyzed and, upon hydrolysis, does ATP $\gamma$ S provide sufficient energy to drive polypeptide translocation in the preincubation syringe? If this occurs, the population of enzyme may not all be bound at the SsrA tag at the carboxy terminus in the pre-incubation syringe (see syringe 1, Fig. 1). Rather, the enzyme may be distributed randomly on the polypeptide substrate upon rapid mixing with ATP. Second, does competition between ATP $\gamma$ S and ATP binding impact the reported kinetic parameters?

Here we report an examination of the effect of the ATP analogue, ATP $\gamma$ S, on ClpA catalyzed polypeptide translocation in both the presence and absence of ClpP. We have employed our previously developed single turnover stopped-flow method to examine the kinetic parameters of ClpA catalyzed polypeptide translocation as a function of increasing ATP $\gamma$ S concentrations.<sup>23; 24</sup> Our results show that in the presence of 1 mM

ATP $\gamma$ S, the rate of polypeptide translocation is affected by competition between ATP $\gamma$ S and hydrolysable ATP binding to ClpA. However, this effect is not present upon addition of ClpP. These observations, when incorporated with our proposed mechanism for ClpA and ClpAP catalyzed polypeptide translocation<sup>25</sup>, suggest that ATP $\gamma$ S competes for ATP binding at the D1 ATP binding site and therefore impacts polypeptide translocation catalyzed by ClpA in the absence of ClpP. No competition between ATP and ATP $\gamma$ S was observed when ClpP was present. Therefore, ATP $\gamma$ S does not appear to effectively compete for binding at the D2 ATP binding site.

## Results

### *Kinetics of ATP $\gamma$ S Hydrolysis Catalyzed by ClpA*

We first set out to determine the steady-state kinetic parameters,  $K_m$  and  $k_{cat}$ , for ClpA catalyzed ATP $\gamma$ S hydrolysis. Experiments were performed by mixing 10  $\mu$ M ClpA monomer with ATP $\gamma$ S supplemented with <sup>35</sup>S-ATP $\gamma$ S (see Materials and Methods). The total ATP $\gamma$ S concentration was varied between 100  $\mu$ M and 1 mM. The initial velocity as a function of the total [ATP $\gamma$ S] is shown in Fig. 2a. The relationship between initial velocity and nucleotide concentration was subjected to NLLS analysis using Eq. (1) to obtain estimates of the Michaelis constant,  $K_m = (134 \pm 46)$   $\mu$ M, and the turnover number,  $k_{cat} = (0.05 \pm 0.004)$   $\text{min}^{-1}$ . Fig. 2a shows that ClpA hydrolyses ATP $\gamma$ S, albeit slowly.

The observation that ClpA hydrolyses ATP $\gamma$ S leads to the question; does hydrolysis of ATP $\gamma$ S provide sufficient energy to fuel polypeptide translocation? If

ATP $\gamma$ S does provide sufficient energy for ClpA to translocate, then this would predict that not all of the ClpA in syringe 1 of Fig. 1 would be statically bound at the carboxy terminus of SsrA-tagged polypeptides. Rather, some molecules may have moved forward by some number of steps. If true, we would predict that the observed time courses would change depending on the amount of time the contents of syringe 1 (see Fig. 1) were allowed to incubate before rapid mixing with the contents of syringe 2. To test this, we collected time courses at various different incubation times. Since the two reactants are rapidly mixed together, a time course is collected over a 400 s time period, and up to ten time courses are collected, the contents of syringe 1 (Fig. 1) are allowed to incubate for up to 4,000 s or 70 minutes by the time the last time course is collected. Fig. 2b shows two time courses collected using the experimental design schematized in Fig. 1, where 1  $\mu$ M ClpA monomer has been allowed to incubate in the presence of 5 mM ATP $\gamma$ S and 100 nM fluorescein-labeled polypeptide for either ~15 (solid blue circles) or ~70 minutes (solid red circles) before mixing with ATP and SsrA peptide (pre-mixing concentrations).

If ATP $\gamma$ S hydrolysis provided enough energy to fuel polypeptide translocation, the extent of the lag would be expected to be decreased or nonexistent after ClpA had been incubated in the presence of 5 mM ATP $\gamma$ S and polypeptide for ~70 minutes. However, the time courses in Fig. 2b demonstrate that the extent of lag and the overall shape of the time courses are identical after 15 and 70 minutes of incubation in the presence of ATP $\gamma$ S. Thus, ClpA catalyzed hydrolysis of ATP $\gamma$ S does not impact the observed time courses for polypeptide translocation over this length of time. Furthermore, the contents of syringe 1 in Fig. 1 must represent a homogenous population of hexamers bound to the SsrA sequence at the carboxy terminus.

### *Competition between ATP and ATP $\gamma$ S*

Preassembling ClpA into hexameric rings using ATP $\gamma$ S is required to perform the single-turnover polypeptide translocation experiments reported here and previously.<sup>6; 9; 13; 16; 18; 19; 21; 22; 23</sup> Upon rapid mixing with hydrolysable ATP, it is likely that ATP $\gamma$ S and ATP compete for binding to ClpA. Moreover, this competition may impact the observed kinetic parameters. To elucidate the impact of the competition between ATP and ATP $\gamma$ S on the kinetic parameters, polypeptide translocation experiments were performed as a function of [ATP $\gamma$ S] by varying the concentration of ATP $\gamma$ S in the preincubation syringe (see Fig. 1, syringe 1).

Single turnover polypeptide translocation experiments were performed as described previously and in Materials and Methods.<sup>23; 24; 25</sup> Syringe 1 of the stopped-flow is loaded with a solution containing 1  $\mu$ M ClpA monomer, 100 nM fluorescein modified polypeptide substrate, and varying concentrations of ATP $\gamma$ S (see Fig. 1). Under the conditions illustrated in Fig. 1, the final mixing concentrations of ATP $\gamma$ S and ATP are 75  $\mu$ M and 5 mM, respectively. Thus, the resultant time courses represent polypeptide translocation under conditions where ATP $\gamma$ S and ATP could compete for binding to ClpA.

Syringe 2 is loaded with a solution containing 10 mM ATP and 200  $\mu$ M SsrA. The inclusion of a non-fluorescently modified SsrA polypeptide in syringe 2 serves as a protein trap that insures single-turnover conditions. Upon mixing of the contents of the two syringes, free ClpA or any ClpA that dissociates will rapidly bind the non-fluorescent SsrA trap, thus insuring that the observed signal is only sensitive to ClpA that was bound

prior to mixing. Reaction progress is monitored by exciting fluorescein at 494 nm and observing the emission at 515 nm and above using a 515 nm long pass filter.

Fig. 3 shows a representative set of time courses for translocation of ClpA on a set of polypeptide substrates that differ only in length in the presence of final mixing concentrations of 75  $\mu\text{M}$  (green circles), 600  $\mu\text{M}$  (blue circles) and 2.5 mM (red circles)  $\text{ATP}\gamma\text{S}$  in the presence of a final concentration of 5 mM ATP. From qualitative inspection of the time courses shown in Fig. 3, it is clear that the rate of translocation is slowed with each increase in  $[\text{ATP}\gamma\text{S}]$ . However, it is unclear if the apparent decrease in translocation rate is an effect of a change in the microscopic rate constants, kinetic step-size, or both.

#### *Global NLLS analysis of translocation data*

To quantify the effect of competition between ATP and  $\text{ATP}\gamma\text{S}$  for binding to ClpA, single-turnover stopped-flow fluorescence experiments were performed as illustrated in Fig. 1. Experiments were carried out with substrates I-III (see Table 1) at final  $\text{ATP}\gamma\text{S}$  concentrations of 75, 126, 250, 355, and 600  $\mu\text{M}$ , and 1, 1.8, and 2.5 mM. Each set of time courses for three polypeptide lengths at a fixed  $\text{ATP}\gamma\text{S}$  concentration was subjected to NLLS analysis to determine the parameters  $k_T$ ,  $m$ ,  $mk_T$ ,  $k_C$ , and  $k_{NP}$ . The data were well described by Scheme 1 at all  $[\text{ATP}\gamma\text{S}]$ , and the resultant parameters are given in Table 2.

The macroscopic rate,  $mk_T$ , and the elementary rate constant,  $k_T$ , decrease with increasing  $[\text{ATP}\gamma\text{S}]$  (see Fig. 4a-b). We previously reported a cooperative dependence of  $mk_T$  and  $k_T$  on  $[\text{ATP}]$  for ClpA catalyzed polypeptide translocation.<sup>23</sup> Consistently, those data were well described by an infinitely cooperative binding model with a Hill

coefficient of  $\sim 2.5$ . In contrast, the dependencies of the kinetic parameters on  $[\text{ATP}\gamma\text{S}]$  do not appear to exhibit isotherms consistent with cooperative binding of  $\text{ATP}\gamma\text{S}$  (see Fig. 4 a-b). That is to say, from a qualitative inspection of the curves, the decreases in rate and rate constant with increasing  $[\text{ATP}\gamma\text{S}]$  do not appear particularly steep.

To determine if cooperativity is present, the dependences of  $mk_T$  and  $k_T$  on  $[\text{ATP}\gamma\text{S}]$  were subjected to NLLS analysis using an infinitely cooperative competition binding model given by Eq. (5) (see Materials and Methods section). In Eq. (5), the parameters that define ATP binding were constrained to the previously determined values, specifically,  $K_{\text{ATP}} = 1.9 \times 10^3 \text{ M}^{-1}$  ( $K_{d,\text{ATP}} = 526 \text{ }\mu\text{M}$ ) or  $1.8 \times 10^3 \text{ M}^{-1}$  ( $K_{d,\text{ATP}} = 556 \text{ }\mu\text{M}$ ), the Hill coefficient for ATP binding,  $\nu = 2.5$  or  $2.2$ , for  $mk_T$  or  $k_T$ , respectively and  $[\text{ATP}] = 5 \text{ mM}$ . The floating parameters are the binding constant for  $\text{ATP}\gamma\text{S}$ ,  $K_{\text{ATP}\gamma\text{S}}$ , the Hill coefficient for  $\text{ATP}\gamma\text{S}$  binding,  $\omega$ , and the maximum translocation rate or rate constant,  $mk_{T,\text{max}}$  or  $k_{T,\text{max}}$ , respectively. For the analysis of  $mk_T$  and  $k_T$  (see Fig. 4a-b) the Hill coefficient for  $\text{ATP}\gamma\text{S}$  was found to be  $\omega = 0.88 \pm 0.03$  and  $\omega = 1.2 \pm 0.2$ , respectively. Since the values are close to one it was concluded that there is not significant cooperativity. Thus, the analysis was performed with the Hill coefficient for  $\text{ATP}\gamma\text{S}$  binding constrained to one, i.e.  $\omega = 1$  in Eq. (5). For the analysis of  $mk_T$  (see Fig. 4a), estimates of the parameters were found to be  $K_{\text{ATP}\gamma\text{S}} = (160 \pm 7) \times 10^3 \text{ M}^{-1}$  ( $K_{d,\text{ATP}\gamma\text{S}} = (6.2 \pm 0.3) \text{ }\mu\text{M}$ ), and  $mk_{T,\text{max}} = (21.6 \pm 0.2) \text{ aa s}^{-1}$ .

The microscopic translocation rate constant,  $k_T$ , is plotted as a function of  $[\text{ATP}\gamma\text{S}]$  in Fig. 4b. Similar to  $mk_T$ , the relationship between  $k_T$  and  $[\text{ATP}\gamma\text{S}]$  was subjected to NLLS analysis using Eq. (5) with  $\omega = 1.0$ . From this analysis the parameters  $K_{\text{ATP}\gamma\text{S}}$  and  $k_{T,\text{max}}$  were found to be  $(104 \pm 13) \times 10^3 \text{ M}^{-1}$  ( $K_{d,\text{ATP}\gamma\text{S}} = (10 \pm 1) \text{ }\mu\text{M}$ ) and

$(1.39 \pm 0.05) \text{ s}^{-1}$ , respectively. The analysis of both  $mk_T$  and  $k_T$  shows that ATP $\gamma$ S binds to ClpA with nearly 100-fold greater affinity than ATP, but does so non-cooperatively.<sup>23</sup> This either indicates that the cooperativity is reduced in the presence of ATP $\gamma$ S or that ATP $\gamma$ S only binds to one of the two nucleotide binding sites on the ClpA monomer.

The kinetic step-size is plotted as a function of [ATP $\gamma$ S] in Fig. 4c and shows no significant dependence upon ATP $\gamma$ S concentration between 75  $\mu$ M and 1 mM. However, at the two highest ATP $\gamma$ S concentrations, the parameter is between 20 and 24 aa step<sup>-1</sup> with large uncertainty. The kinetic step-size averaged over all eight ATP $\gamma$ S concentrations is  $m = (18 \pm 3) \text{ aa step}^{-1}$ , which is within error of our previously reported value of  $m = (14 \pm 1) \text{ aa step}^{-1}$  independent of [ATP].<sup>23</sup> At the two highest [ATP $\gamma$ S], 1.8 and 2.5 mM, the kinetic step-size is observed to increase. If these two data points are removed from the determination of the average, then  $m = (16.3 \pm 0.5) \text{ aa step}^{-1}$ .

#### *Impact of Parameter Correlation on the Determination of the Kinetic Parameters*

We and others have previously reported that the elementary rate constant,  $k_T$ , and the kinetic step-size,  $m$ , are negatively correlated.<sup>23; 26; 27; 28</sup> Because of this, under certain conditions it can be difficult to simultaneously determine both parameters. However, the overall rate of translocation,  $mk_T$ , contains less parameter correlation and tends to be a parameter that can be determined with higher precision.<sup>28; 29</sup> This is a consequence of the fact that the overall rate,  $mk_T$ , represents the product of the kinetic step-size,  $m$ , and the elementary rate constant,  $k_T$ . In this study, both  $mk_T$  and  $k_T$  follow the same trend and are both well described by the same model. Thus, we asked the question; is the deviation in the kinetic step-size observed at high [ATP $\gamma$ S] a consequence of parameter correlation (See Fig. 4c)?

To assess the parameter correlation between the rate constant and the kinetic step-size, we performed Monte Carlo simulations (see Materials and Methods). Fig. 5a is a plot of the translocation rate constant versus the kinetic step-size from two representative Monte Carlo simulations from polypeptide translocation experiments collected in the presence of 75  $\mu\text{M}$  (solid blue spheres) and 2.5 mM (solid red spheres) ATP $\gamma$ S and a fixed [ATP] = 5 mM. Consistent with our previous report, in both cases,  $k_T$  and  $m$  are negatively correlated based on the observation of a negative slope (see Fig. 5a), where the slope represents the correlation coefficient. However, the 75  $\mu\text{M}$  data exhibits a slope of  $-0.096 \pm 0.001$  and the 2.5 mM data exhibits a slope of  $-0.0148 \pm 0.0005$ . If the two parameters had the same degree of correlation, one would expect the correlation coefficient to be -1. However, at both low and high [ATP $\gamma$ S], the correlation coefficient is less than one, in this case, indicating that the kinetic step-size is less well constrained than the elementary rate constant. Furthermore, the observation of different correlation coefficients predicts a different degree of parameter correlation for data collected at low vs. high ATP $\gamma$ S concentrations. That is to say, for each incremental change in the elementary rate constant, a relatively large change in the kinetic steps-size will occur for the shallow slope exhibited at 2.5 mM ATP $\gamma$ S.

To assess how well the kinetic step-size is constrained, we examined the sum of the squared residuals (SSR) as a function of fixed values of the kinetic step-size for the two sets of data (see Fig. 5b). The minimum of these plots represent the best estimates of the kinetic step-size under conditions of 75  $\mu\text{M}$  ATP $\gamma$ S (solid blue line) or 2.5 mM ATP $\gamma$ S (dashed red line). For plotting purposes, we have subtracted the value of the SSR at the minimum of each curve from each data point so the bottom of the parabola is close

to zero (see Fig. 5b). Although both curves exhibit the expected concave up parabolic shape, the 2.5 mM ATP $\gamma$ S data exhibits a parabola with a broader minimum than the 75  $\mu$ M ATP $\gamma$ S data. This observation is consistent with the slopes in the  $k_T$  vs.  $m$  plot shown in Fig. 5a. That is to say, a broad minimum in the parabola indicates that a wide range of kinetic step-sizes yield very similar SSR values.

In order to determine how well the elementary rate constant is constrained, we examined SSR as a function of fixed values of  $k_T$  using the same methodology as applied to the assessment of the kinetic step-size. Similar to Fig. 5b, Fig. 5c shows a plot of SSR versus  $k_T$  for both the 75  $\mu$ M ATP $\gamma$ S (solid green line) and 2.5 mM ATP $\gamma$ S (solid red line) data sets. Both curves exhibit the expected concave up parabolic shape corresponding to the best estimate of the elementary rate constant. From the minimum of each parabola, Fig. 5c shows that the minima in the SSR vs.  $k_T$  plot is 1.2 s<sup>-1</sup> and 0.4 s<sup>-1</sup> for 75  $\mu$ M and 2.5 mM ATP $\gamma$ S, respectively. However, the parabola corresponding to the 75  $\mu$ M ATP $\gamma$ S dataset is observed to have a broader minimum than observed for the 2.5 mM ATP $\gamma$ S dataset, which is opposite to what was observed in the SSR vs. step-size plot in Fig 5b. Thus, the elementary rate constant is better constrained at 2.5 mM ATP $\gamma$ S in comparison to 75  $\mu$ M ATP $\gamma$ S, whereas the kinetic step-size is better constrained at 75  $\mu$ M ATP $\gamma$ S and less well constrained at 2.5 mM ATP $\gamma$ S. These observations are consistent with the initial predictions made from the plot of  $k_T$  versus  $m$  shown in Fig. 5a.

For reasons that are not entirely clear, these results indicate that at elevated [ATP $\gamma$ S], there is a change in the parameter correlation relative to low [ATP $\gamma$ S]. The consequence of this change is a reduced ability to uniquely determine the kinetic step-

size at high [ATP $\gamma$ S]. Although the elementary rate constant is better constrained at high ATP $\gamma$ S concentrations, it is adequately constrained under both conditions.

#### *ClpAP catalyzed polypeptide translocation*

We recently reported that the kinetic step-size for ClpA when ClpP is present, i.e. ClpAP, is  $(4.6 \pm 0.3)$  aa step<sup>-1</sup> compared to  $(14 \pm 1)$  aa step<sup>-1</sup> for ClpA in the absence of ClpP.<sup>23</sup> Similarly, the translocation rate constant and the overall translocation rate were found to be  $(7.9 \pm 0.2)$  s<sup>-1</sup> and  $(36.1 \pm 0.7)$  aa s<sup>-1</sup>, respectively, for ClpAP compared to ClpA alone where  $k_T = (1.39 \pm 0.06)$  s<sup>-1</sup> and  $mk_T = (19.5 \pm 0.7)$  aa s<sup>-1</sup>.<sup>23; 25</sup> Moreover, the rate and rate constant for ClpA in the absence of ClpP exhibit a cooperative dependence on ATP concentration, whereas, ClpAP appears to depend non-cooperatively on ATP concentration. Since the molecular mechanisms for ClpA and ClpAP are emerging to be so different, we asked the question; does ClpAP exhibit the same dependence on [ATP $\gamma$ S] as ClpA in the absence of ClpP?

Single-turnover fluorescence stopped-flow experiments were performed as described in Fig. 1 with the modification that 1.2  $\mu$ M ClpP was added to syringe 1 (see Fig. 1). Experiments were performed with substrates I-III at final ATP $\gamma$ S concentrations of 75, 250, 500, 750 and 1000  $\mu$ M. All data were subjected to global NLLS analysis to determine the parameters  $k_T$ ,  $m$ ,  $mk_T$ ,  $k_C$ , and  $k_{NP}$  for each set of polypeptide lengths at each [ATP $\gamma$ S]. The data were well described by Scheme 1 at each [ATP $\gamma$ S]. The resultant parameters are summarized in Table 3 and plotted in Fig. 4d–f. Strikingly, the rate of translocation,  $mk_T$ , does not exhibit any dependence on ATP $\gamma$ S concentration. On the other hand, the three low ATP $\gamma$ S concentrations exhibit a rate constant,  $k_T$ , between 6 – 8 s<sup>-1</sup> within error of the value we have previously reported (see Fig. 4e). However, the rate

constant drops to between  $2 - 4 \text{ s}^{-1}$  at the two highest ATP $\gamma$ S concentrations. Similarly, the kinetic step-size also increases from a value of  $\sim 5 \text{ aa step}^{-1}$  to values of  $\sim 14$  and  $10 \text{ aa step}^{-1}$  at the two highest ATP $\gamma$ S concentrations. The observed change in the rate constant and kinetic step-size at  $750 \text{ }\mu\text{M}$  and  $1 \text{ mM}$  ATP $\gamma$ S is likely a consequence of parameter correlation since these two parameters are negatively correlated. Consistent with negative parameter correlation, the observed rate constant is observed to decrease and the kinetic step-size increase at the two highest concentrations of ATP $\gamma$ S. Also consistent with parameter correlation, the overall rate of translocation,  $mk_T$  is not observed to depend on ATP $\gamma$ S over the range of [ATP $\gamma$ S] where both  $k_T$  and  $m$  do appear to change.

To determine whether the parameter correlation between the elementary rate constant and kinetic step-size is the same for both ClpA and ClpAP, we performed Monte Carlo simulations using ClpAP polypeptide translocation time courses. A plot of the resulting translocation rate constants versus the kinetic steps-size is shown in Fig. 6a, where representative Monte Carlo simulations are shown from polypeptide translocation experiments collected in the presence of  $75 \text{ }\mu\text{M}$  (solid blue spheres) and  $1 \text{ mM}$  (solid red spheres) ATP $\gamma$ S. As expected, the two parameters are negatively correlated for both  $75 \text{ }\mu\text{M}$  and  $1 \text{ mM}$  ATP $\gamma$ S. However, the correlation coefficients observed for ClpAP are different from the correlation coefficients observed for ClpA in the absence of ClpP (See Fig. 6a). For ClpAP, the  $75 \text{ }\mu\text{M}$  ATP $\gamma$ S data exhibit a slope of  $-0.97 \pm 0.01$  and the  $1 \text{ mM}$  ATP $\gamma$ S data exhibit a slope of  $-0.258 \pm 0.004$ . Unlike ClpA in the absence of ClpP, ClpAP exhibits nearly 1:1 parameter correlation between  $m$  and  $k_T$  at  $75 \text{ }\mu\text{M}$  ATP $\gamma$ S. Although the correlation coefficient decreases to  $\sim -0.26$  at  $1 \text{ mM}$  ATP $\gamma$ S, this correlation

coefficient is approximately an order of magnitude larger than the correlation coefficient exhibited by ClpA in the absence of ClpP of  $\sim -0.015$ .

Fig. 6a predicts that the kinetic step-size should be better constrained at  $75 \mu\text{M}$  ATP $\gamma$ S relative to  $1 \text{ mM}$  ATP $\gamma$ S. To test this hypothesis, we examined the SSR as a function of fixed values of the kinetic step-size for the two sets of data (see Fig. 6b). For plotting purposes, we have again subtracted the value of the SSR at the minimum of each curve from each data point so the bottom of the parabola is close to zero (see Fig. 6b). For both datasets, the plots of SSR versus  $m$  exhibit the concave up parabolic shape that allows for the determination of the best estimate of the kinetic step-size. Although there is a decrease in the correlation coefficient of  $k_T$  vs.  $m$  in Fig. 6a, visually, there is not a substantial difference in the broadness of the minimum in the two SSR vs.  $m$  plots shown in Fig. 6b. From the minima shown in Fig. 6b, the best estimate of the kinetic step-size is  $m = 4.8$  or  $11.2 \text{ aa step}^{-1}$  for  $75 \mu\text{M}$  or  $1 \text{ mM}$  ATP $\gamma$ S, respectively.

To assess how well the elementary rate constant for ClpAP catalyzed polypeptide translocation is constrained under conditions of  $75 \mu\text{M}$  ATP $\gamma$ S and  $1 \text{ mM}$  ATP $\gamma$ S, we examined SSR as a function of fixed values of  $k_T$ . Fig. 6c clearly shows that both curves exhibit the expected concave up shape. The parabola corresponding to the  $75 \mu\text{M}$  ATP $\gamma$ S dataset (solid blue line) is observed to have a broader minimum than observed for the  $1 \text{ mM}$  ATP $\gamma$ S dataset (dashed red line). From this analysis the best estimate of the elementary rate constant is  $5.9 \text{ s}^{-1}$  and  $2.7 \text{ s}^{-1}$  for  $75 \mu\text{M}$  and  $1 \text{ mM}$  ATP $\gamma$ S, respectively.

For both ClpA alone and for ClpA in the presence of ClpP, the degree of parameter correlation between  $k_T$  and  $m$  changes at the highest ATP $\gamma$ S concentrations. However, this transition is not observed to be as dramatic for ClpAP as it is for ClpA in

the absence of ClpP. Although the kinetic parameters for ClpAP exhibit little ATP $\gamma$ S concentration dependence between 75  $\mu$ M and 500  $\mu$ M ATP $\gamma$ S some impact on the kinetic parameters is beginning to occur above 1 mM ATP $\gamma$ S (see Fig. 4d–f).

## Discussion

Including ours, many studies on proteolytic degradation by ClpAP and translocation by ClpA have reported results that come from experiments performed in the presence of ATP $\gamma$ S and ATP.<sup>8; 19; 21; 22; 23; 30</sup> However, the potential competition between the nucleotide analogue and ATP has not been addressed. The question is; does the inclusion of a particular ATP-analogue affect the polypeptide binding or translocation activities of ClpA? We have previously reported that the nucleotide analogues ATP $\gamma$ S, AMP-PNP, AMP-PCP, ADP.BeF, and ADP promote the formation of ClpA hexamers, but only ATP $\gamma$ S and AMP-PNP promote the formation of ClpA hexamers that are active in both polypeptide binding and translocation.<sup>22</sup> However, to fully populate hexamers, we,<sup>22</sup> and others,<sup>17</sup> have observed that higher concentrations of AMP-PNP are required relative to ATP $\gamma$ S. For this reason, ATP $\gamma$ S appears to be the only choice for efficiently pre-assembling and binding ClpA to a polypeptide substrate.

We previously reported an elementary rate constant,  $k_T = (1.39 \pm 0.06) \text{ s}^{-1}$ , and overall rate,  $mk_T = (19.4 \pm 1.3) \text{ aa s}^{-1}$ , for ClpA catalyzed polypeptide translocation in the presence of 5 mM ATP and 75  $\mu$ M ATP $\gamma$ S.<sup>23</sup> By examining the ATP $\gamma$ S concentration dependence of these parameters and extrapolating to zero ATP $\gamma$ S, here we have shown that the  $k_T = (1.39 \pm 0.05) \text{ s}^{-1}$  and  $mk_T = (21.6 \pm 0.2) \text{ aa s}^{-1}$  in the presence of 5 mM ATP. Thus, these parameters are within error of our previous report.<sup>23</sup> Consequently, we

conclude that the kinetic parameters previously reported reflect translocation under conditions where there is little to no competition between ATP and ATP $\gamma$ S. The same conclusion is drawn for ClpAP, since we have shown here that ClpA in the presence of ClpP exhibits no dependence on [ATP $\gamma$ S].

*Model for Polypeptide Translocation catalyzed by ClpA vs. ClpAP*

The strength of the single-turnover experiments applied here is that the kinetic time-courses are sensitive to the events in the active site of the enzyme and are not affected by macromolecular assembly or polypeptide binding. However, they are single-turnover with respect to polypeptide and multiple turnover with respect to ATP. That is to say, multiple rounds of ATP binding and hydrolysis are occurring during a single round of polypeptide translocation. Based on the observation of a lag in the single turnover kinetic time courses for polypeptide translocation, we can conclude that multiple steps with similar or the same rate constants are occurring before the enzyme dissociates.

For a motor protein to translocate a linear lattice, repetitive cycles of similar events must occur. At a minimum, this cycle must include ATP binding, hydrolysis, mechanical movement, ADP and Pi release, and likely conformational changes. The single turnover experiments performed here are sensitive to the slowest repeating step in each of these cycles.

We have shown that, for both ClpA and ClpAP, the observed rate constant reflects a repeating step that immediately follows an ATP binding event within a cycle of translocation.<sup>23; 25</sup> However, for ClpA this step repeats every ~14 amino acids translocated with an observed rate constant of ~1.39 s<sup>-1</sup> and for ClpAP this step repeats every ~2 – 5 amino acids translocated with an observed rate constant of ~6.6 s<sup>-1</sup>. We

have hypothesized that the rate limiting step that we observe for ClpA in the absence of ClpP is coupled to ATP hydrolysis site D1, and, when ClpP is present, the observed repeating rate-limiting step is coupled to D2. This hypothesis is based on our examination of the ATP concentration dependence of both the observed rate constant and the kinetic step-size,<sup>23; 25</sup> steady state ATP hydrolysis rates from Weber-Ban and coworkers,<sup>13</sup> and crosslinking experiments from Horwich and coworkers.<sup>16</sup>

To perform the single-turnover experiments reported here, we pre-bind ClpA to the polypeptide substrate. This is done to eliminate any effects on the kinetic time courses due to macromolecular assembly and polypeptide binding. To accomplish this, we must include a nucleotide analog to form hexameric rings competent for polypeptide binding.<sup>22</sup> In an attempt to eliminate the competing nucleotide analog, we have explored initiating translocation in a variety of other ways. For example, we have prebound ClpA to polypeptide in the presence of ATP and absence of  $Mg^{2+}$  and attempted to initiate translocation by rapidly mixing with  $Mg^{2+}$ . However, no translocation was observed (unpublished result). In summary, we have found that ATP $\gamma$ S is the best and possibly the only practical option for pre-assembling and pre-binding ClpA to the polypeptide. Since we are “stuck” with ATP $\gamma$ S in these experiments, some of the experiments reported here were initiated to control for the fact that ATP $\gamma$ S may compete with ATP during repeating cycles of polypeptide translocation. Surprisingly, the results yielded insight into the differences in the molecular mechanism for ClpA vs. ClpAP catalyzed polypeptide translocation.

The examination of polypeptide translocation catalyzed by ClpA in the absence of ClpP as a function of [ATP $\gamma$ S] reveals that increasing concentrations of ATP $\gamma$ S slows

down polypeptide translocation, which is an observation that has been reported.<sup>31</sup> Such an observation is not surprising and indicates that there is competition between ATP and ATP $\gamma$ S binding. More importantly, it indicates that there is competition between ATP and ATP $\gamma$ S at the ATP binding site that is responsible for coupling ATP binding and hydrolysis to polypeptide translocation.

As stated above, we have previously concluded that the repeating rate limiting step that limits the observation of translocation, in the absence of ClpP, is occurring at the D1 ATPase site. Thus, the competition between ATP and ATP $\gamma$ S is likely occurring at the D1 ATPase site. Further, the dependence of the rate and the observed rate constant on ATP exhibits a Hill coefficient of  $\sim 2.2$  and  $2.5$ , respectively. This indicates that there is cooperativity between ATP binding sites, which, by definition requires at least two ATP binding sites.

Unlike the previously reported dependence on [ATP], the translocation rate and rate constant do not exhibit cooperative dependencies on [ATP $\gamma$ S] for ClpA in the absence of ClpP. This observation suggests that ATP $\gamma$ S does not bind to both ATP binding sites on the monomer of ClpA or that binding to the second site is substantially weaker than the first. However, in order to observe a dependence on [ATP $\gamma$ S] the competition must occur at the site where the repeating rate limiting step is occurring and, based on our model, this site is most likely D1.

In contrast to ClpA alone, the translocation rate and rate constant for ClpA in the presence of ClpP exhibits little to no dependence on [ATP $\gamma$ S]. We have proposed that when ClpP is present, the observed repeating rate limiting step occurs at D2. Since we do

not observe competition between ATP and ATP $\gamma$ S when ClpP is present, this is consistent with ATP $\gamma$ S binding more weakly to D2 than to D1.

It seems unlikely that ATP $\gamma$ S would not bind at all to D2, so we favor the interpretation that ATP $\gamma$ S binds more weakly to D2 than D1. Consistently, at 750  $\mu$ M and 1 mM ATP $\gamma$ S, the kinetic step-size increases and the rate constant decreases. Since these two parameters are negatively correlated, the observation that one parameter goes up while the other goes down is consistent with negative parameter correlation. Also consistent with parameter correlation is the fact that the overall rate does not appear to exhibit any dependence on [ATP $\gamma$ S] even at the most elevated concentrations.

#### *Dependence of Correlation Coefficient on ATP $\gamma$ S*

We, and others, have established that there is negative parameter correlation between the kinetic step-size and the elementary rate constant that is coupled to the observed kinetic step-size.<sup>3; 24; 26; 27; 28; 32; 33</sup> This can often lead to poor constraints on the two parameters and, under some conditions, the parameters cannot be simultaneously determined. Under such conditions, the overall rate,  $mk_T$ , is considered to be a more reliable parameter since the parameter correlation is largely cancelled.

For ClpA in the absence of ClpP, the kinetic step-size increased to  $\sim$ 20 and  $\sim$ 24 at 1.8 and 2.5 mM ATP $\gamma$ S, respectively. With this observation in mind, we asked the question; is this simply due to parameter correlation or are we truly monitoring a different kinetic step that repeats every 20 – 25 amino acids. However, there is not a concomitant decrease in the observed rate constant or an effect on the overall rate. This is inconsistent with the typical effects of negative parameter correlation where it would be expected that the rate constant would decrease with a concomitant increase in the kinetic step-size. On

the other hand, one may argue that the decrease in the rate constants is apparent in the data but the rate constant is already decreasing with increasing [ATP $\gamma$ S] and thus the effect is masked. If this were true, then the dependence of the rate constant on ATP $\gamma$ S would be steeper than the dependence of the overall rate on ATP $\gamma$ S. Upon inspection and comparison of Fig. 4a-b, these two curves do not appear to exhibit vastly different midpoints.

We examined the parameter correlation between the kinetic step-size and the rate constant to determine if the observed change in the kinetic step-size is physically meaningful. Interestingly, the correlation coefficient changes quite significantly at the highest ATP $\gamma$ S concentrations. Specifically, the correlation coefficient is observed to decrease, which reduces the constraints on the kinetic step-size. Consequently, we do not interpret the increase in the kinetic step-size at 1.8 and 2.5 mM ATP $\gamma$ S to be physically meaningful. Rather, it is likely the consequence of the reduced constraints on the parameter.

Surprisingly, even though the kinetic parameters exhibit no dependence on [ATP $\gamma$ S] for ClpA in the presence of ClpP, the correlation coefficients also change with increasing [ATP $\gamma$ S] (see supplemental Table S1). In the case of ClpAP, this indicates that, even though there is little effect on the kinetic parameters, there must still be some impact of high concentrations of ATP $\gamma$ S on translocation catalyzed by ClpAP. One possibility, among others, is that ATP $\gamma$ S binding to D1 may have some influence on translocation even though ATP hydrolysis at D2 is rate limiting. It is tempting to interpret the data in this way since the kinetic step-size increases to  $\sim 14$  and  $\sim 10$  aa step $^{-1}$  at 750  $\mu$ M and 1 mM, respectively, and the rate constant decreases to 2.4 and 3.1 s $^{-1}$ ,

respectively. The temptation occurs because these values are similar to the parameters observed for ClpA in the absence of ClpP, where we conclude that events occurring at D1 are rate limiting. However, due to the fact that the correlation coefficient decreases in this range, resulting in a reduction in the certainty on the kinetic step-size, one is required to conclude that these numbers may be fortuitously similar.

It is important to note that experiments performed at a final mixing concentration above 500  $\mu\text{M}$  ATP $\gamma$ S are not likely to be conditions where we would examine the mechanism of polypeptide translocation. Although we preincubate ClpA with polypeptide substrate in the presence of 1 mM ATP $\gamma$ S, upon rapid mixing with ATP the final concentration of ATP $\gamma$ S is 500  $\mu\text{M}$ . Such high concentrations of ATP $\gamma$ S were only used in this study to further probe the impact on the mechanism.

The single-turnover translocation experiments and the method of analysis presented here have been applied to polypeptide translocation,<sup>23; 24; 25</sup> helicase catalyzed nucleic acid unwinding,<sup>34; 35 27; 33 36</sup> and helicase catalyzed ssDNA translocation.<sup>28; 37; 38</sup> In all of these studies there is concern about the interpretation of the kinetic steps-size and elementary rate constant since it is well known that the two parameters are negatively correlated. However, we contend that under many conditions these two parameters yield insight into the molecular mechanism. With the observation of the changes in the parameter correlation observed here, we propose that an examination of the parameter correlation should accompany the analysis of the kinetic parameters. This will allow the examiner to determine the range over which the parameters can be reliably interpreted.

### *Type 1 AAA+ Molecular Chaperones*

A major thrust of our research is to understand how Type 1 AAA+ protein translocases coordinate the activity of their two ATP binding and hydrolysis sites per monomer (12 per hexamer) to polypeptide translocation. It is striking to us that the hexameric rings of Type 1 AAA+ motors like ClpA, ClpB, Hsp104, NSF, and p97 all contain 12 ATP binding and hydrolysis sites per hexameric ring when most hexameric ring motor proteins only contain six. A fascinating question is; why the need for so many sites when many hexameric ring motors do their work with half as many? One potential answer is that different sets of nucleotide binding and hydrolysis sites are up-regulated or down-regulated depending upon which partner the enzyme is interacting with, i.e. ClpP and/or adapter proteins.

In a series of surprising observations, Wickner and coworkers showed that a mixture of ATP and ATP $\gamma$ S increased the activity of ClpB and Hsp104 catalyzed disaggregation and the rate of ATP hydrolysis.<sup>31</sup> That work represented the first report of a slowly hydrolysable nucleotide analog enhancing the activity of a motor protein. They went on to show, through mutational analysis of the D1 and D2 nucleotide binding sites, that ATP $\gamma$ S differentially competed for the two sites. Moreover, they concluded that ATP $\gamma$ S could elicit a similar impact as cochaperone proteins on ATP hydrolysis and disaggregation. These observations are similar to what we have observed here for ClpA. That is, our results support a hypothesis where D1 binds tighter to ATP $\gamma$ S than D2. Further, if we think of ClpP as a cochaperone, ClpP impacts the activities of D1 and D2 similar to how cochaperones impact ClpB activities.

Substantially more work is required on ClpA, ClpB, Hsp104, and other Type 1 AAA+ motors, to fully understand the role of the D1 and D2 ATP binding and hydrolysis sites. It remains unclear how the two sites coordinate their activities and couple binding and hydrolysis to polypeptide translocation and/or disaggregation.

## **Materials and Methods**

### *Materials*

All solutions were prepared in double-distilled water produced from a Purelab Ultra Genetic system (Siemens Water Technology, Alpharetta, Georgia) using reagent grade chemicals purchased commercially. All peptide substrates were synthesized by CPC Scientific (Sunnyvale, CA), and were judged to be >90% pure by HPLC and mass spectral analysis. Fluorescein was covalently attached to the free cysteine residue at the amino terminus of the polypeptide as previously described. *E. coli* ClpA and ClpP were purified as previously described.<sup>25;39</sup>

### *Methods*

#### *ATPase Activity Assay*

ATP $\gamma$ S hydrolysis was examined by pre-incubating 10  $\mu$ M ClpA in Buffer H (25 mM HEPES, pH 7.5 at 25 °C, 10 mM MgCl<sub>2</sub>, 2 mM 2-mercaptoethanol, 300 mM NaCl, and 10% v/v glycerol) at 25 °C for 45 minutes prior to adding [<sup>35</sup>S]-ATP $\gamma$ S. After 45 minutes, ATP $\gamma$ S that had been supplemented with [<sup>35</sup>S]-ATP $\gamma$ S was added. For determination of the initial velocity, samples were removed and quenched with a 1:1 dilution of 1 M HCl. The pH of each sample was adjusted through addition of a solution

containing 2.5 M NaOH, 0.5 M Tris, and 0.5 M EDTA such that the final pH was neutral. Reaction progress was monitored through separation of [<sup>35</sup>S]-ATP $\gamma$ S from <sup>35</sup>S-thio-phosphate using PEI-Cellulose F Thin Layer Chromatography plates (EMD Chemicals, Inc., Darmstadt, Germany) with 0.6 M KH<sub>2</sub>PO<sub>4</sub> (pH 3.4 at 25 °C) as the mobile phase. TLC plates were exposed to a phosphor imager screen (Molecular Dynamics, Sunnyvale, CA) for a period of 90 minutes. Radioactive counts were then quantified using a Typhoon Trio+ (GE Healthcare, Piscataway, NJ) in phosphor storage mode using the 390 BP 100 phosphor filter. The resulting data was then processed using ImageQuant TL (GE Healthcare, Piscataway, NJ). The resulting initial velocities were plotted versus [ATP $\gamma$ S] and subjected to NLLS analysis using the Michaelis-Menten equation with no linear transformation, given by Eq. (1):

$$v_0 = \frac{k_{cat} [ClpA]_{total}}{1 + \frac{K_m}{[ATP\gamma S]}} \quad (1)$$

#### *Stopped-flow fluorescence assay*

Fluorescence stopped-flow experiments were performed as previously described and shown in Fig. 1. All reactions were prepared in buffer H (25 mM HEPES, pH 7.5 at 25 °C, 10 mM MgCl<sub>2</sub>, 2 mM 2-mercaptoethanol, 300 mM NaCl, and 10% v/v glycerol). All experiments were performed in an SX.20 stopped-flow fluorometer, (Applied Photophysics, Letherhead, UK). Prior to each reaction, 1  $\mu$ M ClpA was preincubated with ATP $\gamma$ S for 25 minutes, concentration indicated in text. Fluorescently modified polypeptide substrate was then added such that the final concentration was 100 nM, and the mixture was loaded into syringe 1 of the stopped-flow fluorometer. Syringe 2

contained a solution of 10 mM ATP and 200  $\mu$ M SsrA peptide prepared in buffer H. Prior to mixing, both solutions were incubated for an additional 10 minutes at 25°C in the stopped-flow instrument. Increasing the incubation time of either solution in the stopped-flow instrument had no effect on the observed fluorescence time courses. Upon mixing, the final concentrations were 0.5  $\mu$ M ClpA monomer, 50 nM peptide substrate, 100  $\mu$ M SsrA peptide, 5 mM ATP, and the final concentration of ATP $\gamma$ S is indicated in the text. Fluorescein was excited at  $\lambda_{\text{ex}} = 494$  nm and fluorescence emission was observed above 515 nm with a 515 nm long pass filter. All kinetic traces shown represent the average of at least 8 individual determinations.

Additional stopped-flow fluorescence experiments were performed in the presence of 1.2  $\mu$ M ClpP. ClpAP was preassembled by incubating ClpA in the presence of ATP $\gamma$ S for 25 minutes, followed by incubation with ClpP for an additional 25 minutes. Fluorescently modified polypeptide substrate was then added such that the initial concentration was 20 nM, and the mixture was loaded into syringe 1 of the stopped-flow fluorometer.

### *NLLS Analysis*

The system of coupled differential equations that result from Scheme 1 was solved using the method of Laplace transforms to obtain an expression for product formation as a function of the Laplace variable,  $S(s)$ , given by Eq. (2),

$$S(s) = \frac{1}{s} \left( \sum_{j=1}^h \frac{k_d k_C^{j-1} (k_{NP} + sx)}{(k_C + k_d + s)^j (k_{NP} + s)} + \sum_{i=1}^{n-1} \frac{k_d k_T^i k_T^{i-1} (k_{NP} + sx)}{(k_C + k_d + s)^i (k_{NP} + s) (k_d + k_T + s)^i} + \frac{(k_T + k_d) k_C^h k_T^{n-1} (k_{NP} + sx)}{(k_C + k_d + s)^h (k_{NP} + s) (k_d + k_T + s)^n} \right) \quad (2)$$

where capital  $S$  represents the substrate and lower case  $s$  is the Laplace variable,  $h$  is the number of steps with rate constant  $k_C$ ,  $n$  is the number of steps with rate constant  $k_T$ ,  $k_{NP}$

is the rate of transition from a nonproductive complex to the productive complex, and  $x$  is the fraction of ClpA bound in the productive form given by Eq. (3).

$$x = \frac{[ClpA \cdot S]_L}{[ClpA \cdot S]_L + [ClpA \cdot S]_{NP}} \quad (3)$$

Eq. (2) was then numerically solved using Eq. (4) to describe product formation as a function of time,  $S(t)$ ,

$$S(t) = A_T \mathcal{L}^{-1} S(s) \quad (4)$$

where  $A_T$  is the total amplitude of the time-course, and  $\mathcal{L}^{-1}$  is the inverse Laplace transform operator. This was accomplished using the NLLS fitting routine, Conlin, and the inverse Laplace transform function using the IMSL C Numerical libraries (Visual Numerics, Houston, TX), as previously described.<sup>24; 32</sup> Uncertainties reported on the parameters in Tables 2 and 3 and Fig. 4 are based on the average of a minimum of two experimental determinations.

The ATP $\gamma$ S concentration dependencies of the macroscopic rate of translocation and microscopic translocation rate constant displayed in Fig. 4a-b was subjected to NLLS analysis using an infinitely cooperative model given by Eq. (5),

$$mk_{T,app} = \frac{mk_{T,max} \cdot (K_{ATP} \cdot [ATP])^\nu}{1 + (K_{ATP} \cdot [ATP])^\nu + (K_{ATP\gamma S} \cdot [ATP\gamma S])^\omega} \quad (5)$$

where  $mk_{T,app}$  is the apparent macroscopic translocation rate. The maximum macroscopic translocation rate is represented as  $mk_{T,max}$ . The association equilibrium constants for ATP- or ATP $\gamma$ S- association with ClpA are represented as  $K_{ATP}$  or  $K_{ATP\gamma S}$ , respectively. The apparent Hill coefficients for nucleotide binding are represented by either  $\nu$  or  $\omega$  for ATP or ATP $\gamma$ S binding, respectively.

For translocation time courses collected 75  $\mu\text{M}$  ATP $\gamma$ S in the absence of ClpP, the “grid-searches” shown in Figs. 5b-c were performed by constraining either the kinetic step-size,  $m$ , or the elementary rate constant,  $k_T$ , to fixed values ranging from 1 to 40 or 0.35 to 10, in intervals of 0.04 or 0.01, respectively, followed by minimization of the SSR. For translocation time courses collected in the presence of 2.5  $\mu\text{M}$  ATP $\gamma$ S in the absence of ClpP, the “grid-searches” shown in Figs. 5b-c were performed by constraining either the kinetic step-size,  $m$ , or the elementary rate constant,  $k_T$ , to fixed values ranging from 1 to 65 or 0.05 to 10, in intervals of 0.06 or 0.01, respectively, followed by minimization of the SSR. For translocation time courses collected in the presence of ClpA, ClpP, and 75  $\mu\text{M}$  ATP $\gamma$ S, the “grid-searches” shown in Figs. 6b-c were performed by constraining either the kinetic step-size,  $m$ , or the elementary rate constant,  $k_T$ , to fixed values ranging from 2 to 21 or 0.6 to 10, in intervals of 0.04 or 0.01, respectively, followed by minimization of the SSR. For translocation time courses collected in the presence of ClpA, ClpP, and 1  $\mu\text{M}$  ATP $\gamma$ S, the “grid-searches” shown in Figs. 6b-c were performed by constraining either the kinetic step-size,  $m$ , or the elementary rate constant,  $k_T$ , to fixed values ranging from 1.25 to 40 or 0.6 to 10, in intervals of 0.04 or 0.01, respectively, followed by minimization of the SSR.

## **Acknowledgements**

We would like to thank Clarissa Weaver and Ryan Stafford for comments on this manuscript. We would also like to thank to J. Woody Robins for use of the fermenter core facility. This work was supported by NSF grant MCB-0843746 to ALL, National Institute of Biomedical Imaging and Bioengineering (NIBIB) grant number T32EB004312 to JMM, and the University of Alabama at Birmingham Department of Chemistry. The content discussed here is solely the responsibility of the authors and does not necessarily represent the official views of the National Institute of Biomedical Imaging and Bioengineering or the National Institutes of Health.

## References

1. Alberts, B. (1998). The cell as a collection of protein machines: preparing the next generation of molecular biologists. *Cell* **92**, 291-4.
2. Neuwald, A. F., Aravind, L., Spouge, J. L. & Koonin, E. V. (1999). AAA+: A class of chaperone-like ATPases associated with the assembly, operation, and disassembly of protein complexes. *Genome Res* **9**, 27-43.
3. Karzai, A. W., Roche, E. D. & Sauer, R. T. (2000). The SsrA-SmpB system for protein tagging, directed degradation and ribosome rescue. *Nat Struct Biol* **7**, 449-55.
4. Gottesman, S. (1996). Proteases and their targets in Escherichia coli. *Annu Rev Genet* **30**, 465-506.
5. Sauer, R. T. & Baker, T. A. (2011). AAA+ Proteases: ATP-Fueled Machines of Protein Destruction. *Annual review of biochemistry* **80**, 587-612.
6. Hoskins, J. R., Pak, M., Maurizi, M. R. & Wickner, S. (1998). The role of the ClpA chaperone in proteolysis by ClpAP. *Proc Natl Acad Sci U S A* **95**, 12135-40.
7. Licht, S. & Lee, I. (2008). Resolving individual steps in the operation of ATP-dependent proteolytic molecular machines: from conformational changes to substrate translocation and processivity. *Biochemistry* **47**, 3595-605.
8. Thompson, M. W., Singh, S. K. & Maurizi, M. R. (1994). Processive degradation of proteins by the ATP-dependent Clp protease from Escherichia coli. Requirement for the multiple array of active sites in ClpP but not ATP hydrolysis. *J Biol Chem* **269**, 18209-15.
9. Maglica, Z., Kolygo, K. & Weber-Ban, E. (2009). Optimal efficiency of ClpAP and ClpXP chaperone-proteases is achieved by architectural symmetry. *Structure* **17**, 508-16.
10. Maurizi, M. R., Singh, S. K., Thompson, M. W., Kessel, M. & Ginsburg, A. (1998). Molecular properties of ClpAP protease of Escherichia coli: ATP-dependent association of ClpA and clpP. *Biochemistry* **37**, 7778-86.

11. Ishikawa, T., Beuron, F., Kessel, M., Wickner, S., Maurizi, M. R. & Steven, A. C. (2001). Translocation pathway of protein substrates in ClpAP protease. *Proc Natl Acad Sci U S A* **98**, 4328-33.
12. Singh, S. K. & Maurizi, M. R. (1994). Mutational analysis demonstrates different functional roles for the two ATP-binding sites in ClpAP protease from *Escherichia coli*. *J Biol Chem* **269**, 29537-45.
13. Kress, W., Mutschler, H. & Weber-Ban, E. (2009). Both ATPase domains of ClpA are critical for processing of stable protein structures. *J Biol Chem* **284**, 31441-52.
14. Guo, F., Maurizi, M. R., Esser, L. & Xia, D. (2002). Crystal structure of ClpA, an Hsp100 chaperone and regulator of ClpAP protease. *J Biol Chem* **277**, 46743-52.
15. Bohon, J., Jennings, L. D., Phillips, C. M., Licht, S. & Chance, M. R. (2008). Synchrotron protein footprinting supports substrate translocation by ClpA via ATP-induced movements of the D2 loop. *Structure* **16**, 1157-65.
16. Hinnerwisch, J., Fenton, W. A., Furtak, K. J., Farr, G. W. & Horwich, A. L. (2005). Loops in the central channel of ClpA chaperone mediate protein binding, unfolding, and translocation. *Cell* **121**, 1029-41.
17. Maurizi, M. R. (1991). ATP-promoted interaction between Clp A and Clp P in activation of Clp protease from *Escherichia coli*. *Biochem Soc Trans* **19**, 719-23.
18. Hoskins, J. R., Singh, S. K., Maurizi, M. R. & Wickner, S. (2000). Protein binding and unfolding by the chaperone ClpA and degradation by the protease ClpAP. *Proc Natl Acad Sci U S A* **97**, 8892-7.
19. Kolygo, K., Ranjan, N., Kress, W., Striebel, F., Hollenstein, K., Neelsen, K., Steiner, M., Summer, H. & Weber-Ban, E. (2009). Studying chaperone-proteases using a real-time approach based on FRET. *J Struct Biol* **168**, 267-77.
20. Kress, W., Mutschler, H. & Weber-Ban, E. (2007). Assembly Pathway of an AAA+ Protein: Tracking ClpA and ClpAP Complex Formation in Real Time. *Biochemistry* **46**, 6183-93.
21. Reid, B. G., Fenton, W. A., Horwich, A. L. & Weber-Ban, E. U. (2001). ClpA mediates directional translocation of substrate proteins into the ClpP protease. *Proc Natl Acad Sci U S A* **98**, 3768-72.
22. Veronese, P. K., Rajendar, B. & Lucius, A. L. (2011). Activity of *Escherichia coli* ClpA Bound by Nucleoside Di- and Triphosphates. *Journal of molecular biology* **409**, 333-47.

23. Rajendar, B. & Lucius, A. L. (2010). Molecular mechanism of polypeptide translocation catalyzed by the Escherichia coli ClpA protein translocase. *J Mol Biol* **399**, 665-79.
24. Lucius, A. L., Miller, J. M. & Rajendar, B. (2011). Application of the Sequential n-Step Kinetic Mechanism to Polypeptide Translocases. *Methods Enzymol* **488**, 239-64.
25. Miller, J. M., Lin, J., Li, T. & Lucius, A. L. (2013). E. coli ClpA Catalyzed Polypeptide Translocation Is Allosterically Controlled by the Protease ClpP. *J Mol Biol*.
26. Lucius, A. L., Jason Wong, C. & Lohman, T. M. (2004). Fluorescence stopped-flow studies of single turnover kinetics of E.coli RecBCD helicase-catalyzed DNA unwinding. *J Mol Biol* **339**, 731-50.
27. Lucius, A. L. & Lohman, T. M. (2004). Effects of temperature and ATP on the kinetic mechanism and kinetic step-size for E.coli RecBCD helicase-catalyzed DNA unwinding. *J Mol Biol* **339**, 751-71.
28. Fischer, C. J. & Lohman, T. M. (2004). ATP-dependent translocation of proteins along single-stranded DNA: models and methods of analysis of pre-steady state kinetics. *J Mol Biol* **344**, 1265-86.
29. Fischer, C. J., Wooten, L., Tomko, E. J. & Lohman, T. M. (2010). Kinetics of motor protein translocation on single-stranded DNA. *Methods Mol Biol* **587**, 45-56.
30. Thompson, M. W. & Maurizi, M. R. (1994). Activity and specificity of Escherichia coli ClpAP protease in cleaving model peptide substrates. *J Biol Chem* **269**, 18201-8.
31. Doyle, S. M., Shorter, J., Zolkiewski, M., Hoskins, J. R., Lindquist, S. & Wickner, S. (2007). Asymmetric deceleration of ClpB or Hsp104 ATPase activity unleashes protein-remodeling activity. *Nature structural & molecular biology* **14**, 114-22.
32. Lucius, A. L., Maluf, N. K., Fischer, C. J. & Lohman, T. M. (2003). General methods for analysis of sequential "n-step" kinetic mechanisms: application to single turnover kinetics of helicase-catalyzed DNA unwinding. *Biophys J* **85**, 2224-39.
33. Lucius, A. L., Vindigni, A., Gregorian, R., Ali, J. A., Taylor, A. F., Smith, G. R. & Lohman, T. M. (2002). DNA unwinding step-size of E. coli RecBCD helicase determined from single turnover chemical quenched-flow kinetic studies. *J Mol Biol* **324**, 409-28.

34. Jankowsky, E., Gross, C. H., Shuman, S. & Pyle, A. M. (2000). The DExH protein NPH-II is a processive and directional motor for unwinding RNA. *Nature* **403**, 447-51.
35. Ali, J. A. & Lohman, T. M. (1997). Kinetic measurement of the step size of DNA unwinding by Escherichia coli UvrD helicase. *Science* **275**, 377-80.
36. Galletto, R., Jezewska, M. J. & Bujalowski, W. (2004). Unzipping mechanism of the double-stranded DNA unwinding by a hexameric helicase: quantitative analysis of the rate of the dsDNA unwinding, processivity and kinetic step-size of the Escherichia coli DnaB helicase using rapid quench-flow method. *J Mol Biol* **343**, 83-99.
37. Fischer, C. J., Maluf, N. K. & Lohman, T. M. (2004). Mechanism of ATP-dependent translocation of E.coli UvrD monomers along single-stranded DNA. *J Mol Biol* **344**, 1287-309.
38. Chisty, L. T., Toseland, C. P., Fili, N., Mashanov, G. I., Dillingham, M. S., Molloy, J. E. & Webb, M. R. (2013). Monomeric PcrA helicase processively unwinds plasmid lengths of DNA in the presence of the initiator protein RepD. *Nucleic Acids Res* **41**, 5010-23.
39. Veronese, P. K., Stafford, R. P. & Lucius, A. L. (2009). The Escherichia coli ClpA Molecular Chaperone Self-Assembles into Tetramers. *Biochemistry* **48**, 9221-9233.

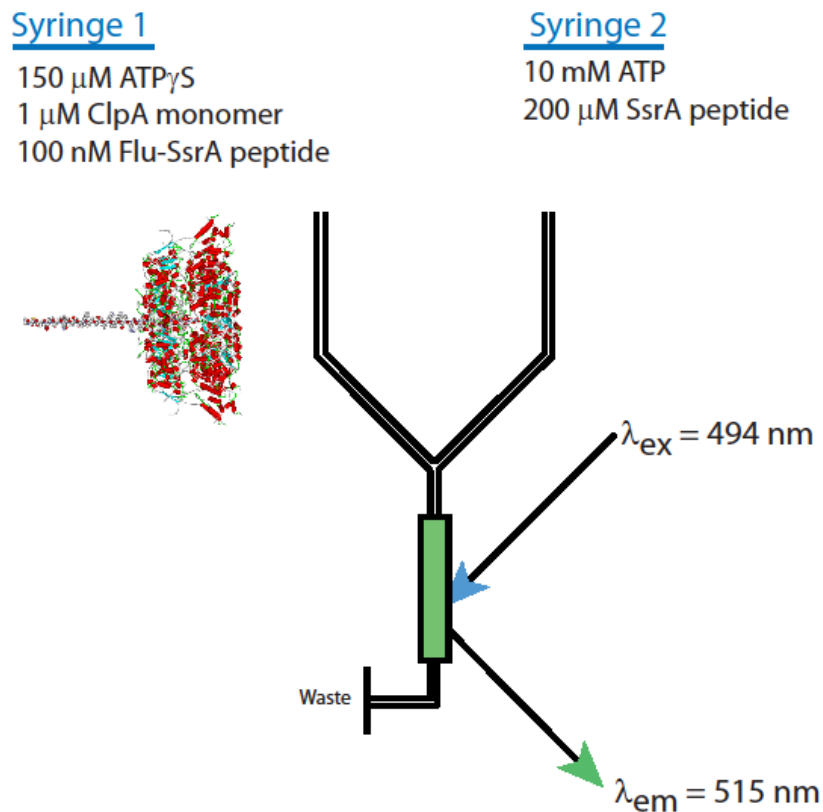


**Figure 1. Schematic representation of single turnover stopped-flow translocation experiments.** Syringe 1 contains the indicated reagents, ClpA, ATP $\gamma\text{S}$ , and fluorescein-labeled polypeptide. The structure schematizes the contents of syringe 1 with ClpA hexamers bound by a single polypeptide. Syringe 2 contains 10 mM ATP and 200  $\mu\text{M}$  SsrA peptide to serve as a trap for unbound ClpA or any ClpA that dissociates from polypeptide during the course of the reaction. The two reactants are rapidly mixed in the green colored chamber and fluorescein is excited at  $\lambda_{\text{ex}} = 494 \text{ nm}$ . Fluorescein emission is observed above 515 nm with a 515 nm long pass filter. Upon mixing, the concentrations are two-fold lower than in the preincubation syringe.

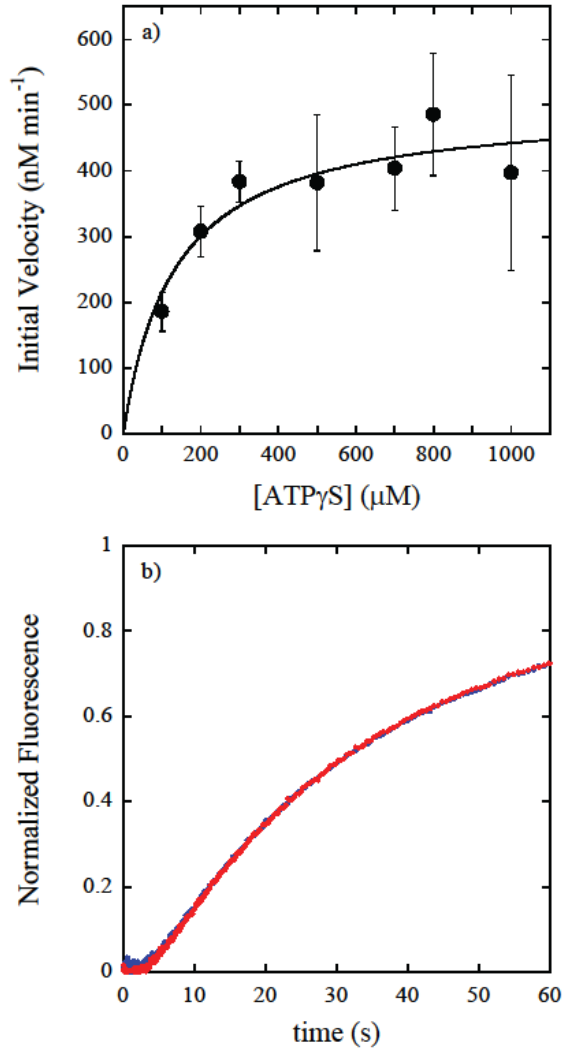


**Figure 2. ClpA catalyzes ATP $\gamma$ S hydrolysis.** a) Steady-state kinetic experiments were performed by mixing 10  $\mu$ M ClpA monomer with ATP $\gamma$ S supplemented with <sup>35</sup>S-ATP $\gamma$ S. The relationship between initial velocity and nucleotide concentration was subjected to NLLS analysis using Eq. (1) to obtain estimates of the Michaelis constant,  $K_m = (134 \pm 46)$   $\mu$ M, and the turnover number,  $k_{cat} = (0.05 \pm 0.004)$  min<sup>-1</sup>. b) Two fluorescence time courses are shown that have been collected using the experimental design schematized in Fig. 1. ClpA has been allowed to incubate in the presence of 5 mM ATP $\gamma$ S and 100 nM fluorescein-labeled polypeptide for either ~15 (solid blue circles) or ~70 minutes (solid red circles) before mixing with ATP and SsrA peptide (pre-mixing concentrations).

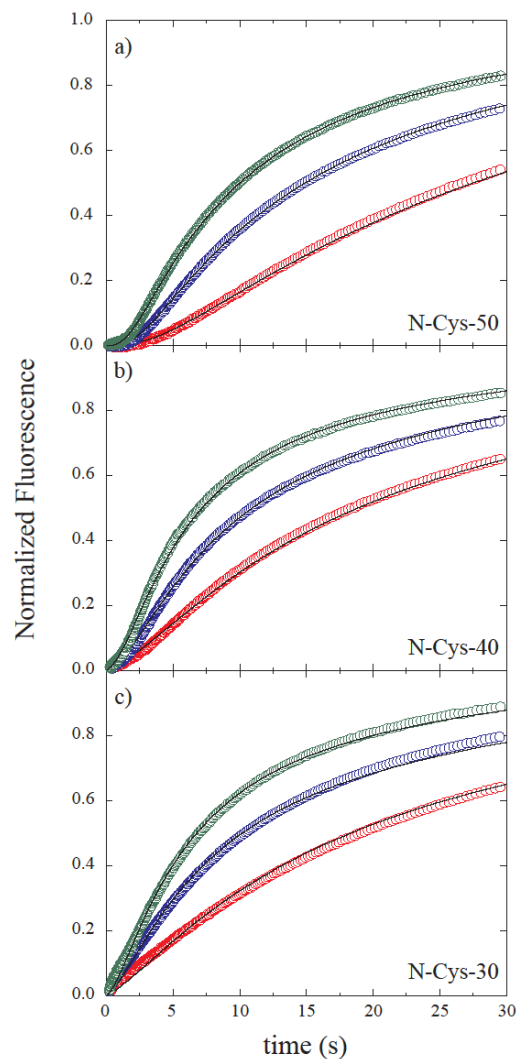


**Figure 3. Fluorescence time-courses for ClpA catalyzed polypeptide translocation.**

As shown in Fig. 1, 1  $\mu\text{M}$  ClpA was pre-assembled in the presence of ATP $\gamma$ S and 100 nM fluorescein-labeled polypeptide substrate prior to rapidly mixing with 10 mM ATP and 200  $\mu\text{M}$  SsrA. Time courses are shown for ClpA catalyzed polypeptide translocation of N-Cys-50, N-Cys-40, and N-Cys-30 (see Table 1) substrates after incubation of ClpA with 75  $\mu\text{M}$  (green circles), 600  $\mu\text{M}$  (blue circles), and 2.5 mM (red circles) ATP $\gamma$ S. The time courses shown illustrate that the extent of the lag phase is dependent upon [ATP $\gamma$ S]. The solid black lines represent a global NLLS fit using Scheme 1 for time-courses collected with substrates I – III in Table 1. The resulting kinetic parameters are summarized in Table 2 for each [ATP $\gamma$ S]. Each time-course was analyzed under a given set of conditions by constraining the parameters  $k_T$ ,  $k_C$ ,  $k_{NP}$ , and  $h$  to be global parameters, while  $A_x$ ,  $x$ , and  $n$  were allowed to float for each polypeptide length.

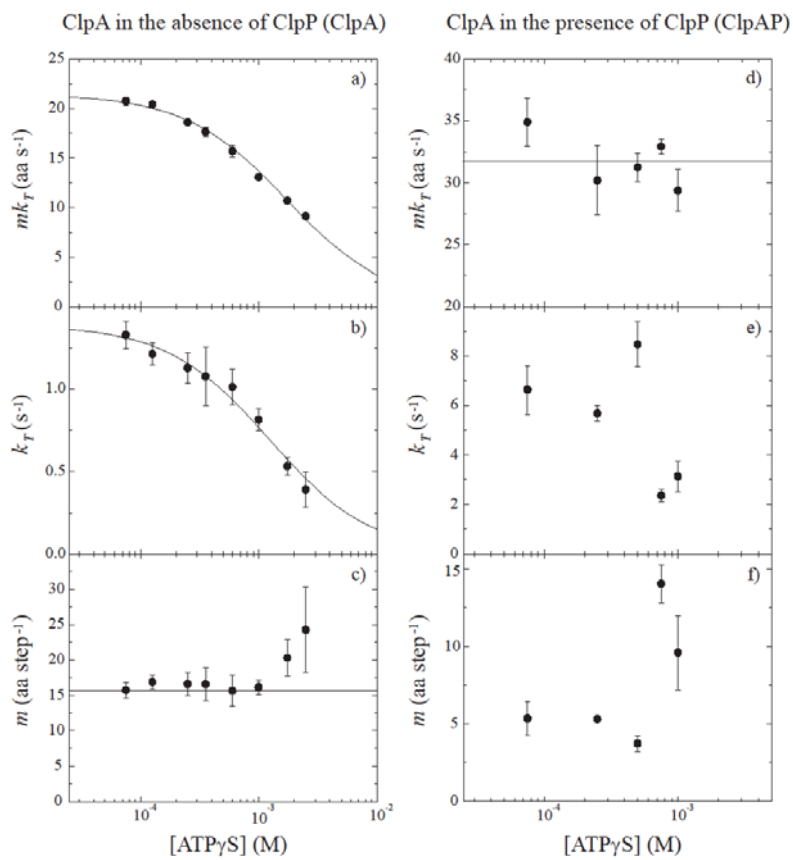


**Figure 4. Molecular mechanism for ClpA catalyzed polypeptide translocation depends on [ATP $\gamma$ S].** a) Dependence of  $mk_T$  on [ATP $\gamma$ S] for ClpA catalyzed polypeptide translocation in the absence of ClpP, where the solid line is the result of a NLLS fit to Eq. (5) with  $K_{ATP\gamma S} = (160 \pm 7) \times 10^3 \text{ M}^{-1}$  and  $mk_{T,max} = 21.6 \pm 0.2 \text{ aa s}^{-1}$ . The number of ATP and ATP $\gamma$ S binding sites,  $\nu = 2.5$  and  $\omega = 1.0$ , respectively, the association equilibrium constant,  $K_{ATP} = 1.9 \times 10^3 \text{ M}^{-1}$ , and [ATP] = 5 mM were treated as constant parameters in this analysis. b) The dependence of  $k_T$  on [ATP $\gamma$ S] was subjected to NLLS analysis using Eq. (5), where the solid line represents the best fit with  $K_{ATP\gamma S} = (104 \pm 13) \times 10^3 \text{ M}^{-1}$  and  $k_{T,max} = (1.39 \pm 0.05) \text{ s}^{-1}$ . For this analysis, the number of ATP and ATP $\gamma$ S binding sites,  $\nu = 2.2$  and  $\omega = 1.0$ , respectively, the association equilibrium constant,  $K_{ATP} = 1.8 \times 10^3 \text{ M}^{-1}$  and [ATP] = 5 mM were treated as constant parameters. c) Dependence of the kinetic step-size on [ATP $\gamma$ S], solid line represents the average of six measurements,  $\langle m \rangle = (16.3 \pm 0.5) \text{ aa step}^{-1}$ . (d) The rate of translocation for ClpA catalyzed polypeptide translocation in the presence of ClpP,  $mk_T$ , does not exhibit any dependence on ATP $\gamma$ S concentration with a mean  $mk_T = (32 \pm 2) \text{ aa s}^{-1}$ , where the solid line represents the average of five measurements. (e-f) The elementary rate constant and kinetic step-size for ClpA catalyzed polypeptide translocation in the presence of ClpP do not exhibit a significant dependence on [ATP $\gamma$ S].

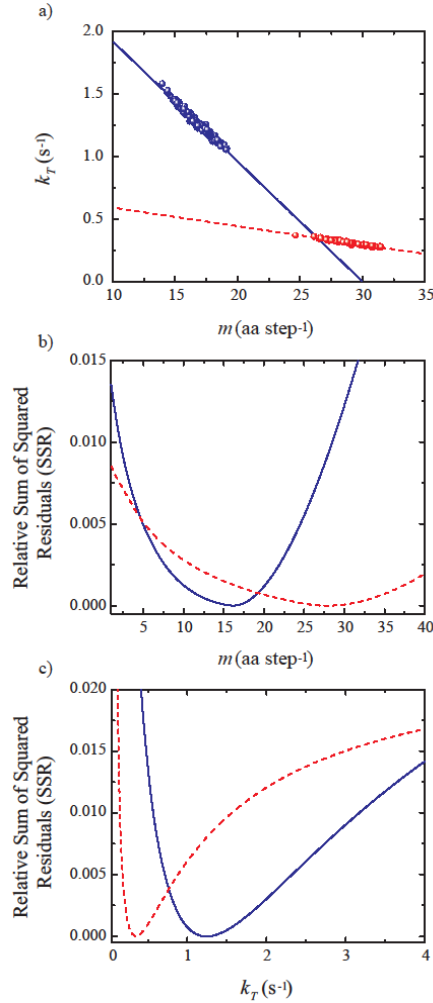


**Figure 5. Parameter correlation between the kinetic step-size and elementary rate constant depends on [ATP $\gamma$ S] for ClpA catalyzed polypeptide translocation in the absence of ClpP.** (a) Plot of the translocation rate constant versus the kinetic step-size from two representative Monte Carlo simulations from polypeptide translocation experiments collected in the presence of 75  $\mu$ M (blue spheres) and 2.5 mM (red spheres) ATP $\gamma$ S. Lines represent linear least-squares fit of 75  $\mu$ M (solid blue line) and 2.5 mM (dashed red line) ATP $\gamma$ S data, where the 75  $\mu$ M data exhibit a slope of  $-0.096 \pm 0.001$  and the 2.5 mM data exhibit a slope of  $-0.0148 \pm 0.0005$ . (b,c) Plots of the sums of the squared residuals as functions of fixed values of the kinetic step-size (b) or fixed values for the elementary rate constant (c) for conditions of 75  $\mu$ M (solid blue line) and 2.5 mM (dashed red line) ATP $\gamma$ S. From the minima shown in Fig. 5b, the best estimate of the kinetic step-size is  $m = 16.2$  or  $27.8$  aa step<sup>-1</sup>, for 75  $\mu$ M or 2.5 mM ATP $\gamma$ S, respectively. For the elementary translocation rate constant, the best estimate from the minima shown in Fig. 5c is  $1.2$  s<sup>-1</sup> or  $0.4$  s<sup>-1</sup> for 75  $\mu$ M or 2.5 mM ATP $\gamma$ S, respectively.

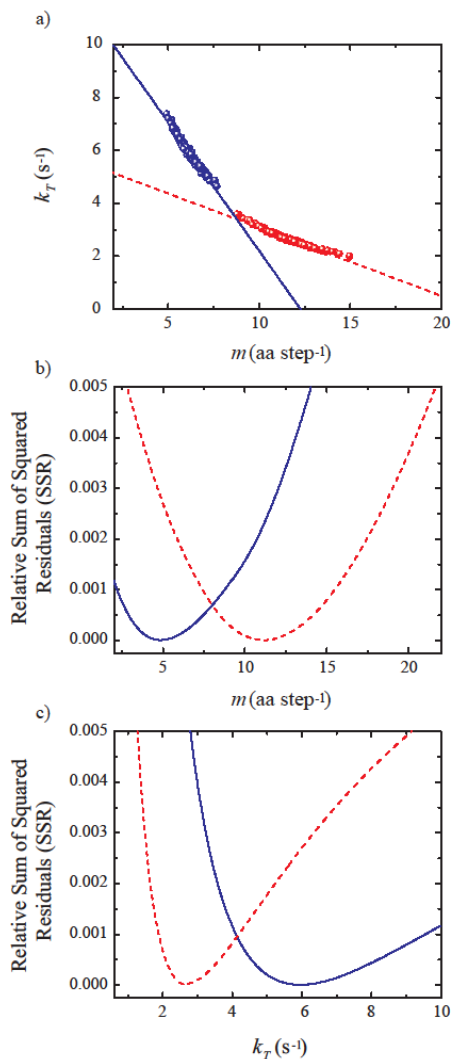
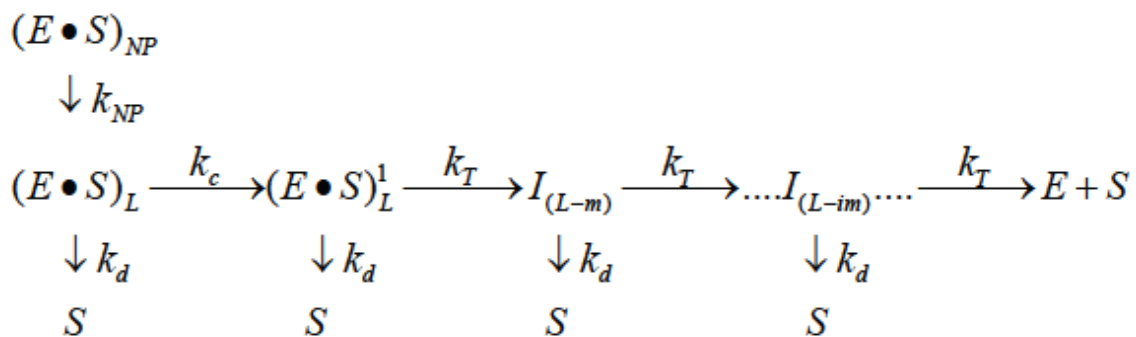


**Figure 6. Parameter correlation between the kinetic step-size and elementary rate constant depends on [ATP $\gamma$ S] for ClpA catalyzed polypeptide translocation in the presence of ClpP.** (a) Plot of the translocation rate constant versus the kinetic step-size from two representative Monte Carlo simulations from polypeptide translocation experiments collected in the presence of 75  $\mu$ M (blue spheres) and 1 mM (red spheres) ATP $\gamma$ S. Solid or dashed lines represent linear least-squares fit of 75  $\mu$ M (solid blue line) and 1 mM (dashed red line) ATP $\gamma$ S data, where the 75  $\mu$ M data exhibit a slope of  $-0.97 \pm 0.01$  and the 1 mM data exhibit a slope of  $-0.258 \pm 0.004$ . (b,c) Plots of the sums of the squared residuals as functions of fixed values of the kinetic step-size (b) or fixed values for the elementary rate constant (c) for conditions of 75  $\mu$ M (solid blue line) and 1 mM (dashed red line) ATP $\gamma$ S. From the minima shown in Fig. 6 b, the best estimate of the kinetic step-size is  $m = 4.8$  or  $11.2$  aa step<sup>-1</sup>, for 75  $\mu$ M or 1 mM ATP $\gamma$ S, respectively. For the elementary translocation rate constant, the best estimate from the minima shown in Fig. 6 c is  $5.9$  s<sup>-1</sup> or  $2.7$  s<sup>-1</sup> for 75  $\mu$ M or 1 mM ATP $\gamma$ S, respectively.

Scheme 1



**Scheme 1. Sequential  $n$ -step model for polypeptide translocation.**  $(E \cdot S)_L$  and  $(E \cdot S)_{NP}$  represent enzyme bound to polypeptide substrate in the productive and nonproductive forms, respectively, and  $S$  is the unbound polypeptide substrate.  $k_T$  is the translocation rate constant,  $k_d$  is the dissociation rate constant,  $L$  is the polypeptide length,  $m$  is the average distance translocated between two rate limiting steps with rate constant  $k_T$ , 'i' in  $I_{(L-im)}$  represents  $i$  number of translocation steps, and the step that occurs with rate constant  $k_c$  represents a step slower than the step with rate constant  $k_T$ .

**Table 1.** Polypeptide translocation Substrates

Substrate	Name	Length (aa)	Sequence
I	N-Cys-50	50	CLILHNKQLGMTGEVSFQAA NTKSAANLKVKELRSKKKLA <b>ANDENYALAA</b>
II	N-Cys40	40	CTGEVSFQAANTKSAANLKV KELRSKKKLA <b>ANDENYALAA</b>
III	N-Cys40	30	CTKSAANLKVKELRSKKKLA <b>ANDENYALAA</b>
* Fluorescein dye covalently attached to N-terminal cysteine residue			

**Table 2.** ClpA Polypeptide Translocation Parameters as a Function of [ATP $\gamma$ S]

[ATP $\gamma$ S] ( $\mu$ M)	$m$ (aa step $^{-1}$ )	$k_T$ (s $^{-1}$ )	$mk_T$ (aa s $^{-1}$ )	$k_{NP}$ (s $^{-1}$ )	$k_C$ (s $^{-1}$ )
75	16 $\pm$ 1	1.3 $\pm$ 0.1	20.8 $\pm$ 0.4	0.039 $\pm$ 0.002	0.15 $\pm$ 0.01
126	17 $\pm$ 1	1.2 $\pm$ 0.1	20.4 $\pm$ 0.1	0.034 $\pm$ 0.001	0.141 $\pm$ 0.004
250	17 $\pm$ 2	1.1 $\pm$ 0.1	18.6 $\pm$ 0.2	0.031 $\pm$ 0.001	0.125 $\pm$ 0.003
355	17 $\pm$ 2	1.1 $\pm$ 0.2	17.6 $\pm$ 0.4	0.029 $\pm$ 0.001	0.118 $\pm$ 0.003
600	16 $\pm$ 2	1.0 $\pm$ 0.1	15.7 $\pm$ 0.6	0.028 $\pm$ 0.001	0.102 $\pm$ 0.004
[ATP $\gamma$ S] (mM)					
1.0	16 $\pm$ 1	0.8 $\pm$ 0.1	13.1 $\pm$ 0.3	0.03 $\pm$ 0.01	0.089 $\pm$ 0.003
1.8	20 $\pm$ 3	0.5 $\pm$ 0.1	10.7 $\pm$ 0.3	0.0163 $\pm$ 0.0004	0.052 $\pm$ 0.001
2.5	24 $\pm$ 6	0.4 $\pm$ 0.1	9.1 $\pm$ 0.3	0.015 $\pm$ 0.001	0.043 $\pm$ 0.004

$k_T$  is the translocation rate constant,  $k_C$  is an additional kinetic step defined by Scheme 1,  $m$  is the kinetic step size,  $k_{NP}$  is a slow conformational change defined by Scheme 1, and  $mk_T$  is the macroscopic rate of translocation.

**Table 3.** ClpAP Polypeptide Translocation Parameters as a Function of [ATP $\gamma$ S]

[ATP $\gamma$ S] ( $\mu$ M)	$m$ (aa step $^{-1}$ )	$k_T$ (s $^{-1}$ )	$mk_T$ (aa s $^{-1}$ )	$k_{NP}$ (s $^{-1}$ )	$k_C$ (s $^{-1}$ )
75	$5 \pm 1$	$6.6 \pm 0.9$	$35 \pm 2$	$0.042 \pm 0.002$	$0.23 \pm 0.01$
250	$5.3 \pm 0.2$	$5.7 \pm 0.3$	$30 \pm 3$	$0.033 \pm 0.001$	$0.18 \pm 0.01$
500	$4 \pm 1$	$8.5 \pm 0.9$	$31 \pm 1$	$0.029 \pm 0.001$	$0.17 \pm 0.01$
750	$14 \pm 1$	$2.4 \pm 0.2$	$33 \pm 1$	$0.0296 \pm 0.0003$	$0.15 \pm 0.002$
1000	$10 \pm 2$	$3.1 \pm 0.6$	$29 \pm 2$	$0.026 \pm 0.001$	$0.14 \pm 0.002$

$k_T$  is the translocation rate constant,  $k_C$  is an additional kinetic step defined by Scheme 1,  $m$  is the kinetic step size,  $k_{NP}$  is a slow conformational change defined by Scheme 1, and  $mk_T$  is the macroscopic rate of translocation.

Chapter Five

*E. coli* ClpAP Complexes Share a Common Polypeptide Translocation Mechanism

By:

Justin M. Miller and Aaron L. Lucius

Submitted to *Journal of Molecular Biology*

Format adapted for dissertation

## **Abstract**

ATP-dependent proteases are required in all organisms for the removal of misfolded and properly folded proteins during cellular homeostasis. ClpAP shares structural homology with many other ATP-dependent proteases where a hexameric ring of ClpA associates with one or both ends of the cylindrically-shaped protease ClpP. Each monomer of ClpA contains two ATP binding and hydrolysis sites, termed Domain 1 (D1) or Domain 2 (D2). We have previously proposed a model for ClpA and ClpAP where the rate-limiting step in polypeptide translocation is coupled to ATP hydrolysis at either D1 or D2, respectively. However, that study was performed under conditions favoring a mixture of ClpAP and free ClpA hexamers. Therefore, it was unclear as to whether the translocation activity of ClpA was affected differently when one versus two ClpA hexamers interacted with ClpP. Here we show that the rate of polypeptide translocation strongly depends on the ClpAP species distribution, and that free ClpA hexamers contribute to a decrease in the apparent overall translocation rate. Using single-turnover stopped flow fluorescence methods, we report that all ClpAP complexes translocate polypeptide with the same mechanism, where the overall rate is  $\sim 31$  amino acids per second and, on average, this step repeats every  $\sim 3$  amino acids translocated. Interpreting these observations alongside our previously proposed model for translocation catalyzed by ClpA vs. ClpAP indicates that the rate-limiting step must occur at D2 for both 1:1 and 2:1 ClpAP complexes.

## Introduction

AAA+ proteases (ATPases Associated with various cellular Activities) are required in all organisms for the ATP-dependent removal of both misfolded and properly folded proteins in cellular quality control pathways. A representative member of this family is the ATP-dependent protease *E. coli* ClpAP, which degrades N-end polypeptide substrates, SsrA-tagged polypeptides, and other polypeptides displaying a degradation tag (commonly termed degron).<sup>1; 2</sup> ClpAP is assembled through the interaction of ClpA hexamers with one or both ends of the cylindrically-shaped protease ClpP, where ClpP contains serine protease active sites insulated from bulk solution.<sup>5; 8; 9; 10; 11; 12; 13</sup> Upon assembly of the ClpAP complex, ClpA will couple the energy of ATP binding and hydrolysis to translocate polypeptide substrates into ClpP for proteolytic degradation.

In addition to a conserved N-terminal domain, monomers of ClpA contain two nucleotide binding domains, each with the canonical Walker A and Walker B motifs.<sup>3; 4</sup> The nucleotide binding domains have been labeled as Domain 1 and Domain 2, D1 and D2, respectively. Each domain has been thought to serve a particular function, where D1 is hypothesized to be responsible for ClpA hexamerization and D2 was previously proposed to be primarily responsible for polypeptide translocation.<sup>5</sup> However, more recent work has shown that ClpA mutants deficient in ATPase activity at either D1 or D2 both support polypeptide translocation.<sup>6</sup> Therefore, both ATP binding and hydrolysis sites are likely involved in polypeptide translocation.

In general, ATP-dependent proteases share a common architecture where a ring-shaped AAA+ ATPase can associate with either end of a cylindrically-shaped protease.<sup>1</sup> For ClpAP, the schematic shown in Figure 1 illustrates that ClpA hexamers (Fig. 1a) can

associate with a single face of ClpP<sub>14</sub> to form a ClpAP complex with one hexamer per ClpP tetradecamer, 1:1 ClpAP (Fig. 1b). Alternatively, ClpA hexamers can associate with both faces of ClpP<sub>14</sub> to form a ClpAP complex with two hexamers per ClpP tetradecamer, 2:1 ClpAP (Fig. 1c). In principle, the 2:1 ClpAP complex can bind one (Fig. 1c) or two (Fig. 1d) polypeptide substrates per active complex **to form a 2:1 ClpAP<sub>1P</sub> complex or a 2:1 ClpAP<sub>2P</sub> complex, respectively, where the subscripts 1P and 2P indicate the number of bound polypeptides.** Therefore, a dynamic equilibrium of free ClpA hexamers, 1:1 ClpAP, and 2:1 ClpAP complexes with either one or two bound polypeptides is possible.

The distribution of 1:1 ClpAP and 2:1 ClpAP complexes has been previously reported to depend on the ratio of ClpA hexamers to ClpP tetradecamers.<sup>7</sup> In the absence of nucleotide, ClpA has been demonstrated to reside in a monomer-dimer-tetramer equilibrium,<sup>8; 9</sup> and requires nucleoside triphosphate to assemble hexamers that are competent for ClpP<sub>14</sub> association, polypeptide binding, and translocation of polypeptide substrates.<sup>7; 10; 11</sup> When the concentration of ClpA hexamers is in excess of the concentration of ClpP tetradecamers, only free ClpA hexamers and the 2:1 ClpAP complex are observed in sedimentation velocity experiments performed in the presence ATPγS.<sup>7</sup> However, when the [ClpP<sub>14</sub>] exceeds the [ClpA<sub>6</sub>], a mixture of free ClpP, 1:1 ClpAP, and 2:1 ClpAP is observed in the presence of ATPγS.

We have previously reported a single-turnover stopped-flow fluorescence method that allows for the observation of ClpA catalyzed polypeptide translocation in the absence of proteolysis.<sup>12; 13</sup> Preassembled ClpA that is prebound with polypeptide substrate is rapidly mixed with ATP and protein trap in a stopped-flow fluorometer to initiate

translocation. In this experimental design, fluorescence time courses only reflect the kinetics of translocation since we have removed the contributions of assembly and polypeptide binding kinetics by prebinding ClpA to polypeptide substrate. Therefore, the resulting kinetic time courses reflect only a single cycle of polypeptide translocation. The strength in this approach is that the kinetic time courses are sensitive to the molecular events in polypeptide translocation.

This translocation assay is single-turnover with respect to polypeptide translocation, but is multiple-turnover with respect to ATP binding and hydrolysis. For a motor protein to translocate along a linear lattice, repeating cycles of certain events must occur. At a minimum, each cycle must include ATP binding, ATP hydrolysis,  $P_i$  release, potential conformational changes, etc. Therefore, each round of translocation requires that this cycle of events repeat multiple times until translocation is complete. Consequently, our single-turnover method is sensitive to the slowest repeating step in the cycle.

By coupling observations from our single-turnover polypeptide translocation experiments<sup>14</sup> to steady state ATP hydrolysis rates from Weber-Ban and coworkers<sup>6</sup> and crosslinking experiments from Horwich and coworkers,<sup>15</sup> we have proposed models for ClpA and ClpAP catalyzed polypeptide translocation.<sup>12; 14</sup> In these models, the rate-limiting step in translocation takes place at D1 when ClpP is absent, whereas the observed rate-limiting step occurs at D2 in the presence of ClpP.<sup>14</sup> We proposed that at D1 the rate-limiting step repeats every  $\sim 14$  amino acids translocated with an observed rate constant of  $\sim 1.39 \text{ s}^{-1}$ , and at D2 the rate-limiting step repeats every  $\sim 2 - 5$  amino acids translocated with an observed rate constant of  $\sim 6.6 \text{ s}^{-1}$ .<sup>16; 18</sup>

In experiments performed to examine ClpA catalyzed polypeptide translocation in the absence of ClpP, only ClpA hexamers are capable of translocation. In contrast, for the same experiments performed in the presence of ClpP, Fig. 1 illustrates that up to four possible forms of ClpA and ClpAP may exist in solution, dependent on the molar ratio of ClpA hexamers to ClpP tetradecamers, where all are competent for polypeptide translocation. Therefore, translocation time courses may contain contributions from multiple species. As a result, the contribution of each individual species to translocation time courses remains unclear.

Maurizi and coworkers have reported that the proteolytic activities of 2:1 ClpAP and 1:1 ClpAP are approximately equivalent.<sup>7</sup> They arrived at this conclusion using the method of continuous variation, where casein degradation was measured using different ratios of ClpA hexamers to ClpP tetradecamers while maintaining a constant total molar concentration of ClpA<sub>6</sub> and ClpP<sub>14</sub>. It should be noted that the total ClpA population was assumed to reside in the hexameric state in this study. Maximal activity was observed when the [ClpA<sub>6</sub>] was 2-fold larger than the [ClpP<sub>14</sub>], but the observed proteolytic activity was decreased only slightly when the concentrations of ClpA<sub>6</sub> and ClpP<sub>14</sub> were equivalent. Therefore, it was concluded that the addition of a second ClpA hexamer to the ClpAP complex does not further activate ClpP for polypeptide degradation.

In contrast to what Maurizi and coworkers reported,<sup>7</sup> Weber-ban and coworkers have proposed that a 2:1 ClpAP complex with two polypeptides bound, as shown in Fig. 1d, can translocate polypeptide from both ends of ClpP<sub>14</sub> simultaneously and independently.<sup>16</sup> In that study, to observe translocation by 1:1 or 2:1 ClpAP complexes, a λRSsrA construct was prepared with donor and acceptor fluorophores far away in the

primary structure, but close in tertiary structure. Thus, an increase in donor fluorescence and a decrease in sensitized emission would be expected upon unfolding and translocation of the fluorescently-modified polypeptide construct. Stopped-flow fluorescence experiments were performed that incubated the fluorescently-labeled  $\lambda$ RSsrA construct with ClpAP that had been preassembled using either a ClpP mutant that only allowed ClpA to bind at one end of the ClpP tetradecamer to form 1:1 ClpAP complexes or with wild-type ClpP, where 2:1 ClpAP complexes would be favored. Fluorescence time courses collected in the presence of the mutant ClpP or wild-type ClpP were observed to be identical when a 2-fold higher concentration of 1:1 ClpAP complexes was used relative to the concentration of 2:1 ClpAP complexes. From this, it was concluded that 2:1 ClpAP complexes must translocate polypeptide from both ends of ClpP<sub>14</sub> simultaneously and independently.

The apparent disagreement in the ClpAP literature led us to ask the question; do 1:1 ClpAP complexes utilize the same mechanism as 2:1 ClpAP complexes to catalyze translocation of a single polypeptide? It is clear that ClpP allosterically modulates the translocation activity of ClpA hexamers.<sup>12; 14</sup> However, it is unclear whether the addition of a second ClpA hexamer that is not ligated with polypeptide to a ClpAP complex with a single polypeptide bound further impacts the translocation mechanism of ClpA when associated with ClpP.

To begin to investigate this question, we used our previously reported single-turnover stopped-flow fluorescence method to examine the impact of the total [ClpP<sub>14</sub>] on the translocation mechanism for ClpA catalyzed translocation of a single polypeptide substrate.<sup>12; 13; 14</sup> We show here that the best model to describe polypeptide translocation

catalyzed by 1:1 or 2:1 ClpAP complexes is one where both complexes translocate a single polypeptide with the same translocation mechanism. We have measured the apparent kinetic step-size for ClpAP complexes as  $m_{app} = (2.6 \pm 0.2) \text{ aa step}^{-1}$ , which is consistent with our previous report that  $m_{app} = \sim 2 - 5 \text{ aa step}^{-1}$ . Therefore, we conclude that, since the same rate-limiting step is observed for conditions that favor 1:1 ClpAP versus 2:1 ClpAP, the addition of a second ClpA hexamer with no bound polypeptide to a 1:1 ClpAP complex with polypeptide bound (Fig. 1b) does not impact the polypeptide translocation mechanism of ClpAP.

## Results

We have reported that ClpP induces modifications in the ClpA catalyzed polypeptide translocation mechanism for a mixture of 1:1 and 2:1 ClpAP complexes.<sup>14</sup> However, it remains unclear as to whether 1:1 ClpAP complexes translocate a single polypeptide differently than 2:1 ClpAP complexes. Two models have been proposed to describe ClpAP catalyzed polypeptide translocation, where one model concludes that both ClpA hexamers in a 2:1 ClpAP complex translocate polypeptide simultaneously into ClpP<sub>14</sub>, and the other model concludes that translocation occurs only from one end of ClpP<sub>14</sub>.<sup>20;7</sup> From this, we asked; do 1:1 ClpAP and 2:1 ClpAP share a common translocation mechanism or does 2:1 ClpAP translocate a single polypeptide with a unique mechanism? To test this, we set out to examine the effect of a varied ClpAP species distribution on a single-turnover of polypeptide translocation by 1:1 and 2:1 ClpAP complexes.

### *Application of single-turnover stopped-flow fluorescence method*

To examine the dependence of the molecular mechanism of ClpA catalyzed polypeptide translocation on the distribution of 1:1 ClpAP, 2:1 ClpAP, and free ClpA hexamers, we employed single-turnover stopped-flow fluorescence.<sup>12; 13; 14</sup> Figure 2 illustrates the experimental design. Syringe 1 of the stopped-flow apparatus contains a solution of 1  $\mu\text{M}$  ClpA monomer, 1 mM ATP $\gamma$ S, 20 nM fluorescein labeled polypeptide substrate (see Table 1 for sequences), and 333 nM ClpP tetradecamer. We have included 1 mM ATP $\gamma$ S in syringe 1 to form ClpA hexamers active in polypeptide binding, translocation, and ClpP association.<sup>7; 10; 12; 14</sup> Further, we have chosen conditions that maintain enzyme concentration in excess of polypeptide concentration to favor the binding of a single polypeptide per ClpAP complex, when 2:1 ClpAP is present (see Fig. 1b-c for schematic representation of ClpAP complexes).

All polypeptide substrates contain the SsrA sequence, AANDENYALAA, at the carboxy terminus for specific binding by ClpA hexamers and a single cysteine residue at the amino terminus that has been labeled with fluorescein-5-maleimide. Whether in complex with ClpP or not, ClpA will bind at the carboxy terminus of the polypeptide substrate and translocate directionally from the carboxy- to the amino-terminus.<sup>12; 17</sup> We have previously reported that ClpA binding to the short polypeptide substrates shown in Table 1 results in quenched emission.<sup>12</sup> Therefore, an enhancement in our fluorescence signal will occur on dissociation of the enzyme from fluorescently-modified polypeptide.

We have reported that the concentration of ClpA hexamers is  $(130 \pm 11)$  nM when 1  $\mu\text{M}$  total ClpA monomer is pre-incubated in the presence of 150  $\mu\text{M}$  ATP $\gamma$ S.<sup>14</sup> This constitutes an  $\sim 22\%$  lower hexamer concentration relative to the 167 nM hexamer

concentration predicted if the total ClpA concentration,  $[\text{ClpA}]_T$ , is assumed to be in the hexameric state, i.e.  $[\text{ClpA}]_T / 6$ . Further, we have observed no significant dependence of the hexamer concentration on  $[\text{ATP}\gamma\text{S}]$  higher than 150  $\mu\text{M}$  (J. Lin, Manuscript in preparation). Moreover, preassembled ClpAP complexes with a single polypeptide bound are predicted since the concentration of enzyme complex is in excess of the concentration of polypeptide substrate. Thus, the conditions depicted in Fig. 2 represent an  $\sim 2.6$ -fold excess of  $[\text{ClpP}_{14}]_T$  over  $[\text{ClpA}_6]_T$  and predominantly 1:1 ClpAP complexes with one polypeptide bound are predicted to be present in syringe 1 based on mass action.

As shown in Fig. 2, syringe 2 contains a solution of 10 mM ATP and 300  $\mu\text{M}$  SsrA polypeptide. The inclusion of a non-fluorescently modified SsrA polypeptide in syringe 2 serves as a protein trap that insures single-turnover conditions. Upon mixing of the contents of the two syringes, free enzyme or any enzyme that dissociates will rapidly bind the non-fluorescently modified SsrA trap, thus insuring that the observed signal is only sensitive to ClpA hexamers or ClpAP complexes that were bound at time zero. Reaction progress is monitored by exciting fluorescein at 494 nm and observing fluorescence emission at 515 nm and above using a 515 nm long pass filter (see Materials and Methods).

The schematic ClpAP structure shown in Figure 3a represents the contents of syringe 1 as illustrated in Fig. 2, where assembly of 1:1 ClpAP complexes is favored since the concentration of ClpP tetradecamers is in excess of the concentration of ClpA hexamers. Since the 1:1 ClpAP complex contains only one polypeptide binding site, there is a single polypeptide bound. Figures 3b-d show representative fluorescence time courses collected from rapidly mixing the contents of syringe 1 and 2 under the

conditions illustrated in Fig. 2. The time courses shown in Fig. 3b-d are from experiments performed with polypeptide substrate lengths of 50 (blue circles), 40 (red circles), and 30 amino acids (green circles) (see Table 1 for sequences).

Consistent with our previous reports, the time courses shown in Figures 3b-d exhibit a lag followed by a fluorescence enhancement upon dissociation of enzyme from fluorescently-modified polypeptide.<sup>12</sup> Furthermore, the extent of the lag increases with increasing polypeptide substrate length. The observation of a lag phase indicates that two or more rate-limiting steps must occur in the translocation mechanism prior to dissociation of the enzyme from the polypeptide lattice.<sup>13; 18; 19</sup> Therefore, in the experiments reported here, each increase in polypeptide substrate length yields a kinetic time course consistent with multiple rate-limiting steps occurring prior to dissociation of the enzyme from the polypeptide lattice.

Figures 3f-h shows representative time courses resulting when the  $[\text{ClpP}_{14}]_{\text{T}}$  is decreased in syringe 1 to  $[\text{ClpP}_{14}]_{\text{T}} = 19 \text{ nM}$ . This was done to test whether a change in the distribution of ClpAP species would affect translocation time courses. Based on mass action, conditions where 130 nM ClpA<sub>6</sub> is incubated in the presence of 19 nM ClpP<sub>14</sub> in syringe 1 favor the assembly of a mixture of 2:1 ClpAP complexes and free ClpA hexamers as schematized in Figure 3e. Despite having two polypeptide binding sites in each 2:1 ClpAP complex, 2:1 ClpAP complexes with a single polypeptide are statistically favored since the concentration of 2:1 ClpAP complex is much larger than the concentration of polypeptide substrate. Identical to Fig. 3b-d, the resulting time courses shown in Fig. 3f-h exhibit a lag phase that increases with increasing polypeptide substrate length.

Comparison of time courses shown in Figs. 3b-d and 3f-h show that time courses collected under conditions favoring the assembly of 1:1 ClpAP complexes (Fig. 3b-d) exhibit shorter lag phases than time courses collected for conditions where 2:1 ClpAP and free ClpA hexamers are favored (Fig. 3f-h). For example, Figs. 3b and 3f show time courses collected under conditions where enzyme has been prebound to a 50 aa polypeptide substrate. For conditions favoring 1:1 ClpAP complexes (Fig. 3b), the extent of the lag phase is  $\sim 1$  second, but increases to  $\sim 2$  seconds for conditions favoring a mixture of 2:1 ClpAP complexes and free ClpA hexamers (Fig. 3f). It is unclear whether this is the result of 1:1 ClpAP and 2:1 ClpAP complexes translocating polypeptide with different mechanisms.

To determine whether the difference between the time courses in Fig. 3b and Fig. 3f is due to a different translocation mechanism for 1:1 versus 2:1 ClpAP complexes, we subjected the time courses to global NLLS analysis to estimate the apparent overall translocation rate,  $mk_{T,app}$ , the apparent elementary rate constant,  $k_{T,app}$ , and the apparent kinetic step-size,  $m_{app}$ , for each set of polypeptide lengths collected at each  $[\text{ClpP}_{14}]_T$ . All data were well described by Scheme 1, and the best fit for each condition is represented by the solid black line in each panel of Fig. 3. The resultant parameters for conditions where 130 nM ClpA<sub>6</sub> was incubated with 333 nM ClpP<sub>14</sub> (Fig. 3b-d) were  $mk_{T,app} = (30.6 \pm 0.1) \text{ aa s}^{-1}$ ,  $k_{T,app} = (10.8 \pm 0.6) \text{ s}^{-1}$ , and  $m_{app} = (2.8 \pm 0.1) \text{ aa step}^{-1}$ . When 130 nM ClpA<sub>6</sub> was incubated in the presence of a decreased  $[\text{ClpP}_{14}]_T = 18 \text{ nM}$  (Fig. 3f-h), the best fit parameters were  $mk_{T,app} = (19.0 \pm 0.4) \text{ aa s}^{-1}$ ,  $k_{T,app} = (3.4 \pm 0.6) \text{ s}^{-1}$ , and  $m_{app} = (5.8 \pm 0.9) \text{ aa step}^{-1}$ . Therefore, the observation of a shorter lag phase in Fig. 3b versus Fig. 3f is a result of an increased overall translocation rate for conditions that favor the assembly of

1:1 ClpAP complexes (Fig. 3a) compared to conditions favoring a mixture of 2:1 ClpAP complexes (Fig. 3e) and free ClpA hexamers. Furthermore, the increase in overall rate for increased  $[\text{ClpP}_{14}]_T$  is a consequence of both an increase in the translocation rate constant and a decrease in the frequency that the rate-limiting step repeats.

*Apparent translocation rate depends on the  $[\text{ClpP}_{14}]_T$*

Conditions that favor 1:1 ClpAP complexes clearly exhibit different translocation parameters than conditions that favor 2:1 ClpAP complexes and free ClpA hexamers. However, it is possible that this difference is the result of translocation by free ClpA hexamers for conditions that favor the assembly of 2:1 ClpAP complexes and free ClpA hexamers. To examine the differences between these conditions, experiments were performed over a full range of  $[\text{ClpP}_{14}]_T$  to differentially populate 1:1 ClpAP, 2:1 ClpAP, and free ClpA hexamers.

Single-turnover stopped-flow fluorescence experiments were performed as described in Fig. 2 by varying  $[\text{ClpP}_{14}]_T$  in syringe 1. This was done to investigate the dependence of the kinetic parameters on the ClpAP species distribution. Before rapid mixing in the stopped-flow, the initial  $[\text{ClpA}]_T$  was 1  $\mu\text{M}$  and the  $[\text{ClpP}_{14}]_T$  values were 334, 167, 111, 84, 67, 56, 48, 33, 28, 24, and 19 nM. For these conditions of  $[\text{ATP}\gamma\text{S}]$  and  $[\text{ClpA}]_T$ , we predict that the  $[\text{ClpA}_6]_T = 130$  nM in syringe 1 before rapid mixing based on our previous report.<sup>14</sup> Therefore, the ratio of  $\text{ClpA}_6$  to  $\text{ClpP}_{14}$  in this range of  $[\text{ClpP}_{14}]_T$  is predicted to span from  $\sim 0.4$  to  $\sim 7$ . All data were subjected to global NLLS analysis using Scheme 1 such that the parameters  $k_{T,app}$ ,  $m_{app}$ ,  $mk_{T,app}$ ,  $k_{C,app}$ , and  $k_{NP,app}$  were estimated for each set of polypeptide lengths at each  $[\text{ClpP}_{14}]_T$ . The resultant parameters are given in Table 2.

Figure 4a shows the apparent overall translocation rate  $mk_{T,app}$  plotted as a function of  $[\text{ClpP}_{14}]_T$ . The dependence of  $mk_{T,app}$  on  $[\text{ClpP}_{14}]_T$  exhibits an apparent plateau in the translocation rate at  $[\text{ClpP}_{14}]_T > \sim 84$  nM. Under the assumption that all ClpA monomers reside in the hexameric state, we replotted Fig. 4a by dividing the fixed  $[\text{ClpA}_6]_T$  by the  $[\text{ClpP}_{14}]_T$  to replot the data in Figure 4b as a ratio. Fig. 4b demonstrates that when the molar ratio of ClpA hexamers to ClpP tetradecamers,  $[\text{ClpA}_6]_T / [\text{ClpP}_{14}]_T$ , is less than approximately two, the apparent overall translocation rate is observed to fluctuate about a mean value  $mk_{T,app} = (31 \pm 1)$  aa  $s^{-1}$ . However, when the molar ratio equals approximately two ( $[\text{ClpA}_6]_T / [\text{ClpP}_{14}]_T = \sim 2$ ), a breakpoint is observed where the overall translocation rate steeply decreases as the molar ratio of ClpA hexamers to ClpP tetradecamers increases.

Fig. 4b shows the dependence of the apparent translocation rate on the molar ratio of  $\text{ClpA}_6$  to  $\text{ClpP}_{14}$ . Over the range of  $[\text{ClpA}_6]_T / [\text{ClpP}_{14}]_T = 0 - 1$ , the ClpAP species distribution favors the assembly of only 1:1 ClpAP complexes. However, when  $[\text{ClpA}_6]_T / [\text{ClpP}_{14}]_T = 1 - 2$ , both 1:1 and 2:1 ClpAP complexes may be populated, thereby causing a shift in the ClpAP species distribution relative to  $[\text{ClpA}_6]_T / [\text{ClpP}_{14}]_T = 0 - 1$ . The observation in Fig. 4b of an apparent plateau in  $mk_{T,app}$  that spans molar ratios from 0 - 2 may suggest that 2:1 ClpAP and 1:1 ClpAP translocate polypeptide with the same overall rates under conditions where only one polypeptide is bound to either ClpAP complex. However, this conclusion may not be correct since we have previously demonstrated that the total ClpA monomer concentration is not 100 % hexameric.<sup>8; 9; 10; 14</sup> Therefore, calculating the molar ratio of ClpA hexamers to ClpP tetradecamers by

assuming that the total ClpA population is entirely hexameric by simply dividing by a factor of 6 is not likely to yield the correct ratio.

***1:1 and 2:1 ClpAP complexes translocate polypeptide with similar rates***

To investigate whether 1:1 and 2:1 ClpAP complexes with one polypeptide bound share a common translocation mechanism, we derived an expression to describe the dependence of the overall translocation rate on the ClpAP species distribution given by Eq. (1) below.

$$mk_{T,app} = \frac{mk_{T,1:1} \cdot 2K_{app}[ClpP_{14}] + mk_{T,2:1} \cdot 2K_{app}^2[ClpP_{14}][ClpA_6] + mk_{T,A}}{1 + 2K_{app}[ClpP_{14}] + 2K_{app}^2[ClpP_{14}][ClpA_6]} \quad (1)$$

In Eq. (1), ClpA hexamers interact with each end of ClpP<sub>14</sub> with an apparent association equilibrium constant,  $K_{app}$ . This model also includes terms to describe the dependence of the translocation activity of each individual species on the ClpAP species distribution, where the translocation rates for free ClpA hexamers, 1:1 ClpAP, and 2:1 ClpAP are given as  $mk_{T,A}$ ,  $mk_{T,1:1}$ , and  $mk_{T,2:1}$ , respectively. The floating parameters in this analysis were the apparent association equilibrium constant,  $K_{app}$ , and the translocation rates for 2:1 ClpAP and free ClpA hexamers.

As the  $[ClpP_{14}]_T$  is increased, this, by mass action, drives the equilibrium towards the assembly of 1:1 ClpAP, and thus the apparent plateau shown in Fig. 4a must extrapolate to the overall translocation rate for the 1:1 ClpAP complex. Fig. 4a illustrates that high  $[ClpP_{14}]_T$  lead to an extrapolated value for  $mk_{T,app} = (31 \pm 1) \text{ aa s}^{-1}$ . For these reasons, we have constrained  $mk_{T,1:1} = (31 \pm 1) \text{ aa s}^{-1}$  in our analysis using Eq. (1).

Our initial attempts to subject the data in Fig. 4a to NLLS analysis using Eq. (1) treated the  $[\text{ClpA}_6]_{\text{T}}$  as a floating parameter. We observed in our analysis that  $[\text{ClpA}_6]_{\text{T}}$  converged to a value similar to the for the reported value of  $[\text{ClpA}_6]_{\text{T}} = 130 \text{ nM}$  for conditions of  $1 \text{ }\mu\text{M}$  ClpA and  $150 \text{ }\mu\text{M}$  ATP $\gamma$ S, which contrasts the  $[\text{ATP}\gamma\text{S}] = 1 \text{ mM}$  used here.<sup>14</sup> However, it was unclear whether the similar  $[\text{ClpA}_6]_{\text{T}}$  was the result of poor constraints in our analysis of the data shown in Fig. 4a. Therefore, we asked the question; do the data shown in Fig. 4a contain information on the concentration of free ClpA hexamers? We set out to answer this question by observing the impact on the goodness of fit when the  $[\text{ClpA}_6]_{\text{T}}$  is constrained in Eq. (1) and systematically varied. The constrained ClpA hexamer concentrations in Eq. (1) were  $[\text{ClpA}_6]_{\text{T}} = 97, 103, 108, 114, 119, 125, 130, 136, 141, 147, 152, 158, 163, 169, 174, 180,$  and  $186 \text{ nM}$ . The floating parameters in this analysis were the apparent association equilibrium constant  $K_{app}$  and the translocation rates for free ClpA hexamers and 2:1 ClpAP complexes,  $mk_{T,A}$  and  $mk_{T,2:1}$ , respectively, whereas the translocation rate for 1:1 ClpAP was constrained to  $mk_{T,1:1} = (31 \pm 1) \text{ aa s}^{-1}$ .

Figure 4c represents a plot of the sum of squared deviations (SSD) as a function of the  $[\text{ClpA}_6]_{\text{T}}$ . A broad minimum is observed in Fig. 4c. However, an absolute minimum is observed to occur when the  $[\text{ClpA}_6]_{\text{T}} = 147 \text{ nM}$ , which predicts that  $\sim 88 \%$  of the total  $[\text{ClpA}]$  resides in the hexameric state. This is in contrast to our previous report where  $\sim 78 \%$  of the  $[\text{ClpA}]_{\text{T}}$  was observed to be hexameric in the absence of ClpP and polypeptide.<sup>14</sup> Consequently, the increased hexamer concentration observed here may be due to the presence of polypeptide, ClpP, or an increase in the  $[\text{ATP}\gamma\text{S}]$ . The solid vertical line in Fig. 4c denotes the condition where 100 % of the  $[\text{ClpA}]_{\text{T}}$  is hexameric. Therefore,  $[\text{ClpA}_6]_{\text{T}}$  values to the right of the solid line in Fig. 4c represent ClpA

hexamer concentrations that are not physically possible. Additionally, it should be noted that all subsequent analyses to be discussed assume that the concentration of ClpA hexamers equals 147 nM.

When the overall translocation rate for 2:1 ClpAP,  $mk_{T,2:1}$ , is allowed to float independent of the overall translocation rates for 1:1 ClpAP and free ClpA hexamers,  $mk_{T,2:1} = (32 \pm 2) \text{ aa s}^{-1}$ . This is statistically identical to the overall translocation rate for the 1:1 ClpAP complex,  $mk_{T,1:1} = (31 \pm 1) \text{ aa s}^{-1}$ , determined from the apparent plateau in overall translocation rate in Fig. 4a at high  $[\text{ClpP}_{14}]_T$ . This observation led us to constrain  $mk_{T,2:1} = mk_{T,1:1}$  in our analysis, where  $mk_{T,1:1}$  and  $mk_{T,2:1}$  were constrained to equal  $(31 \pm 1) \text{ aa s}^{-1}$  and the translocation rate for free ClpA hexamers and the apparent association equilibrium constant  $K_{app}$  were treated as floating parameters. The solid line in Fig. 4a represents the resulting fit with the translocation rate for free ClpA hexamers  $mk_{T,A} = (15.5 \pm 0.6) \text{ aa s}^{-1}$  and the apparent association equilibrium constant  $K_{app} = (2 \pm 14) \times 10^{10} \text{ M}^{-1}$ . This estimate of the association equilibrium constant corresponds to a dissociation equilibrium constant of  $(50 \pm 338) \text{ pM}$ , which is several orders of magnitude smaller than our lowest concentration of  $\text{ClpP}_{14}$ . Because the concentrations of  $[\text{ClpP}_{14}]_T$  and  $[\text{ClpA}_6]_T$  presented here are well above the dissociation equilibrium constant and binding is very tight for these conditions,  $K_{app}$  could not be determined accurately.

The broken line in Fig. 4a represents NLLS analysis using Eq. (1) with equivalent translocation rates for 2:1 ClpAP complexes and free ClpA hexamers. As shown, the resulting fit does not adequately describe the data in Fig. 4a. We also attempted to analyze the data in Fig. 4a using Eq. (1) without a term for 2:1 ClpAP complexes,  $mk_{T,2:1} = 0 \text{ aa s}^{-1}$ . The resulting fit is shown in Fig. 4a as a dashed line, and also does not describe

the data. Taken together, the three fits shown in Fig. 4a predict a model where 1:1 and 2:1 ClpAP complexes translocate a single polypeptide with the same overall rates.

When the dissociation equilibrium constant is much smaller than the concentrations of ligand and macromolecule, stoichiometric binding conditions can be achieved. For conditions of stoichiometric binding, the maximum binding stoichiometry can be determined from the breakpoint in a plot of the degree of binding versus the ratio of the monomeric concentrations of total ligand to total macromolecule,  $[X]_T / [M]_T$ . Under single-turnover conditions, the overall translocation rate shown in Fig. 4a is proportional to the degree of binding since the kinetic time courses are sensitive only to translocation activity from enzyme that was bound at time zero. Therefore, the data shown in Fig. 4a can be replotted with  $[ClpA]_T / [ClpP]_T$  on the x-axis and used in the determination of the maximum binding stoichiometry of ClpA hexamers by ClpP tetradecamers for these conditions.

Figure 4d shows a plot of the apparent translocation rate versus the ratio of the total ClpA monomer concentration to the total ClpP monomer concentration. The solid line in Fig. 4d represents the best fit of the data shown in Fig. 4a where the data and the fit have been replotted with the ratio of the total monomer concentrations of each component,  $[ClpA]_T / [ClpP]_T$ , on the x-axis. The data shown in Fig. 4d exhibit a sigmoidal dependence of  $mk_{T,app}$  on the molar ratio with a breakpoint at  $[ClpA]_T / [ClpP]_T = 0.96$ , which is illustrated by the dashed line. Therefore, the maximum stoichiometry describing ClpP monomers binding ClpA monomers is 0.96, which indicates a nearly 1:1 mixture of ClpA monomers and ClpP monomers for these conditions. It is important to recall that this conclusion is predicated on the assumption that the macromolecule

concentration is much greater than the dissociation equilibrium constant,  $[\text{ClpP}_{14}]_{\text{T}} \gg K_d$ , which are conditions that favor tight binding of ClpA hexamers by ClpP tetradecamers.

The maximum stoichiometry represents the ratio of ClpA monomers to ClpP monomers. Therefore, the product of the maximum stoichiometry and the number of ClpP monomers present in the active complex allows for the prediction of the number of ClpA monomers present. Since it has been established that ClpP exists as a tetradecamer, a 14 subunit complex,<sup>7; 20; 21; 22; 23; 24</sup> the product of the maximum stoichiometry from Fig. 4d, 0.96, and 14 is 13.4, i.e.  $0.96 \times 14 = 13.4$ . One would expect that this product would equal 12 if two ClpA hexamers were bound by a single ClpP tetradecamer. For that case, the binding stoichiometry would equal  $\sim 0.86$ , since the ratio of ClpA monomers to ClpP monomers would be  $12 / 14 = 0.86$ .

The observation of a stoichiometry equal to 0.96 represents an 11.6 % deviation from the stoichiometry equal to  $\sim 0.86$  predicted if the entire population of ClpA resides in the hexameric state. Consequently, 11.6 % more ClpA monomers are required to fully saturate ClpP<sub>14</sub> binding of ClpA hexamers. This is likely due to the fact that the entire ClpA population is not hexameric, but instead resides in a dynamic equilibrium of monomers, dimers, tetramers, and hexamers.<sup>8; 9; 10</sup> Moreover, the 11.6 % difference predicts that the hexamer concentration is 147.3 nM, which is in contrast to the hexamer concentration equal to 166.7 nM if the entire ClpA population is hexameric. This is consistent with the NLLS analysis shown in Fig. 4c, where we have predicted the concentration of ClpA hexamers to equal  $\sim 147$  nM for these conditions of  $[\text{ClpA}]_{\text{T}}$ ,  $[\text{ClpP}_{14}]_{\text{T}}$ ,  $[\text{ATP}\gamma\text{S}]$ , and  $[\text{polypeptide}]$ . Therefore, we favor  $\sim 147$  nM as the most likely

ClpA hexamer concentration based on the minimum of the SSD plot shown in Fig. 4c and the 11.6 % deviation between the observed and predicted ClpA binding stoichiometry.

#### Dependence of *kinetic parameters on molar ratio*

We have replotted the apparent translocation rate in Figure 5a as a function the molar ratio using our best estimate of the ClpA hexamer concentration equal to 147 nM. The solid line in Fig. 5a represents the best fit of the data shown in Fig. 4a where the data has been replotted with the molar ratio on the x-axis using  $[\text{ClpA}_6]_{\text{T}} = 147 \text{ nM}$ . The plot shown in Fig. 4b of the apparent translocation rate versus molar ratio assumed that the entire population of ClpA was hexameric, whereas the plot shown in Fig. 5a has accounted for the fact that ~ 88% of the total ClpA monomer concentration is hexameric. However, for both Fig. 4b and Fig. 5a, the apparent translocation rate is observed to fluctuate about a mean value  $mk_{T,app} = (31 \pm 1) \text{ aa s}^{-1}$  for molar ratios in the range of 0 to ~ 2, and is observed to decrease at molar ratios greater than ~ 2. Therefore, our earlier conclusion that 1:1 ClpAP and 2:1 ClpAP complexes translocate polypeptide with identical rates appears to be independent of the concentration of ClpA hexamers since the same conclusion has been reached from a plot of  $mk_{T,app}$  versus molar ratio using different values for  $[\text{ClpA}_6]_{\text{T}}$ .

While it is clear from Fig. 5a that the overall translocation rate depends on the molar ratio when the concentration of ClpA hexamers exceeds the concentration of ClpP tetradecamers by a factor of ~ 2, it is not clear if this is the result of a similar dependence in the kinetic step-size, rate constant, or both. Figure 5b shows the translocation rate constant  $k_{T,app}$  plotted as a function of the molar ratio of ClpA hexamers to ClpP tetradecamers. Similar to the overall translocation rate, Fig. 5b shows an apparent plateau

in the translocation rate constant for molar ratios in the range of 0 to  $\sim 1.5$ , where conditions favor a mixture of 1:1 and 2:1 ClpAP complexes. At sufficiently low molar ratios of ClpA hexamers to ClpP tetradecamers, only 1:1 ClpAP complexes will be present, and the apparent translocation rate constant will represent the rate constant for only 1:1 ClpAP complexes. Therefore, the apparent plateau shown in Fig. 5b must extrapolate at low molar ratios to the translocation rate constant for the 1:1 ClpAP complex,  $k_{T,1:1} = (11.9 \pm 0.9) \text{ s}^{-1}$ .

Figure 5c shows the apparent kinetic step-size  $m_{app}$  plotted as a function of the molar ratio of ClpA hexamers to ClpP tetradecamers. Identical to Fig. 5a-b, Fig. 5c shows that the apparent kinetic step-size remains constant over the range of molar ratios from 0 to  $\sim 1.5$ , where the mean value of  $m_{app} = (2.6 \pm 0.2) \text{ aa step}^{-1}$ . For this range of molar ratios, 1:1 and 2:1 ClpAP complexes will be populated. Identical to the overall translocation rate and rate constant, the apparent plateau shown in Fig. 5c must also extrapolate at low ratios of  $[\text{ClpA}_6]_{\text{T}} / [\text{ClpP}_{14}]_{\text{T}}$  to the kinetic step-size for only 1:1 ClpAP complexes,  $m_{1:1} = (2.6 \pm 0.2) \text{ aa step}^{-1}$ .

Figs. 5b-c illustrate that when the molar ratio of ClpA hexamers to ClpP tetradecamers is greater than  $\sim 1.5$ , the translocation rate constant  $k_{T,app}$  is observed to decrease (see Fig. 5b) and the kinetic step-size  $m_{app}$  is observed to increase (see Fig. 5c). Both parameters are observed to transition at slightly lower molar ratios than the overall translocation rate, where the overall translocation rate was observed to decrease at molar ratios greater than  $\sim 2$  and both the kinetic step-size and rate constant change when the molar ratio exceeds  $\sim 1.5$ . Since transitions for the kinetic parameters are only observed under conditions where ClpP<sub>14</sub> binding of ClpA<sub>6</sub> is most likely saturated, the

dependencies of each parameter on ClpAP species distribution must be the result of an increasing population of free ClpA hexamers, and not due to the relative populations of 1:1 and 2:1 ClpAP complexes. Furthermore, this predicts a transition to a different rate-limiting step as free ClpA hexamers are populated relative to ClpAP complexes.

The kinetic step-size and rate constant both exhibit an apparent plateau when the total ClpA hexamer concentration exceeds the total ClpP tetradecamer concentration by a factor of at least 2.5. These are conditions that favor the population of 2:1 ClpAP complexes and free ClpA hexamers. For the range of molar ratios equal to  $\sim 2.5$  to  $\sim 8$ , the average values of the translocation rate constant and the kinetic step-size are  $k_{T,app} = (3.4 \pm 0.6) \text{ s}^{-1}$  and  $m_{app} = (6.9 \pm 0.8) \text{ aa step}^{-1}$ .

The dependencies of the kinetic parameters on the ClpAP species distribution indicate a different rate-limiting step for ClpAP complexes versus free ClpA hexamers. This is consistent with our previous report that the presence of ClpP affects the ClpA catalyzed polypeptide translocation mechanism, where the rate-limiting step for ClpAP was reported to occur every 2 - 5 amino acids translocated with a rate constant of  $\sim 8 \text{ s}^{-1}$ .<sup>14</sup> Since we observe here that 1:1 and 2:1 ClpAP complexes translocate polypeptide with identical mechanisms, we can refine our earlier report to conclude that the rate-limiting step for ClpAP complexes must occur every  $(2.6 \pm 0.2)$  amino acids translocated with a rate constant equal to  $(11.9 \pm 0.9) \text{ s}^{-1}$ . Furthermore, we are able to conclude that the primary reason for the dependence of the kinetic parameters on the ClpAP species distribution is due to an increase in the population of free ClpA hexamers, since 1:1 and 2:1 ClpAP complexes catalyze polypeptide translocation with a common translocation mechanism.

## Discussion

### *Polypeptide translocation catalyzed by 1:1 ClpAP versus 2:1 ClpAP*

Recently, the Weber-ban group proposed that 2:1 ClpAP complexes can translocate polypeptide from either end of ClpP simultaneously and independently.<sup>16</sup> In that study, translocation by 1:1 or 2:1 ClpAP complexes was observed using a  $\lambda$ RSsrA construct prepared with donor and acceptor fluorophores far away in the primary structure, but close in the tertiary structure. Upon unfolding and translocation of the  $\lambda$ RSsrA construct by ClpAP, an increase in donor fluorescence was observed. Stopped-flow fluorescence experiments were performed where the fluorescently-labeled  $\lambda$ RSsrA construct was incubated with ClpAP that had been preassembled using a ClpP construct that could only interact with ClpA at one end of the ClpP tetradecamer to form 1:1 ClpAP complexes or with wild-type ClpP, where 2:1 ClpAP complexes would be favored. Fluorescence time courses collected in the presence of mutant ClpP or wild-type ClpP were observed to be identical when a 2-fold higher concentration of 1:1 ClpAP was used relative to the concentration of 2:1 ClpAP. From this, it was concluded that a 2-fold higher concentration of 1:1 ClpAP complexes is required to approximate the translocation activity of 2:1 ClpAP complexes. This observation led to the proposal that translocation can initiate from either end of ClpP<sub>14</sub> simultaneously and independent of the events taking place at the opposite end of ClpP<sub>14</sub>.

In contrast to the model proposed by Weber-ban and coworkers,<sup>16</sup> Maurizi and coworkers have concluded that the proteolytic activities of 2:1 ClpAP and 1:1 ClpAP are approximately equivalent.<sup>7</sup> In that study, casein degradation was measured using different

ratios of ClpA hexamers to ClpP tetradecamers while maintaining a constant total molar concentration of ClpA<sub>6</sub> and ClpP<sub>14</sub>. Maurizi and coworkers observed that the maximum proteolytic activity occurred under conditions where the concentrations of ClpA hexamers and ClpP tetradecamers were nearly equivalent. In fact, the observed proteolytic activity was nearly identical for conditions where the molar ratio of ClpA hexamers to ClpP tetradecamers was in the range of 1 to ~ 2.3, where assembly of only 1:1 ClpAP or 2:1 ClpAP is favored. However, the ratio of ClpA hexamers to ClpP tetradecamers was calculated assuming that the total ClpA concentration was hexameric, which is not consistent with our more recent findings that ClpA resides in a dynamic equilibrium of monomers, dimers, tetramers, and hexamers.<sup>8; 10</sup> Using our estimate reported here that ~ 88% of the ClpA population is hexameric for these conditions of [ClpA]<sub>T</sub>, [ClpP]<sub>T</sub>, [polypeptide], and [ATPγS], we have recalculated their range of molar ratios corresponding to maximum proteolytic activity to span from ~ 0.9 to ~ 2. Therefore, interpreting their observations alongside our own allows for the conclusion that, whether the total ClpA concentration is entirely hexameric or not, conditions favoring the addition of a second ClpA hexamer to the ClpAP complex do not appear to further activate ClpP for polypeptide degradation.

Maurizi and coworkers proposed that their observation of nearly identical proteolytic activities for 1:1 ClpAP versus 2:1 ClpAP was a result of inefficient initiation of a second translocation event.<sup>7; 25</sup> From electron microscopy experiments, when the related ATP-dependent protease ClpXP was incubated with excess concentrations of polypeptide substrate and ATP for two hours, 2:1 ClpXP was observed to translocate polypeptide only from one end of the ClpP tetradecamer in ~ 95 % of complexes despite

having two polypeptides bound.<sup>25</sup> From this, it was proposed that negative cooperativity between the two ClpP-associated ClpX hexamers may affect polypeptide translocation, but not the polypeptide binding activity since polypeptide was observed bound to both ends of 2:1 ClpXP complexes. It is possible that ClpP employs a similar mechanism to modulate the translocation of ClpA hexamers associated with ClpP<sub>14</sub>. Therefore, the proteolytic activities reported previously for 1:1 and 2:1 ClpAP complexes may have been identical because polypeptide is only translocated from one end of ClpP<sub>14</sub>.<sup>7</sup>

We have previously reported models for ClpA and ClpAP catalyzed polypeptide translocation.<sup>12; 14</sup> Whether ClpP is present or not, the rate limiting step in ClpA catalyzed polypeptide translocation is a step that immediately follows ATP binding.<sup>12; 14</sup> For ClpA, this step repeats every ~ 14 amino acids translocated with an observed rate constant of ~ 1.4 s<sup>-1</sup>, whereas for ClpAP this step repeats every ~ 2 – 5 amino acids translocated with an observed rate constant of ~ 6.6 s<sup>-1</sup>. By comparing the results from our single-turnover polypeptide translocation experiments<sup>14</sup> to steady state ATP hydrolysis rates from Weber-Ban and coworkers<sup>6</sup> and crosslinking experiments from Horwich and coworkers,<sup>15</sup> we proposed that the repeating rate-limiting step observed for ClpA in the absence of ClpP is coupled to ATP hydrolysis at D1, whereas, in the presence of ClpP, the repeating rate-limiting step is coupled to ATP hydrolysis at D2.<sup>16; 18</sup>

Here, we have applied our previously reported single-turnover stopped-flow fluorescence method to examine the dependence of the ClpAP translocation mechanism on the distribution of ClpAP species. The single-turnover experiments reported here were performed under conditions where the concentration of enzyme is in excess of the concentration of polypeptide, thereby statistically favoring the formation of ClpAP

complexes with a single polypeptide bound. This is in contrast to many other reports for ClpAP where conditions are commonly used with the polypeptide concentration in large excess of the enzyme concentration, thereby favoring the assembly of ClpAP complexes with two polypeptides bound.<sup>6; 7; 15; 16; 26</sup> Because our conditions favor ClpAP complexes with a single polypeptide bound, we cannot discern whether polypeptide is translocated from both ends of ClpP<sub>14</sub> simultaneously, as proposed by Weber-ban and coworkers, or if translocation initiates only from one side of a ClpAP complex as proposed by Maurizi and coworkers.<sup>7; 16</sup> However, the single-turnover experiments reported here allow for the examination of the impact on the translocation mechanism of the addition of a second ClpA hexamer to a ClpAP complex with a single polypeptide bound. Since there clearly is an allosteric impact on the translocation mechanism of ClpA when associated with ClpP, it is not unreasonable to think that addition of a second ClpA hexamer unligated with polypeptide may have an effect on the polypeptide-ligated ClpA hexamer associated at the opposite end of ClpP<sub>14</sub>.

From NLLS analysis of translocation time courses collected as a function of [ClpP<sub>14</sub>]<sub>T</sub>, we conclude here that 1:1 and 2:1 ClpAP complexes translocate a single polypeptide with identical translocation mechanisms. For conditions favoring 1:1 or 2:1 ClpAP complexes with a single polypeptide bound (see Fig. 1b-c), the overall translocation rate is  $(31 \pm 1)$  aa s<sup>-1</sup>, and repeats every ~ 3 amino acids translocated, consistent with our previous report that the rate-limiting step repeats every 2 – 5 amino acids translocated.<sup>14</sup> Moreover, since we observe that 1:1 and 2:1 ClpAP complexes utilize identical mechanisms to translocate a single polypeptide, we are able to conclude that the addition of a second ClpA hexamer unligated with polypeptide does not impact

the translocation activity of the polypeptide-ligated ClpA hexamer associated at the opposite end of ClpP<sub>14</sub>. This is an important finding since it demonstrates that the allosteric impact of ClpP on the mechanism of ClpA catalyzed polypeptide translocation occurs via the interaction of a single ClpP tetradecamer with a single polypeptide-bound ClpA hexamer.

### ***Binding of ClpA hexamers by ClpP tetradecamers***

Under stoichiometric binding conditions, the maximum binding stoichiometry can be determined from the breakpoint in a plot of the extent of binding versus the ratio of the total ligand and macromolecule concentrations. The single-turnover method applied here is sensitive only to enzyme that is bound with fluorescently-modified polypeptide when translocation is initiated by rapid mixing with ATP in the stopped-flow fluorometer. Therefore, the overall rate of translocation is proportional to the extent of binding. Because of this, a plot of the translocation rate versus the ratio of the total ligand and macromolecule concentrations can be used to determine the maximum binding stoichiometry. However, this approach is only valid under conditions where the enzyme concentration is at least two orders of magnitude larger than the apparent dissociation equilibrium constant.

A plot of the apparent translocation rate versus the ratio of the total ClpA monomer concentration to the total ClpP monomer concentration yields a maximum binding stoichiometry equal to 0.96 (see Fig. 4d). Thus, a maximum stoichiometry equal to 0.96 indicates that for each ClpP tetradecamer, ~ 13 ClpA monomers are present. This observation is in contrast to the predicted maximum stoichiometry equal to ~ 0.86 if a

maximum of 12 ClpA monomers, i.e. 2 ClpA hexamers, interact with each ClpP tetradecamer.

The observation of a ClpA binding stoichiometry that is larger than the stoichiometry predicted if the entire population of ClpA resides in the hexameric state indicates that additional ClpA monomers are required to fully saturate binding of ClpA by ClpP. That is to say, the observation of a binding stoichiometry larger than predicted suggests that a higher concentration of ClpA monomers is required to fully saturate ClpP binding. This is potentially a direct result of a decrease in the concentration of ClpA hexamers, uncertainty in the ClpA<sub>6</sub>:ClpP<sub>14</sub> binding affinity, or both.

The predicted ClpA binding stoichiometry equal to  $\sim 0.86$  assumes that 100 % of the total ClpA monomer concentration exists in the hexameric state, which is an assumption that we have previously reported to be incorrect.<sup>8; 9; 10; 14</sup> The 11.6 % deviation between the observed and predicted ClpA binding stoichiometries predicts that the actual concentration of ClpA hexamers is equal to 147.3 nM for these conditions of [ClpA]<sub>T</sub>, [ClpP<sub>14</sub>]<sub>T</sub>, [ATP $\gamma$ S], and [polypeptide]. A hexamer concentration of 147.3 nM is less than the concentration predicted if 100 % of ClpA is hexameric, and corresponds to a ClpA population where  $\sim 88$  % of the total ClpA monomer concentration is hexameric. This is in contrast to our previous report where  $\sim 78$  % of the total population of ClpA was observed to be hexameric for 1  $\mu$ M ClpA in the absence of ClpP and polypeptide.<sup>14</sup> The increase in ClpA hexamer concentration is consistent with an increase in the apparent association equilibrium constant describing ClpA hexamerization,  $L_{6,app}$ , due to [ClpP]<sub>T</sub>, [polypeptide], or an increased [ATP $\gamma$ S]. It should be noted that we predicted in our previous report that no additional hexamers would form at [ATP $\gamma$ S] higher than  $\sim 150$

$\mu\text{M}$ , since an apparent plateau was observed in the ClpA hexamer concentration when plotted versus  $[\text{ATP}\gamma\text{S}]$ . Thus, the increase in hexamer concentration observed here is most likely a result of ClpP or polypeptide. Whether or not the increased hexamer concentration is due to the presence of ClpP or polypeptide, the population of ClpA monomers is not 100 % hexameric. Therefore, higher  $[\text{ClpA}]_{\text{T}}$  are required to saturate ClpP binding relative to conditions where 100 % of the  $[\text{ClpA}]_{\text{T}}$  resides in the hexameric state, which subsequently must lead to an apparent increase in the ClpA binding stoichiometry.

An alternate explanation for the apparent deviation between the observed and predicted ClpA binding stoichiometries is that the  $\text{ClpA}_6:\text{ClpP}_{14}$  binding affinity is weaker than previously reported. To date, we have assumed that binding is tight based on the reported affinity constant  $K_d = 4 \text{ nM}$  for the  $\text{ClpA}_6:\text{ClpP}_{14}$  interaction.<sup>7</sup> However, if the affinity is weaker than reported, it is possible that the maximum binding stoichiometry could be overestimated since increased concentrations of monomeric ClpA, and subsequently increased ratios of the total monomer concentrations of ClpA and ClpP, would be required to fully saturate binding of ClpA hexamers by  $\text{ClpP}_{14}$ . Therefore, the observation of a binding stoichiometry equal to  $\sim 0.96$ , instead of the predicted stoichiometry equal to  $\sim 0.86$ , may suggest that the affinity constant describing the  $\text{ClpA}_6:\text{ClpP}_{14}$  interaction is weaker than previously reported.

### ***Proposed mechanism for ClpAP activation in the cytoplasm***

From the predicted dependence of the association equilibrium constant for ClpA hexamerization on  $[\text{polypeptide}]$ ,  $[\text{ClpP}]_{\text{T}}$ , or both, we propose a model where hexamerization is directly affected by solution conditions in the cytoplasm. We have

previously reported that the equilibrium constant describing ClpA hexamerization,  $L_{6,app}$ , is dependent on the type of polypeptide substrate that ClpA is bound by, where more hexamers are populated in the presence of  $\alpha$ s1 casein polypeptides relative to SsrA-tagged polypeptides.<sup>27</sup> Thus, the accumulation of certain types of polypeptide could lead to the population of additional hexamers.

Since the polypeptide translocation activity of ClpAP complexes is dependent on the molar ratio of ClpA hexamers to ClpP tetradecamers, a mechanism where hexamerization is linked to polypeptide concentration and type would provide a direct pathway for activation of ClpAP complexes. Cytoplasmic conditions that favor the accumulation of polypeptide substrates recognized by ClpA would function much like an on/off switch to regulate the proteolytic activity of ClpAP complexes. Because ClpP is known to degrade only short polypeptides when in the absence of an ATPase partner, a lack of polypeptide substrates for ClpA would lead to a decreased concentration of ClpA hexamers, and subsequently, a decrease in the proteolytic activity resulting from ClpAP complexes. Furthermore, ClpP would become available for association with cytoplasmic ClpX hexamers when polypeptide substrates for ClpA were absent. Therefore, the activity of ClpAP/XP complexes is predicted to be controlled through the dependence of the association equilibrium constant for either ClpA or ClpX hexamerization on solution conditions like [polypeptide], polypeptide type, [ClpP]<sub>T</sub>, and the presence of adaptor proteins like ClpS and SspB.<sup>2</sup>

## Materials and Methods

### *Materials*

All solutions were prepared in double-distilled water produced from a Purelab Ultra Genetic system (Siemens Water Technology) and using reagent grade chemicals purchased commercially. All peptide substrates were synthesized by CPC Scientific (Sunnyvale, CA). All peptides were >90% pure as judged by HPLC and mass spectral analysis. Fluorescein was covalently attached to the free cysteine residue at the amino terminus of the polypeptide as previously described. *E. coli* ClpA and ClpP were purified as described and the concentrations were determined spectrophotometrically in buffer H (25 mM HEPES, pH 7.5 at 25 °C, 10 mM MgCl<sub>2</sub>, 2 mM 2-mercaptoethanol, 300 mM NaCl, and 10% v/v glycerol).<sup>8; 14</sup>

### *Methods*

Fluorescence stopped-flow experiments were performed as previously described and shown in Fig. 2.<sup>12</sup> All reactions were prepared in buffer H (25 mM HEPES, pH 7.5 at 25 °C, 10 mM MgCl<sub>2</sub>, 2 mM 2-mercaptoethanol, 300 mM NaCl, and 10% v/v glycerol). All experiments were performed in an SX.20 stopped-flow fluorometer, Applied Photophysics (Letherhead, UK). Prior to each reaction, 1 μM ClpA was preincubated with 1 mM ATPγS for 25 minutes. ClpP was then added using concentrations stated above and incubated for another 25 minutes to allow for assembly of ClpAP complexes competent for polypeptide translocation. Finally, fluorescently modified polypeptide substrate was added such that the concentration was 20 nM, and the mixture was loaded into syringe 1 of the stopped-flow apparatus. Syringe 2 contained a solution of 10 mM

ATP and 300  $\mu\text{M}$  SsrA peptide prepared in buffer H. Prior to mixing, both solutions were incubated for an additional 10 minutes at 25°C in the stopped-flow instrument to allow for thermal equilibration. Increasing the incubation time of either solution in the stopped-flow instrument had no effect on the observed fluorescence time courses. Upon mixing, the final concentrations were 0.5  $\mu\text{M}$  ClpA monomer, 150  $\mu\text{M}$  SsrA peptide, 500  $\mu\text{M}$  ATP $\gamma\text{S}$ , 5 mM ATP, 10 nM fluorescein-modified polypeptide, and the final concentrations of ClpP<sub>14</sub> are indicated in the text. Fluorescein dye was excited at  $\lambda_{\text{ex}} = 494$  nm and fluorescence emission was observed above 515 nm with a 515 nm long pass filter. All kinetic traces shown represent the average of at least 8 individual determinations.

### *NLLS Analysis*

The system of coupled differential equations that result from Scheme 1 was solved using the method of Laplace transforms to obtain an expression for product formation as a function of the Laplace variable,  $S(s)$ , given by Equation (2),

$$S(s) = \frac{1}{s} \left( \sum_{j=1}^h \frac{k_d k_C^{j-1} (k_{NP} + sx)}{(k_C + k_d + s)^j (k_{NP} + s)} + \sum_{i=1}^{n-1} \frac{k_d k_T^h k_T^{i-1} (k_{NP} + sx)}{(k_C + k_d + s)^h (k_{NP} + s) (k_d + k_T + s)^i} + \frac{(k_T + k_d) k_C^h k_T^{n-1} (k_{NP} + sx)}{(k_C + k_d + s)^h (k_{NP} + s) (k_d + k_T + s)^n} \right) \quad (2)$$

where capital  $S$  represents the substrate and lower case  $s$  is the Laplace variable,  $h$  is the number of steps with rate constant  $k_C$ ,  $n$  is the number of steps with rate constant  $k_T$ ,  $k_{NP}$  is the rate of transition from a nonproductive complex to the productive complex, and  $x$  is the fraction of enzyme bound in the productive form given by Equation (3).

$$x = \frac{[ClpAP \cdot S]_L}{[ClpAP \cdot S]_L + [ClpAP \cdot S]_{NP}} \quad (3)$$

Equation (2) was then numerically solved using Equation (4) to describe product formation as a function of time,  $S(t)$ ,

$$S(t) = A_T \mathcal{L}^{-1} S(s) \quad (4)$$

where  $A_T$  is the total amplitude of the time-course, and  $\mathcal{L}^{-1}$  is the inverse Laplace transform operator. This was accomplished using the NLLS fitting routine, Conlin, and the inverse Laplace transform function using the IMSL C Numerical libraries from Visual Numerics (Houston, TX), as previously described.<sup>13; 18</sup> Uncertainties reported on the parameters in Table 2 are based on the average of a minimum of two independent experiments, analysis, and Monte Carlo simulations.<sup>28</sup> A minimum of 100 cycles were used in all Monte Carlo simulations.

## **Acknowledgements**

We would like to thank members of the Lucius lab for critical discussion of this manuscript. Thanks to J. Woody Robins for use of the fermenter core facility. This work was supported by NSF grant MCB-0843746 to ALL, National Institute of Biomedical Imaging and Bioengineering (NIBIB) grant number T32EB004312 to JMM, and the University of Alabama at Birmingham Department of Chemistry. The content discussed here is solely the responsibility of the authors and does not necessarily represent the official views of the National Institute of Biomedical Imaging and Bioengineering or the National Institutes of Health.

## References

1. Gottesman, S. (1996). Proteases and their targets in Escherichia coli. *Annu Rev Genet* **30**, 465-506.
2. Sauer, R. T. & Baker, T. A. (2011). AAA+ Proteases: ATP-Fueled Machines of Protein Destruction. *Annual review of biochemistry* **80**, 587-612.
3. Neuwald, A. F., Aravind, L., Spouge, J. L. & Koonin, E. V. (1999). AAA+: A class of chaperone-like ATPases associated with the assembly, operation, and disassembly of protein complexes. *Genome Res* **9**, 27-43.
4. Guo, F., Maurizi, M. R., Esser, L. & Xia, D. (2002). Crystal structure of ClpA, an Hsp100 chaperone and regulator of ClpAP protease. *J Biol Chem* **277**, 46743-52
5. Singh, S. K. & Maurizi, M. R. (1994). Mutational analysis demonstrates different functional roles for the two ATP-binding sites in ClpAP protease from Escherichia coli. *J Biol Chem* **269**, 29537-45.
6. Kress, W., Mutschler, H. & Weber-Ban, E. (2009). Both ATPase domains of ClpA are critical for processing of stable protein structures. *J Biol Chem* **284**, 31441-52.
7. Maurizi, M. R., Singh, S. K., Thompson, M. W., Kessel, M. & Ginsburg, A. (1998). Molecular properties of ClpAP protease of Escherichia coli: ATP-dependent association of ClpA and clpP. *Biochemistry* **37**, 7778-86.
8. Veronese, P. K., Stafford, R. P. & Lucius, A. L. (2009). The Escherichia coli ClpA Molecular Chaperone Self-Assembles into Tetramers. *Biochemistry* **48**, 9221-9233.
9. Veronese, P. K. & Lucius, A. L. (2010). Effect of Temperature on the Self-Assembly of the Escherichia coli ClpA Molecular Chaperone. *Biochemistry* **49**, 9820-9.
10. Veronese, P. K., Rajendar, B. & Lucius, A. L. (2011). Activity of Escherichia coli ClpA Bound by Nucleoside Di- and Triphosphates. *Journal of molecular biology* **409**, 333-47.

11. Maurizi, M. R. (1991). ATP-promoted interaction between Clp A and Clp P in activation of Clp protease from Escherichia coli. *Biochem Soc Trans* **19**, 719-23.
12. Rajendar, B. & Lucius, A. L. (2010). Molecular mechanism of polypeptide translocation catalyzed by the Escherichia coli ClpA protein translocase. *J Mol Biol* **399**, 665-79.
13. Lucius, A. L., Miller, J. M. & Rajendar, B. (2011). Application of the Sequential n-Step Kinetic Mechanism to Polypeptide Translocases. *Methods Enzymol* **488**, 239-64.
14. Miller, J. M., Lin, J., Li, T. & Lucius, A. L. (2013). E. coli ClpA Catalyzed Polypeptide Translocation Is Allosterically Controlled by the Protease ClpP. *J Mol Biol*.
15. Hinnerwisch, J., Fenton, W. A., Furtak, K. J., Farr, G. W. & Horwich, A. L. (2005). Loops in the central channel of ClpA chaperone mediate protein binding, unfolding, and translocation. *Cell* **121**, 1029-41.
16. Maglica, Z., Kolygo, K. & Weber-Ban, E. (2009). Optimal efficiency of ClpAP and ClpXP chaperone-proteases is achieved by architectural symmetry. *Structure* **17**, 508-16.
17. Reid, B. G., Fenton, W. A., Horwich, A. L. & Weber-Ban, E. U. (2001). ClpA mediates directional translocation of substrate proteins into the ClpP protease. *Proc Natl Acad Sci U S A* **98**, 3768-72.
18. Lucius, A. L., Maluf, N. K., Fischer, C. J. & Lohman, T. M. (2003). General methods for analysis of sequential "n-step" kinetic mechanisms: application to single turnover kinetics of helicase-catalyzed DNA unwinding. *Biophys J* **85**, 2224-39.
19. Ali, J. A. & Lohman, T. M. (1997). Kinetic measurement of the step size of DNA unwinding by Escherichia coli UvrD helicase. *Science* **275**, 377-80.
20. Wang, J., Hartling, J. A. & Flanagan, J. M. (1997). The structure of ClpP at 2.3 Å resolution suggests a model for ATP-dependent proteolysis. *Cell* **91**, 447-56.
21. Effantin, G., Maurizi, M. R. & Steven, A. C. (2010). Binding of the ClpA unfoldase opens the axial gate of ClpP peptidase. *J Biol Chem* **285**, 14834-40.
22. Beuron, F., Maurizi, M. R., Belnap, D. M., Kocsis, E., Booy, F. P., Kessel, M. & Steven, A. C. (1998). At sixes and sevens: characterization of the symmetry mismatch of the ClpAP chaperone-assisted protease. *Journal of structural biology* **123**, 248-59.

23. Kessel, M., Maurizi, M. R., Kim, B., Kocsis, E., Trus, B. L., Singh, S. K. & Steven, A. C. (1995). Homology in structural organization between E. coli ClpAP protease and the eukaryotic 26 S proteasome. *J Mol Biol* **250**, 587-94.
24. Bewley, M. C., Graziano, V., Griffin, K. & Flanagan, J. M. (2006). The asymmetry in the mature amino-terminus of ClpP facilitates a local symmetry match in ClpAP and ClpXP complexes. *Journal of structural biology* **153**, 113-28.
25. Ortega, J., Lee, H. S., Maurizi, M. R. & Steven, A. C. (2002). Alternating translocation of protein substrates from both ends of ClpXP protease. *The EMBO journal* **21**, 4938-49.
26. Weber-Ban, E. U., Reid, B. G., Miranker, A. D. & Horwich, A. L. (1999). Global unfolding of a substrate protein by the Hsp100 chaperone ClpA. *Nature* **401**, 90-3.
27. Li, T. & Lucius, A. L. (2013). Examination of the Polypeptide Substrate Specificity for Escherichia coli ClpA. *Biochemistry*.
28. Straume, M. & Johnson, M. L. (1992). Monte Carlo method for determining complete confidence probability distributions of estimated model parameters. *Methods Enzymol* **210**, 117-29.

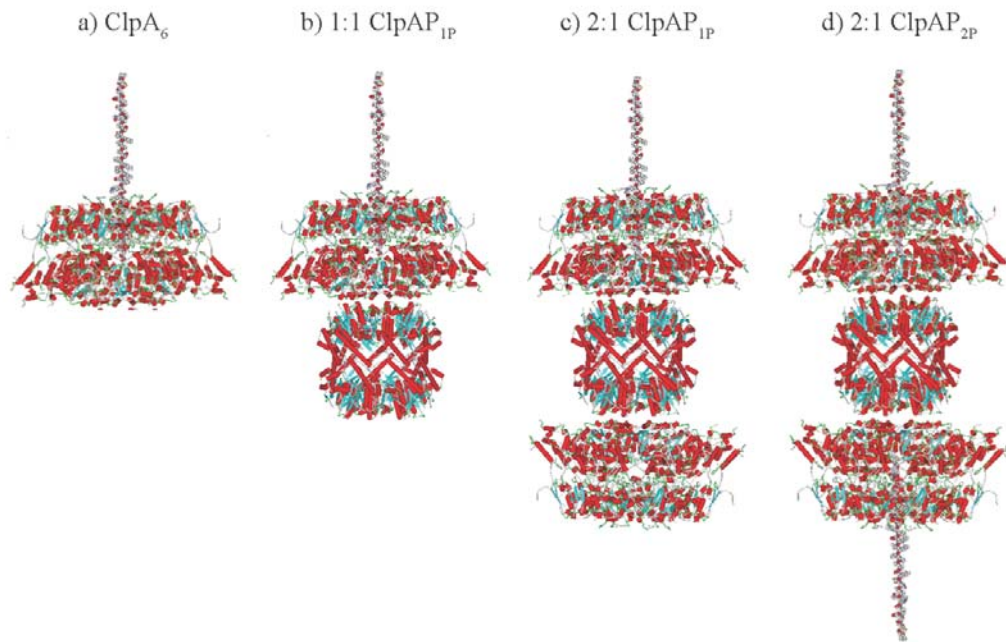


**Figure 1. Schematic representation of the possible ClpAP association states.** Free ClpA hexamers may catalyze polypeptide translocation independent of ClpP<sub>14</sub> (a). Alternatively, ClpA hexamers can associate with a single face of ClpP<sub>14</sub> to form the 1:1 ClpAP complex (b) or with both faces of ClpP<sub>14</sub> to form the 2:1 ClpAP complex (c). In principle, the 2:1 ClpAP complex can bind one (c) or two (d) polypeptide substrates per active complex to form a 2:1 ClpAP<sub>1P</sub> complex or a 2:1 ClpAP<sub>2P</sub> complex, respectively.

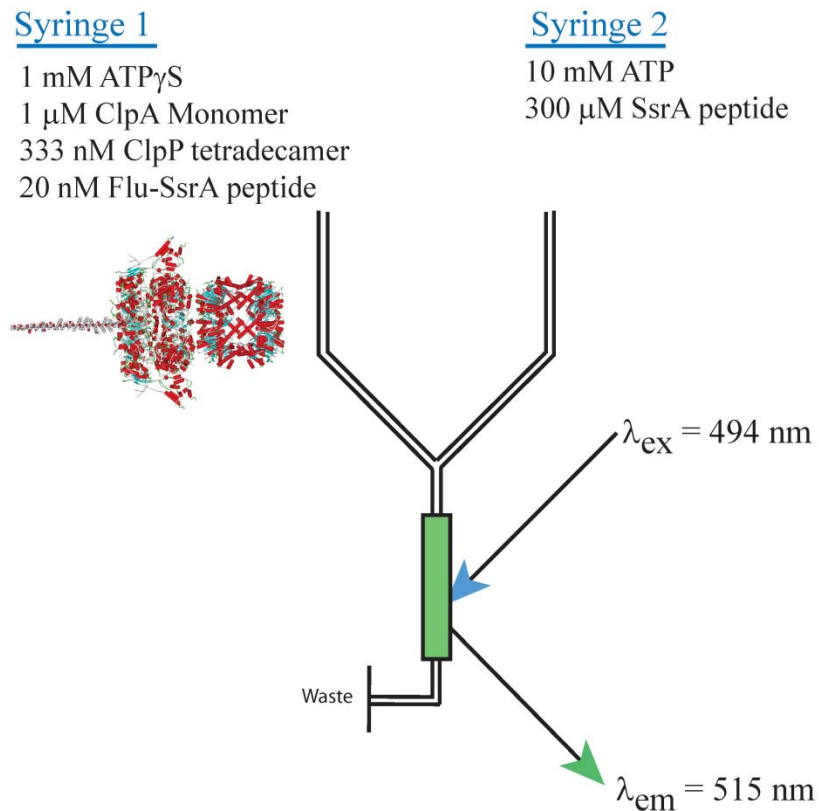


**Figure 2. Schematic representation of single turnover stopped-flow translocation experiments.** Syringe 1 contains the indicated reagents, 1  $\mu$ M ClpA monomer, 333 nM ClpP<sub>14</sub>, 1 mM ATP $\gamma$ S, and 20 nM fluorescein-labeled polypeptide. The structure shown illustrates the contents of syringe 1 with the formation of the 1:1 ClpAP complex with a single polypeptide bound. Syringe 2 contains 10 mM ATP and 300  $\mu$ M SsrA peptide to serve as a trap for unbound ClpAP or any ClpAP that dissociates from fluorescently-modified polypeptide during the course of the reaction. The contents of the two syringes are rapidly mixed in the green colored chamber and fluorescein is excited at  $\lambda_{\text{ex}} = 494$  nm. Fluorescein emissions are observed above 515 nm with a 515 nm long pass filter. Upon mixing, the concentrations are two-fold lower than in the preincubation syringe.

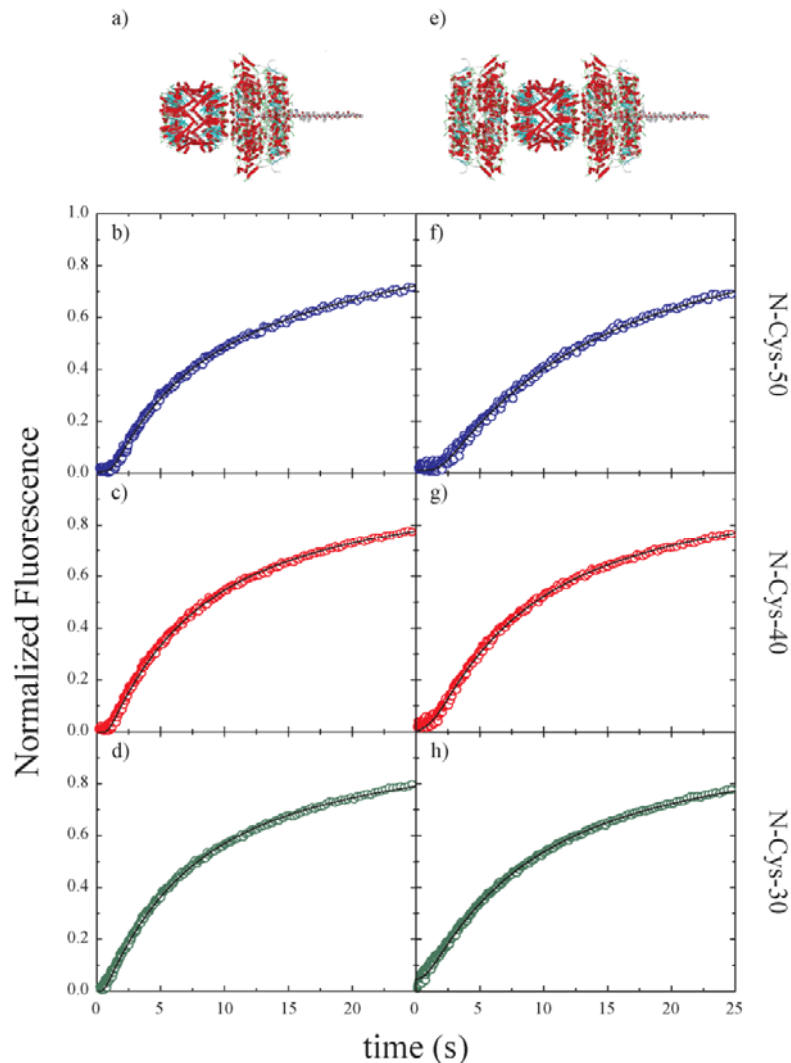


**Figure 3. Representative Fluorescence time-courses for ClpAP catalyzed polypeptide translocation.** 1:1 ClpAP (a) or 2:1 ClpAP (e) complexes were preassembled and prebound with polypeptide by incubating 1  $\mu\text{M}$  ClpA monomer, 1 mM ATP $\gamma\text{S}$ , and 20 nM fluorescein-labeled polypeptide substrate in the presence of 333 nM ClpP $_{14}$  or 19 nM ClpP $_{14}$ , respectively, prior to rapid mixing in the stopped-flow fluorometer with 10 mM ATP and 300  $\mu\text{M}$  SsrA. Representative fluorescence time-courses are shown for either 1:1 ClpAP catalyzed translocation (b-d) or 2:1 ClpAP catalyzed translocation (f-h) using N-Cys-50 (blue circles), N-Cys-40 (red circles), and N-Cys-30 (green circles) polypeptide substrates. The solid black lines represent a global NLLS fit for each  $[\text{ClpP}_{14}]_T$  using Scheme 1 for time-courses collected with substrates I – III in Table 1. The resulting kinetic parameters are summarized in Table 2. Each time-course was analyzed under a given set of conditions by constraining the parameters  $k_T$ ,  $k_C$ ,  $k_{NP}$ , and  $h$  to be global parameters, while  $A_x$ ,  $x$ , and  $n$  were allowed to float for each polypeptide length.

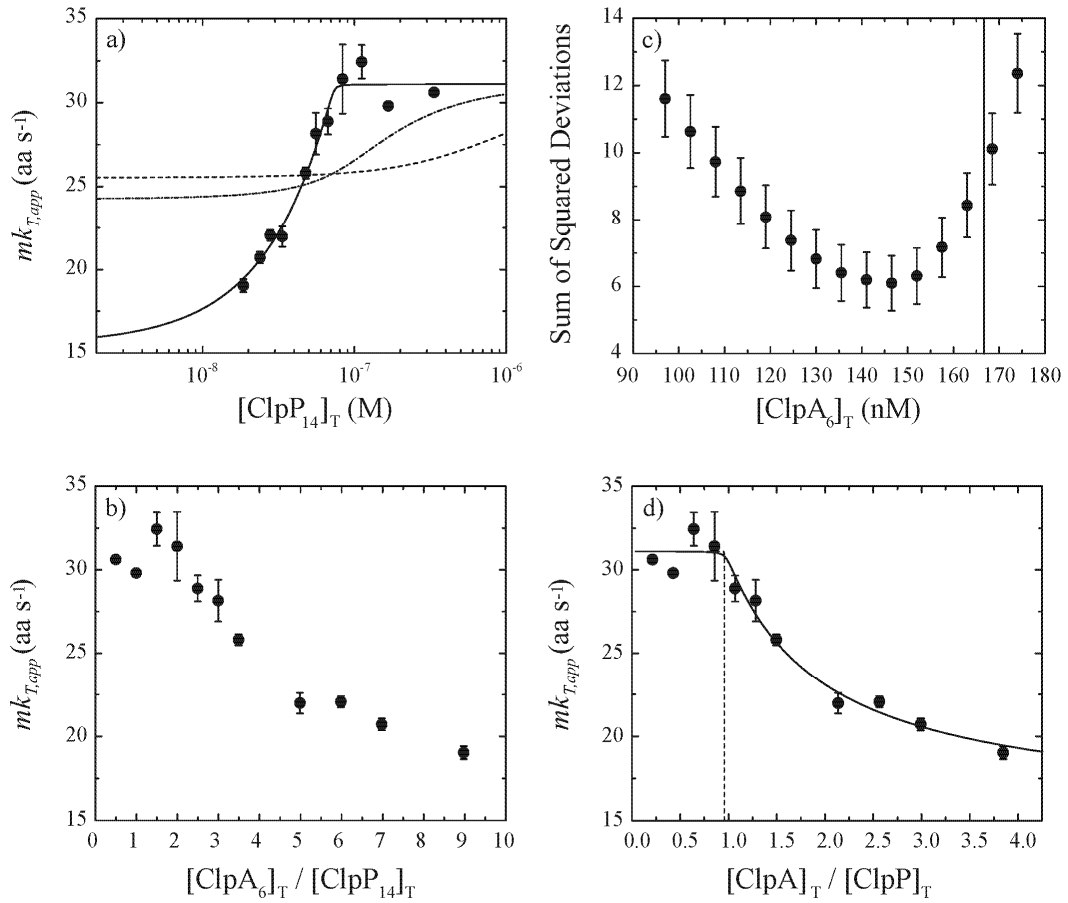


**Figure 4. The apparent overall rate of translocation  $mk_{T,app}$  depends on  $[\text{ClpP}_{14}]_T$ .** (a) Dependence of apparent overall translocation rate  $mk_{T,app}$  on  $[\text{ClpP}_{14}]_T$  for ClpAP catalyzed polypeptide translocation. The solid line is the result of a NLLS fit to Eq. (1) with  $K_{app} = (2 \pm 14) \times 10^{10} \text{ M}^{-1}$  and  $mk_{T,A} = (15.5 \pm 0.6) \text{ aa s}^{-1}$ , where the overall translocation rates for 1:1 and 2:1 ClpAP complexes were constrained to equal  $(31 \pm 1) \text{ aa s}^{-1}$ . The broken and dashed lines represent NLLS analysis using Eq. (1) with either equivalent translocation rates for 2:1 ClpAP complexes and free ClpA hexamers or with  $mk_{T,2:1} = 0 \text{ aa s}^{-1}$ , respectively. (b) Dependence of the translocation rate  $mk_{T,app}$  on the ratio of the concentrations of ClpA hexamers to ClpP tetradecamers,  $[\text{ClpA}_6]_T / [\text{ClpP}_{14}]_T$ . (c) Dependence of the goodness of fit for the analysis of  $mk_{T,app}$  versus  $[\text{ClpP}_{14}]_T$  on the constrained  $[\text{ClpA}_6]_T$  in Eq. (1). The solid vertical line denotes the condition where 100% of the  $[\text{ClpA}]_T$  is hexameric. (d) The apparent translocation rate plotted as a function of the ratio of the total monomer concentrations of ClpA and ClpP. The solid line represents the best fit of the data shown in Fig. 4a where the data has been replotted with the ratio of the total monomer concentrations of each component,  $[\text{ClpA}]_T / [\text{ClpP}]_T$ , on the x-axis. The dashed line represents the observed breakpoint at  $[\text{ClpA}]_T / [\text{ClpP}]_T = 0.96$ , which defines the maximum stoichiometry describing ClpP monomers binding ClpA monomers.

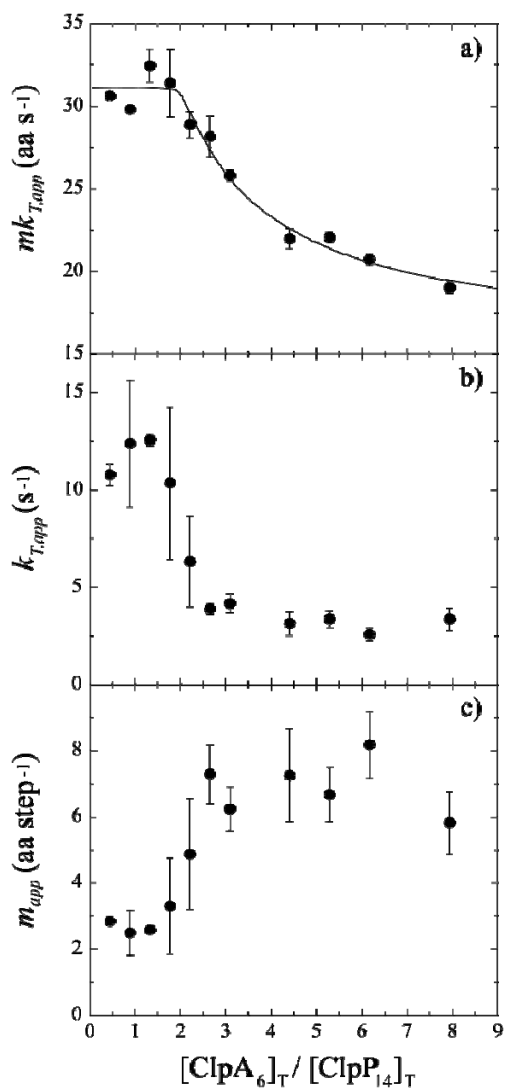
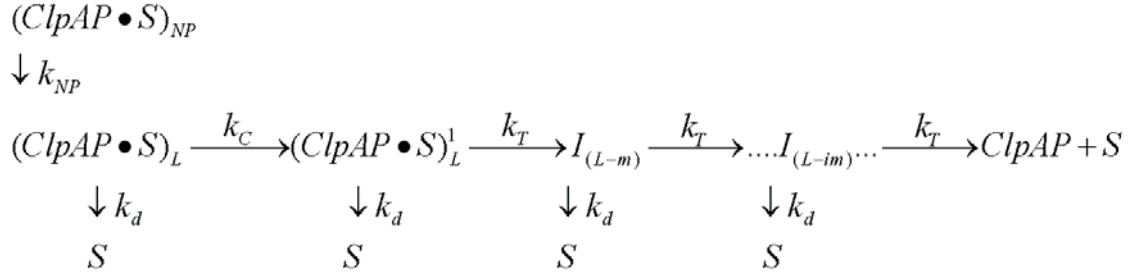


**Figure 5. Dependence of the apparent kinetic parameters on ClpAP species distribution.** (a) Dependence of apparent overall translocation rate  $mk_{T,app}$  on  $[\text{ClpA}_6]_T / [\text{ClpP}_{14}]_T$  for ClpAP catalyzed polypeptide translocation where  $[\text{ClpA}_6]_T = 147 \text{ nM}$ . The solid line is the result of a NLLS fit to Eq. (1) with  $K_{app} = (2 \pm 14) \times 10^{10} \text{ M}^{-1}$  and  $mk_{T,A} = (15.5 \pm 0.6) \text{ aa s}^{-1}$ , where the overall translocation rates for 1:1 and 2:1 ClpAP complexes were constrained to equal  $(31 \pm 1) \text{ aa s}^{-1}$ . (b-c) The translocation rate constant  $k_{T,app}$  (b) and the apparent kinetic step-size  $m_{app}$  (c) are plotted as functions of the molar ratio of ClpA hexamers to ClpP tetradecamers. Both parameters remain constant for conditions favoring a mixture of 1:1 and 2:1 ClpAP complexes, where  $k_{T,app} = (11.9 \pm 0.9) \text{ s}^{-1}$  and  $m_{app} = (2.6 \pm 0.2) \text{ aa step}^{-1}$  for molar ratios in the range of  $\sim 0$  to  $\sim 1.5$ .



**Scheme 1. Sequential  $n$ -step model for polypeptide translocation.**  $(Cl pAP \bullet S)_L$  and  $(Cl pAP \bullet S)_{NP}$  represent ClpAP bound to polypeptide substrate in the productive and nonproductive forms, respectively, and  $S$  is the unbound polypeptide substrate.  $k_T$  is the translocation rate constant,  $k_d$  is the dissociation rate constant,  $L$  is the polypeptide length,  $m$  is the average distance translocated between two steps with rate constant  $k_T$ , ' $i$ ' in  $I_{(L-im)}$  represents  $i$  number of translocation steps, and the step that occurs with rate constant  $k_c$  represents a step slower than translocation.

**Table 1.** Polypeptide translocation Substrates

Substrate	Name	Length (aa)	Sequence
I	N-Cys-50	50	CLILHNKQLGMTGEVSFQAA NTKSAANLKVKELRSKKKLA <b>ANDENYALAA</b>
II	N-Cys40	40	CTGEVSFQAANTKSAANLKV KELRSKKKLA <b>ANDENYALAA</b>
III	N-Cys40	30	CTKSAANLKVKELRSKKKLA <b>ANDENYALAA</b>
* Fluorescein dye covalently attached to N-terminal cysteine residue			

**Table 2.** ClpAP Polypeptide Translocation Parameters as a Function of [ClpP<sub>14</sub>]<sub>T</sub>

$\frac{[ClpA_6]_T}{[ClpP_{14}]_T}$	[ClpP <sub>14</sub> ] <sub>T</sub> (nM)	$k_{T,app}$ (s <sup>-1</sup> )	$m_{app}$ (aa step <sup>-1</sup> )	$mk_{T,app}$ (aa s <sup>-1</sup> )	$k_{C,app}$ (s <sup>-1</sup> )	$k_{NP,app}$ (s <sup>-1</sup> ) x 10 <sup>-2</sup>
0.4	334	10.8 ± 0.6	2.8 ± 0.1	30.6 ± 0.1	0.179 ± 0.005	(3.10 ± 0.03)
0.9	168	12 ± 3	2.5 ± 0.7	29.8 ± 0.2	0.18 ± 0.03	(3.3 ± 0.2)
1.3	112	12.6 ± 0.3	2.58 ± 0.02	32 ± 1	0.191 ± 0.001	(3.2 ± 0.02)
1.7	84	10 ± 4	3 ± 1	31 ± 2	0.169 ± 0.002	(3.000 ± 0.0002)
2.2	66	6 ± 2	5 ± 2	28.9 ± 0.8	0.153 ± 0.007	(2.8 ± 0.1)
2.6	56	3.9 ± 0.3	7.3 ± 0.9	28 ± 1	0.1417 ± 0.0002	(2.8 ± 0.1)
3.1	48	4.2 ± 0.5	6.2 ± 0.7	25.8 ± 0.3	0.142 ± 0.007	(2.80 ± 0.02)
4.3	34	3.1 ± 0.6	7 ± 1	21.9 ± 0.6	0.131 ± 0.006	(2.80 ± 0.04)
5.2	28	3.4 ± 0.4	6.7 ± 0.8	22.1 ± 0.3	0.127 ± 0.002	(2.70 ± 0.04)
6.1	24	2.6 ± 0.3	8 ± 1	20.7 ± 0.4	0.121 ± 0.003	(2.8 ± 0.1)
8.1	19	3.4 ± 0.6	5.8 ± 0.9	19.0 ± 0.4	0.120 ± 0.003	(2.7 ± 0.1)

$k_T$  is the translocation rate constant,  $k_C$  is an additional kinetic step defined by Scheme 1,  $m$  is the kinetic step size,  $k_{NP}$  is a slow conformational change defined by Scheme 1, and  $mk_T$  is the macroscopic rate of translocation, where all parameters have been measured for each [ClpP<sub>14</sub>]<sub>T</sub> in the presence of 1 μM ClpA monomer, 1 mM ATPγS, and 20 nM Flu-polypeptide.

## Chapter Six

### Conclusions

The translocation activity of the AAA+ unfoldase *E.coli* ClpA has traditionally been viewed through the lens of proteolysis from steady-state degradation assays using model substrates like green fluorescent protein<sup>24</sup> and casein<sup>14; 25</sup>, or through the observation of FRET upon substrate entry into ClpP.<sup>26; 27</sup> However, these approaches have not allowed for the observation of ClpA catalyzed polypeptide translocation in the absence of ClpP. Therefore, the question of whether ClpP allosterically impacts the translocation mechanism for ClpA has not been resolved using any previously reported method.

We have presented in Chapter 2 the first reported method that allows for the observation of ClpA polypeptide translocation in the absence of the proteolytic component ClpP. In this method, ClpA that is prebound with polypeptide substrate is rapidly mixed in a stopped-flow fluorometer with ATP and protein trap to initiate translocation. Because ClpA is preassembled and prebound to polypeptide substrate, time courses only reflect the kinetics of translocation since any contribution from the kinetics of assembly or polypeptide binding have been removed. Thus, time courses resulting from this method only reflect a single cycle of polypeptide translocation. Furthermore, the strength of this method lies in the fact that kinetic time courses are sensitive only to the molecular events taking place in the active site. The details of this method were

presented in Chapter 2, where we discussed the experimental design and also presented a series of simulations to provide insight into potential outcomes for example translocation mechanisms.

In order for a motor protein like ClpA to function, it must harness the energy of ATP binding and hydrolysis to fuel translocation. For each translocation event, repeating cycles of certain events must occur. At a minimum, these events include ATP binding, ATP hydrolysis,  $P_i$  release, potential conformational changes, etc. In order to investigate the allosteric impact of ClpP on the mechanism of ClpA catalyzed polypeptide translocation, we used the fact that our single-turnover methodology is sensitive to the slowest repeating step in this cycle to examine the ClpAP translocation mechanism as a function of [ATP] (Chapter 3). The rationale for doing this was rooted in the fact that ATP binding and hydrolysis is absolutely required for translocation to occur. Therefore, by systematically lowering the [ATP], we could potentially force ATP binding to become rate-limiting, and parameter trends would reveal the identity of the rate-limiting step and provide insight into the translocation mechanism for ClpAP.

In Chapter 3, we applied our single-turnover stopped-flow fluorescence method to examine the dependence of ClpAP catalyzed polypeptide translocation on [ATP]. We reported that ClpA, in the presence of ClpP, translocates polypeptide substrate with an overall rate of  $\sim 36 \text{ aa s}^{-1}$ , in contrast to our previous report of  $\sim 20 \text{ aa s}^{-1}$  in the absence of ClpP. Our data showed that this was a consequence of both an increase in the elementary rate constant for translocation and a decrease in the frequency that the observed rate-limiting step repeats. Furthermore, we were able to conclude from the dependence of the translocation mechanism on [ATP] that the repeating rate-limiting step for ClpA

catalyzed translocation, both in the presence and absence of ClpP, is a step that immediately follows ATP binding.

From our data presented in Chapter 3, steady state ATP hydrolysis rates from Weber-Ban and coworkers,<sup>23</sup> and crosslinking experiments from Horwich and coworkers,<sup>12</sup> we proposed models to describe ClpA and ClpAP catalyzed polypeptide translocation. We proposed that, when ClpP is absent, the rate-limiting step in translocation occurs at D1, whereas the observed rate-limiting step occurs at D2 in the presence of ClpP.<sup>29</sup> Additionally, this model was consistent with previous reports that ClpA mutants deficient in ATPase activity at either D1 or D2 both support polypeptide translocation.<sup>23</sup>

Because our single-turnover stopped-flow fluorescence method requires the presence of an ATP analogue to assemble ClpA hexamers, a significant probability exists for competition between ATP and the nucleotide analogue. We have previously reported that the best analogue to assemble ClpA hexamers active in both polypeptide binding and translocation is ATP $\gamma$ S. In an effort to minimize competition between ATP and ATP $\gamma$ S, we chose to use a low [ATP $\gamma$ S], so that [ATP] remains in large excess of [ATP $\gamma$ S].<sup>19</sup> However, despite the large excess of [ATP], the potential for competition between ATP and ATP $\gamma$ S remains.

In order to determine whether our models for ClpA and ClpAP catalyzed polypeptide translocation were influenced by the presence of ATP $\gamma$ S, we investigated the dependence of ClpA catalyzed polypeptide translocation on [ATP $\gamma$ S] in the presence and absence of ClpP. In Chapter 4, we reported the results of this study where we found that the rate of ClpA catalyzed translocation exhibits a dependence on [ATP $\gamma$ S] in the absence

of ClpP, but exhibits no such dependence in the presence of ClpP. This observation was consistent with competition between ATP and ATP $\gamma$ S in the absence of ClpP, but not in the presence of ClpP. By incorporating these findings with our models for ClpA and ClpAP catalyzed polypeptide translocation, we proposed that ATP $\gamma$ S only competes for binding at the D1 ATP binding and hydrolysis site, but not at the D2 site. Furthermore, this led to the conclusion that D1 and D2 bind ATP $\gamma$ S with different affinities, where we reported an affinity constant equal to  $\sim 6 \mu\text{M}$  for ATP $\gamma$ S binding at D1.

Once we had proposed comprehensive models for ClpA and ClpAP catalyzed polypeptide translocation, we then asked; do 1:1 and 2:1 ClpAP share a common translocation mechanism? Two models had been proposed that attempted to answer this question. The first model concluded that 1:1 and 2:1 ClpAP complexes could catalyze polypeptide translocation simultaneously and independently from either end of ClpP<sub>14</sub>,<sup>30</sup> whereas the second model proposed that translocation can only occur from one end of ClpP<sub>14</sub>.<sup>25</sup> Furthermore, it was clear that ClpP allosterically modulated the ClpA catalyzed polypeptide translocation mechanism. However, it was unclear whether translocation of a single polypeptide by ClpAP occurred with the same mechanism when one or two ClpA hexamers associated with a ClpP tetradecamer. That is to say, do 1:1 and 2:1 ClpAP complexes translocate a single polypeptide using the same mechanism or not?

In Chapter 5, we applied the single-turnover stopped-flow fluorescence methodology presented here to investigate the dependence of the translocation mechanism on the ClpAP species distribution for conditions where a single polypeptide was bound to ClpAP. This allowed us to investigate whether a ClpAP complex with one hexamer bound utilizes a different translocation mechanism than a ClpAP complex with

two hexamers bound. In Chapter 5, we reported that 1:1 and 2:1 ClpAP complexes translocate a single polypeptide using identical mechanisms. Thus, the simplest interpretation is consistent with a model where the addition of a second ClpA hexamer to ClpAP does not further activate ClpAP for polypeptide translocation.

However, the single-turnover stopped-flow fluorescence used in Chapter 5 did not allow for the determination of whether polypeptide was bound and translocated from one or both ends of ClpP<sub>14</sub> in 2:1 ClpAP complexes. The experimental conditions employed in Chapter 5 favored the formation of ClpAP complexes with a single polypeptide bound. Since we observed identical translocation mechanisms for conditions favoring 1:1 ClpAP versus 2:1 ClpAP, we concluded that ClpAP complexes with one or two ClpA hexamers associated translocate polypeptide with identical mechanisms, which means that 1:1 and 2:1 ClpAP complexes translocate polypeptide with the same overall rate, kinetic step-size, rate constants, etc. Therefore, the allosteric impact of ClpP on the ClpA catalyzed polypeptide translocation mechanism must be the result of the association of a single ClpP tetradecamer with a single ClpA hexamer.

#### *Future Directions*

While we have presented comprehensive models to describe polypeptide translocation by ClpA and ClpAP, much work remains to fully understand the contributions of D1 and D2 to translocation. This should include a rigorous examination of the dependence of the translocation mechanism on both [ATP] and [ATP $\gamma$ S] using ClpA mutants that are deficient in the ability to hydrolyze ATP at either of the ATPase domains. Such a strategy would allow for the determination of the translocation mechanism utilized by each individual ATP binding and hydrolysis domain. Further, by

performing these studies in both the presence and absence of ClpP, the specifics of how ClpP allosterically impacts ClpA catalyzed polypeptide translocation will emerge.

The elucidation of the translocation mechanism for each individual domain will provide a wealth of information on the contribution of either ATP binding domain to ClpA and ClpAP catalyzed polypeptide translocation. However, the role of ClpP in modulating the translocation activity of ClpA will never fully be understood until the energetics of the ClpA<sub>6</sub>:ClpP<sub>14</sub> interaction have been rigorously examined. A thermodynamic model to describe the distribution of ClpAP assembly states will aid significantly in the interpretation of both existing and future kinetic data derived from ClpAP complexes. Furthermore, the coupling of this data to a rigorous examination of the polypeptide binding activities of ClpAP will allow for a model to be proposed that will answer the question of whether polypeptide is bound and translocated from both ends of ClpP<sub>14</sub> for conditions favoring the assembly of 2:1 ClpAP complexes.

Lastly, information gained from a rigorous examination of the energetics of the ClpA<sub>6</sub>:ClpP<sub>14</sub> association will guide the application of X-ray crystallographic techniques to study ClpAP. Once an initial X-ray crystal structure of the ClpAP complex has been determined, the solution conditions could be modified to allow for the investigation of global conformational changes that accompany polypeptide translocation. Furthermore, X-ray crystallographic experiments for the ClpAP complex with polypeptide bound in the presence of ATP $\gamma$ S, ADP, or transition state analogues will yield a comprehensive picture of the chemical interactions required for the affinity of ClpA for polypeptide substrate to cycle between the high- and low-affinity states that make polypeptide translocation possible.

## References

1. Rubinsztein, D. C. (2006). The roles of intracellular protein-degradation pathways in neurodegeneration. *Nature* **443**, 780-6.
2. Wang, H., Megill, A., He, K., Kirkwood, A. & Lee, H. K. (2012). Consequences of inhibiting amyloid precursor protein processing enzymes on synaptic function and plasticity. *Neural Plast* **2012**, 272374.
3. Matyskiela, M. E. & Martin, A. (2013). Design principles of a universal protein degradation machine. *J Mol Biol* **425**, 199-213.
4. Finley, D. (2009). Recognition and processing of ubiquitin-protein conjugates by the proteasome. *Annu Rev Biochem* **78**, 477-513.
5. Sauer, R. T. & Baker, T. A. (2011). AAA+ Proteases: ATP-Fueled Machines of Protein Destruction. *Annual review of biochemistry* **80**, 587-612.
6. Horwich, A. L., Weber-Ban, E. U. & Finley, D. (1999). Chaperone rings in protein folding and degradation. *Proc Natl Acad Sci U S A* **96**, 11033-40.
7. Lander, G. C., Estrin, E., Matyskiela, M. E., Bashore, C., Nogales, E. & Martin, A. (2012). Complete subunit architecture of the proteasome regulatory particle. *Nature* **482**, 186-91.
8. Gottesman, S. (1996). Proteases and their targets in *Escherichia coli*. *Annu Rev Genet* **30**, 465-506.
9. Tomko Jr, R. J. & Hochstrasser, M. (2013). Molecular Architecture and Assembly of the Eukaryotic Proteasome. *Annu Rev Biochem*.
10. Neuwald, A. F., Aravind, L., Spouge, J. L. & Koonin, E. V. (1999). AAA+: A class of chaperone-like ATPases associated with the assembly, operation, and disassembly of protein complexes. *Genome Res* **9**, 27-43.
11. Guo, F., Maurizi, M. R., Esser, L. & Xia, D. (2002). Crystal structure of ClpA, an Hsp100 chaperone and regulator of ClpAP protease. *J Biol Chem* **277**, 46743-52.
12. Hinnerwisch, J., Fenton, W. A., Furtak, K. J., Farr, G. W. & Horwich, A. L. (2005). Loops in the central channel of ClpA chaperone mediate protein binding, unfolding, and translocation. *Cell* **121**, 1029-41.

13. Martin, A., Baker, T. A. & Sauer, R. T. (2008). Pore loops of the AAA+ ClpX machine grip substrates to drive translocation and unfolding. *Nat Struct Mol Biol* **15**, 1147-51.
14. Farbman, M. E., Gershenson, A. & Licht, S. (2008). Role of a conserved pore residue in the formation of a prehydrolytic high substrate affinity state in the AAA+ chaperone ClpA. *Biochemistry* **47**, 13497-505.
15. Bohon, J., Jennings, L. D., Phillips, C. M., Licht, S. & Chance, M. R. (2008). Synchrotron protein footprinting supports substrate translocation by ClpA via ATP-induced movements of the D2 loop. *Structure* **16**, 1157-65.
16. Farbman, M. E., Gershenson, A. & Licht, S. (2007). Single-Molecule Analysis of Nucleotide-Dependent Substrate Binding by the Protein Unfoldase ClpA. *J Am Chem Soc.*
17. Veronese, P. K. & Lucius, A. L. (2010). Effect of Temperature on the Self-Assembly of the Escherichia coli ClpA Molecular Chaperone. *Biochemistry* **49**, 9820-9.
18. Veronese, P. K., Stafford, R. P. & Lucius, A. L. (2009). The Escherichia coli ClpA Molecular Chaperone Self-Assembles into Tetramers. *Biochemistry* **48**, 9221-9233.
19. Veronese, P. K., Rajendar, B. & Lucius, A. L. (2011). Activity of Escherichia coli ClpA Bound by Nucleoside Di- and Triphosphates. *Journal of molecular biology* **409**, 333-47.
20. Maurizi, M. R. (1991). ATP-promoted interaction between Clp A and Clp P in activation of Clp protease from Escherichia coli. *Biochem Soc Trans* **19**, 719-23.
21. Singh, S. K., Guo, F. & Maurizi, M. R. (1999). ClpA and ClpP remain associated during multiple rounds of ATP-dependent protein degradation by ClpAP protease. *Biochemistry* **38**, 14906-15.
22. Singh, S. K. & Maurizi, M. R. (1994). Mutational analysis demonstrates different functional roles for the two ATP-binding sites in ClpAP protease from Escherichia coli. *J Biol Chem* **269**, 29537-45.
23. Kress, W., Mutschler, H. & Weber-Ban, E. (2009). Both ATPase domains of ClpA are critical for processing of stable protein structures. *J Biol Chem* **284**, 31441-52.
24. Weber-Ban, E. U., Reid, B. G., Miranker, A. D. & Horwich, A. L. (1999). Global unfolding of a substrate protein by the Hsp100 chaperone ClpA. *Nature* **401**, 90-3.
25. Maurizi, M. R., Singh, S. K., Thompson, M. W., Kessel, M. & Ginsburg, A. (1998). Molecular properties of ClpAP protease of Escherichia coli: ATP-dependent association of ClpA and clpP. *Biochemistry* **37**, 7778-86.

26. Reid, B. G., Fenton, W. A., Horwich, A. L. & Weber-Ban, E. U. (2001). ClpA mediates directional translocation of substrate proteins into the ClpP protease. *Proc Natl Acad Sci U S A* **98**, 3768-72.
27. Kolygo, K., Ranjan, N., Kress, W., Striebel, F., Hollenstein, K., Neelsen, K., Steiner, M., Summer, H. & Weber-Ban, E. (2009). Studying chaperone-proteases using a real-time approach based on FRET. *J Struct Biol* **168**, 267-77.
28. Rajendar, B. & Lucius, A. L. (2010). Molecular mechanism of polypeptide translocation catalyzed by the Escherichia coli ClpA protein translocase. *J Mol Biol* **399**, 665-79.
29. Miller, J. M., Lin, J., Li, T. & Lucius, A. L. (2013). E. coli ClpA Catalyzed Polypeptide Translocation Is Allosterically Controlled by the Protease ClpP. *J Mol Biol*.
30. Maglica, Z., Kolygo, K. & Weber-Ban, E. (2009). Optimal efficiency of ClpAP and ClpXP chaperone-proteases is achieved by architectural symmetry. *Structure* **17**, 508-16.

## Appendix 1

Mathematical representation of [ATP]-dependent polypeptide translocation using the method of Laplace transforms

*Journal of Molecular Biology*

Copyright 2013

Used by permission

Format adapted for dissertation

In the single turnover polypeptide translocation experiments reported here, the signal is sensitive to release of polypeptide substrate. Fig. 6a in Chapter 3 gives the simplest  $n$ -step sequential mechanism, where an enzyme,  $E$ , is prebound to polypeptide substrate,  $S$ , to form the  $ES$  complex. Upon mixing with ATP, the enzyme can proceed through a rate limiting step,  $k_{obs}$ , to form the first intermediate,  $E \cdot I_1$ . Fig. 6b in Chapter 3 illustrates that each rate limiting step,  $k_{obs}$ , at a minimum, represents a cycle of ATP binding, ATP hydrolysis, and ADP/P<sub>i</sub> release that must repeat for the formation of each translocation intermediate,  $E \cdot I_n$ , where  $n$  represents the number of translocation steps. This cycle of ATP binding, ATP hydrolysis, and ADP/P<sub>i</sub> release is limited by the slowest step in the cycle, which will repeat  $n$  times until the substrate is released to form  $S^*$ . Thus,  $k_{obs}$  represents the slowest step in the cycle. In translocation, the polypeptide substrate exits the reaction without covalent modification, which means that the 1° structure of  $S$  and  $S^*$  are identical. However, because the experiments are performed under single-turnover conditions,  $S^*$  is not able to be translocated again.

To describe the kinetic time courses with the scheme in Fig. 6a in Chapter 3, an equation must be derived that describes the time-dependent release of polypeptide. For simplification, we will use the fraction of polypeptide translocated as a function of time,  $f_p(t)$ , given by Eq. (S.1),

$$f_p(t) = \frac{S^*(t)}{(ES)_0} \quad (\text{S.1})$$

where  $(ES)_0$  is the concentration of enzyme peptide complex at  $t = 0$ , and  $S^*(t)$  is the concentration of peptide released as a function of time. The system of coupled differential

equations that results from the scheme in Fig. 6a in Chapter 3 is solved using the Laplace transform method as previously described.<sup>1; 2</sup> The strength of using this method is that it reduces the system of coupled differential equations to a system of coupled algebraic equations that can be solved using matrix methods. Moreover, the resulting Laplace transform of  $f_p(t)$  is a continuous function of the number of steps,  $n$ , and is given by Eq. (S.2),

$$\mathcal{L}f_p(t) = F_p(s) \quad (\text{S.2})$$

where,  $\mathcal{L}$  is the Laplace transform operator and  $F_p(s)$  is the Laplace transform of  $f_p(t)$ . For the Scheme in Fig. 6a in Chapter 3, the resulting Laplace transform of the fraction of peptide released as a function of time,  $f_p(t)$ , is given by Eq. (S.3),

$$F_p(s) = \frac{k_{obs}^{n_{obs}}}{s(k_{obs} + s)^{n_{obs}}} \quad (\text{S.3})$$

where  $s$  is the Laplace variable,  $k_{obs}$  is the observed rate constant, and  $n_{obs}$  is the observed number of steps required to fully translocate the polypeptide substrate. In order to analyze experimental time-courses, one must determine  $f_p(t)$ , which is accomplished by finding the inverse Laplace transform of  $F_p(s)$  as described by Eq. (S.4),

$$\mathcal{L}^{-1}F_p(s) = f_p(t) \quad (\text{S.4})$$

where  $\mathcal{L}^{-1}$  is the inverse Laplace transform operator.

For this discussion, we will not focus on finding  $f_p(t)$ , but will instead make predictions about  $f_p(t)$  based on inspecting or taking limits of  $F_p(s)$ . For example,  $F_p(s)$  for the Scheme in Fig. 6b in Chapter 3 is given by Eq. (S.5),

$$F_p(s) = \frac{(k_1[ATP])^n k_2^n k_3^n}{s(k_1[ATP](k_2 + s) + s(k_{-1} + k_2 + s))^n (k_3 + s)^n} \quad (\text{S.5})$$

where Eq. (S.5) is identical to what has been previously reported.<sup>3</sup> At high concentrations of ATP, we assume that  $k_1[ATP] \gg k_2$  and  $k_3$ . Taking the limit of Eq. (S.5) as  $k_1[ATP]$  approaches infinity yields Eq. (S.6).

$$\lim_{k_1[ATP] \rightarrow \infty} \frac{(k_1[ATP])^n k_2^n k_3^n}{s(k_1[ATP](k_2 + s) + s(k_{-1} + k_2 + s))^n (k_3 + s)^n} = \frac{k_2^n k_3^n}{s(k_2 + s)^n (k_3 + s)^n} \quad (\text{S.6})$$

Under conditions where  $k_3 \gg k_2$ , Eq. (S.6) simplifies to Eq. (S.7).

$$\lim_{k_3 \rightarrow \infty} \frac{k_2^n k_3^n}{s(k_2 + s)^n (k_3 + s)^n} = \frac{k_2^n}{s(k_2 + s)^n} \quad (\text{S.7})$$

By relating Eq. (S.7) to Eq. (S.3), we find that under conditions of excess [ATP] and  $k_3 \gg k_2$ , the observed rate constant  $k_{obs} = k_2$  and the apparent number of steps,  $n$ , is equal to the number of times the cycle in Fig. 6b in Chapter 3 repeats. Similarly, if we assume that  $k_2 \gg k_3$ , Eq. (S.6) simplifies to Eq. (S.8).

$$\lim_{k_2 \rightarrow \infty} \frac{k_2^n k_3^n}{s(k_2 + s)^n (k_3 + s)^n} = \frac{k_3^n}{s(k_3 + s)^n} \quad (\text{S.8})$$

By relating Eq. (S.8) to Eq. (S.3), we find that under conditions of excess [ATP] and  $k_2 \gg k_3$  that the observed rate constant  $k_{obs} = k_3$  and the apparent number of steps,  $n$ , is equal to the number of times the cycle in Fig. 6b in Chapter 3 repeats.

On the other hand, if  $k_2 = k_3$  then Eq. (S.6) simplifies to Eq. (S.9).

$$\lim_{k_3 \rightarrow k_2} \frac{k_2^n k_3^n}{s(k_2 + s)^n (k_3 + s)^n} = \frac{k_2^{2n}}{s(k_2 + s)^{2n}} \quad (\text{S.9})$$

By equating Eq. (S.9) to Eq. (S.3), we find that  $k_{obs} = k_2 = k_3$  and the observed number of steps is two-fold larger than the number of times the cycle repeats, i.e.  $n_{obs} = 2n$ . Under conditions where  $n_{obs} = 2n$ , the observed kinetic step-size,  $m$ , given by Eq. (S.10),

$$m_{obs} = \frac{L}{n_{obs}} \quad (\text{S.10})$$

would be reduced by a factor of 2.

## References

1. Lucius, A. L., Maluf, N. K., Fischer, C. J. & Lohman, T. M. (2003). General methods for analysis of sequential "n-step" kinetic mechanisms: application to single turnover kinetics of helicase-catalyzed DNA unwinding. *Biophys J* 85, 2224-39.
2. Lucius, A. L., Miller, J. M. & Rajendar, B. (2011). Application of the Sequential n-Step Kinetic Mechanism to Polypeptide Translocases. *Methods Enzymol* **488**, 239-64.
3. Lucius, A. L. & Lohman, T. M. (2004). Effects of temperature and ATP on the kinetic mechanism and kinetic step-size for E.coli RecBCD helicase-catalyzed DNA unwinding. *J Mol Biol* 339, 751-71.